Using tracers to determine groundwater fluxes in a coastal aquitard-aquifer system

Michelle Lee Irvine

Bachelor of Applied Science (Environmental Health)

Master of Environmental and Business Management

Thesis submitted as a requirement in full for the degree of *Doctor of Philosophy* in the School of the Environment, Flinders University, South Australia

12 August 2016

Declaration

I certify that this thesis does not incorporate without acknowledgment any material previously submitted for a degree or diploma in any other university; and that to the best of my knowledge and belief it does not contain any material previously published or written by another person except where due reference is made in the text.

Michelle Irvine

Co-authorship

This PhD thesis is a presented as a series of journal papers in preparation for publication in leading scientific journals. Chapters 3 and 4 are to be submitted for publication with co-authorship as listed below. I am the first author on all publications and was responsible for leading and conducting the majority of research contained within.

Chapter 3. Time varying recharge in a coastal groundwater system estimated using geochemical methods and a numerical model. Irvine M, Cook P, Harrington G.

Chapter 4. Using aquitard porewater chemistry to reveal long-term changes in regional groundwater chemistry. Irvine M, Harrington G, Cook P, Hendry J, Smith S, Banks E.

Acknowledgements

This pHD would not be possible without the funding support from National Centre for Groundwater Research and Training, and SA Water.

I would like to thank my supervisors Peter Cook and Glenn Harrington for their patience, support, involvement and encouragement throughout my pHD. Their combined experience, insight and willingness to allow the data and research find its own way to tell a story was both inspirational and reassuring.

I would like to thank my colleagues at Flinders who provided advice and a sounding board throughout the research process, Vincent Post, James McCallum, Eddie Banks and Cameron Wood. Vincent Post for the exciting detour into researching the source of hypersaline waters encountered in the basin, and a sounding board for the coastal sea level change and characterising the offshore extent of the basin. James McCallum for his willingness to trouble shoot any numerical modelling problems at very short notice, and sharing his significant knowledge in modelling of age tracers. Eddie Banks for his advice, and countless hours in the field with me collecting groundwater samples in all kinds of weather conditions always ensuring that data collection was systematic and precise. Cameron Wood who has shared his pHD journey with me, through the proximity of a shared office, who tolerated both my joys and disasters with his characteristic dry sense of humour.

And last but not least all of my family. Special thanks go to my sister Haley, and my mother Marie, who provided stability during this rollercoaster ride with their support and good humour.

This work is dedicated to my children April and Danny, who were my inspiration to follow this through to completion.

Summary

Groundwater managers make assessments of the sustainable yield of groundwaters, based on estimates of the parameters of recharge, storage, travel time, and discharge on a regional scale. Many of these parameters are difficult to estimate. In many cases these systems comprise several overlying aquifers whose hydraulics are controlled by aquitards, so estimating fluxes between aquifers is also important component of the groundwater balance.

Environmental tracers are a common method used to constrain recharge estimates, and to measure fluxes across aquitards. The use of tracers to determine fluxes in coastal connected systems is influenced by changing sea levels and changing recharge rates from land clearing.

This research was based in Willunga Basin in South Australia, a system of two regional aquifers separated by an aquitard and hydraulically connected to the coast. The vertical hydraulic gradient between the regional aquifers varies along the flowpath. The system has an upwards gradient at the high point of the system, and a strong downwards vertical gradient in the centre of the basin. The vertical gradient becomes neutral as the aquifers near the coast.

The first part of this study assesses how the spatial distribution of carbon-14, chloride and helium-4 in groundwater can inform the conceptual model of recharge in a layered system. Age tracers in coastal aquifers are assumed to have been influenced by sea level change in the past, increasing velocities of groundwater flow resulting in younger ages than expected based on current hydraulic conditions. Sea level change in the last glacial maxima was shown using a three dimensional regional numerical model to change hydraulic conditions in this groundwater system by up to 20 m when compared to a model with a constant head coastal boundary condition. Despite the change in hydraulic gradients, both models generate a similar distribution for groundwater carbon-14 with variation of up to 3 pmC within 4km of the coast at the end of the Holocene.

Age tracers as a calibration target should constrain the use of numerical models to estimate recharge, by constraining velocity where hydraulic conductivity estimates are uncertain. Recharge changes over time, and is influenced by changes in climate. Anthropogenic changes such as land clearing also influence recharge rates, such as land clearing following European settlement in Australia 200 years ago, and pumping of groundwater for irrigation. A series of model calibrations to single target (head) and dual target calibrations (head and carbon-14) are used to show that age tracer calibration is able to improve model calibration and refine recharge estimates. The model results demonstrate that head as a calibration tool provides a non-unique solution, and that carbon-14 can be used as a calibration target to constrain the estimate of recharge. The model calibration predicts a post-land clearing (0-150 yrs BP) recharge between 15 and 60 mm/yr, with pre-land clearing recharge of 15 to 55 mm/yr. A chloride mass balance assessment of recharge is also made of 15-16 mm/yr. Previous literature estimates for the Willunga Basin are 20 to 34 mm/yr, within the range of the calibration results.

The second part of this study uses the 3D numerical model of the basin to develop an understanding of how sea level fluctuation since the last glacial maxima changed the vertical gradients between the aquifers. At the peak of the sea level decline 18 kyrs BP, the vertical hydraulic gradients across the aquitard at the coast and at the high point increased in magnitude, and at the centre of the basin the direction of the vertical hydraulic gradient was reversed during the last glacial maxima. While the vertical gradients changed, this was shown not to have an influence on solute movement across the aquitard where diffusion is the dominant process for solute transport.

The measurement of flux using aquitard solute profiles is shown to be complicated when aquifer solute concentrations are dynamic. The hydraulic conductivity of the aquitard is constrained to be $1x10^{-7}$ m/d or less, and the flux varies depending on location and size of the vertical gradient. The maximum downward flux is shown to be 0.014 mm/yr at the centre of the system, and maximum

upward flux is 0.002 mm/yr at the top of the flowpath. Increased concentrations of chloride and deuterium enrichment in the aquifers are inferred through the modelling of aquitard solute profiles, and attributed to climatic changes in temperature and precipitation associated with the last glacial maxima, warming periods and late Holocene events.

Table of Contents

List of Figures

List of Photos

List of Tables

Chapter 1 Introduction

1.1 The research problem

When managing groundwater systems, resource managers rely on water budgets to characterise systems and allocate the resource to users. A water budget typically comprises of some conceptual understanding of the groundwater system and the amounts of water available for use that are replenished by recharge (Healy and Cook 2002, Mazor 2004, Seiler and Gat 2007). Resource management relies on balancing the recharge, storage, consumption and discharge from aquifers to estimate a sustainable yield which aims to protect use of the resource over the long term.

Recharge, the amount of water that reaches the aquifer, is a critical component of the water balance that is difficult to quantify. Recharge can be dependent on climate, rainfall, soil and vegetation characteristics, all of which change over time (Allison and Hughes 1978, Healy and Cook 2002, Seiler and Gat 2007). Direct measurements include seepage measurements, and indirect methods include water table fluctuations and stream flow separation methods (Healy and Cook 2002, Seiler and Gat 2007, Batlle-Aguilar and Cook 2012).

A common method of determining parameters such as recharge is inverse modelling, in which a groundwater model is calibrated to observations of hydraulic head by varying the recharge rate. However, when groundwater models are calibrated to hydraulic head data, estimates of groundwater recharge are highly sensitive to values of hydraulic conductivity that are usually not well known. Using an additional target of an age tracer should constrain this estimate of recharge (Sanford 2011, Turnadge and Smerdon 2014). The use of two different calibration targets that measure the recharge over different time frames can cause problems; for example, head is a recent response to recharge, and age tracers are a measure of velocity over the longer term.

Geochemical methods have been widely used for understanding flow systems and estimating recharge rates (Allison and Hughes 1978, Cook and Herczeg 2000, Fetter 2001, McCallum, Engdahl et al. 2014). Groundwater systems have travel times to hundreds and thousands of years (Cook and Herczeg 2000, Mazor 2004), so recharge rates will potentially have changed over several climatic regimes.

In addition to recharge being a function of the climate, hydraulic conditions of coastal groundwater resources are also influenced by sea level variations (Love, Herczeg et al. 1994). Coastal groundwater models generally assume that the current coastline is the appropriate hydraulic boundary condition for these systems for all time (Reilly, Plummer et al. 1994, Sanford, Plummer et al. 2004, Sanford 2011). The assumption of steady state conditions for coastal boundaries in groundwater management is expedient, since knowledge of the offshore extent of aquifers is rare due to a lack of offshore data. Numerical modelling of transient coastal conditions increases the computational requirements of models with no verification that offshore assumptions are correct. Love, Herczeg et al. (1996) proposed that in coastal areas the potential of sea level decline in the last glacial maxima should have influenced age tracer distributions. Changing sea levels from the current shoreline changes the hydraulic gradient, changing the velocity of the groundwater flow.

The Willunga Basin, located south of Adelaide, comprises two regional aquifers separated by an aquitard, all connected to the ocean. Groundwater in the Willunga Basin aquifer system is up to 35,000 years old (Herczeg and Leaney 2002). The last glacial maxima occurred at 18-22 kyr before present (BP), and was accompanied by a colder drier climate (Calvo, Pelejero et al. 2007, Petherick, Bostock et al. 2013, Reeves, Barrows et al. 2013). After the last glacial maxima (LGM) two rapid warming events were associated with the sea level rise to current levels, warmer temperatures and increased precipitation. This warming was separated by a small cooling event between 12.5 – 13.8 kyrs BP, known as the Antarctic cold reversal. During the Holocene, sea levels have been relatively

steady at their current levels (7 kyr BP to present), and a slight cooling of the climate has occurred (Calvo, Pelejero et al. 2007, Petherick, Bostock et al. 2013).

Other major hydrological changes that would have affected the Willunga Basin are land clearing following European settlement in Australia, and irrigation using groundwater. Allison, Cook et al. (1990) calculated increased recharge rates in the Murray Basin following wholesale land clearing. Large scale land clearing of the Willunga Basin is documented as occurring 150 years before present (Denham, Lentfer et al. 2012). Groundwater extraction of the basin for irrigation of crops was noticeably increased in the 1970- 80's (Denham, Lentfer et al. 2012). Extraction from the aquifers peaked in 1994/95 with 9,000 ML recorded. Currently the annual allowable allocation of groundwater extraction in the McLaren Vale Prescribed Wells Area (PWA) is 6,000 ML.

In the first part of this study, geochemical methods and numerical modelling are used to estimate recharge using both chloride mass balance, and groundwater age. The spatial distribution of the environmental tracers chloride, carbon-14 and helium-4 are used to provide insights into groundwater flow in the basin. 3D regional groundwater modelling using both a constant sea level head boundary condition and at transient sea level change boundary condition to reflect the last glacial maxima are used to compare predicted distributions of carbon-14 and heads in the system. This modelling component was used to determine if sea level variation has a significant influence on carbon-14 distributions in regional aquifers, and to determine how the hydraulic gradients of aquifers have varied over time.

The 3D regional groundwater flow and solute transport model was calibrated to determine post land clearing recharge by calibrations to head alone, and dual calibrations to both head and carbon-14. This modelling component was to determine if the use of carbon-14 as a calibration target improves estimates of recharge.

The second part of this study examines groundwater flow between the two aquifers separated by the aquitard, and how this has changed over time. The flux of water across aquitards is a function of the vertical hydraulic gradient that exists between aquifers, which will also vary over time with changes in sea level. While regional groundwater models used for system management usually include aquitards, hydraulic parameters or the flux across these layers are rarely measured.

The flux of water moving across aquitards is not easily measured. Physical methods of measuring hydraulic conductivity include triaxial methods and centrifuge measurements (Van Der Kamp 2001). Vertical solute profiles have been used in recent times to determine flux and provide insight into the changing chemistry of groundwater resources (Timms, Acworth et al. 2000, Mazurek, Alt-Epping et al. 2009, Hendry and Wassenaar 2011, Harrington, Gardner et al. 2013). The analysis of solute profiles is always assumed under steady state hydraulic conditions. Harrington, Walker et al. (1999) proposed that in coastal connected systems aquifer hydraulic conditions changed with past sea level fluctuations, and tested this with a model in the Otway Basin South Australia. In this paper we propose that changes in sea level will also influence the hydraulic gradients of aquitards in coastal connected systems.

This study attempts to measure flux on a regional basis across an aquitard subject to vertical hydraulic fluctuations. Solute profiles for chloride, deuterium and helium-4 of the aquitard are created at five locations , and provide the first regional data set to link both groundwater and aquitard solute profile data in a comprehensive way. Changes in hydraulic gradient across the aquitard caused by sea level change are inferred from the calibrated 3D groundwater model, and applied to 1D solute profile models for each core site. The aquitard solute profiles provide an insight into changing aquifer conditions under previous climates.

1.2 Research questions

The aim of this research is to:

1. Explore how sea level change influences the use of age tracers to determine recharge in a coastal aquifer-aquitard system.
2. To investigate the relative usefulness of hydraulic heads and age tracer data in numerical modelling to determine recharge, based on the relative time scale difference of these two parameters.
3. Interrogate how solute profiles across an aquitard can inform our understanding of groundwater conditions in the past.

Chapter 2 Hydrogeology of the Willunga Basin

2.1 Location

The field site is the Willunga Basin, located 25 km south of Adelaide, in South Australia. Willunga Basin comprises a thick sequence of Cainozoic sediments that provide critical groundwater supplies for the established wine and horticulture industries in the McLaren Vale region. The basin covers an area of 250 km^2. The basin structure is a gently-dipping trough, bounded to the east and south by the steeply-dipping Willunga Fault and Gulf St Vincent to the west (Cooper and McKenzie 1979).

Figure 2.1: Location map of the McLaren Vale Prescribed Wells area.

2.2 Geology

The Willunga Basin is a narrow wedge of Cainozoic sediments on the downthrown side of the Willunga Fault (Cooper and McKenzie 1979), which were deposited during a series of marine incursions during the Eocene to Miocene.

The basin is bounded on its southern margin by the Willunga Fault. It is bounded to the north, south and east by late Precambrian and Cambrian succession of the Adelaide Geosyncline. The sedimentary basin is thinnest in the north and east, and thickens towards the coast and the Willunga Fault. The basement rocks within the embayment are flat lying or dip gently toward the fault where they are sharply upturned (Cooper and McKenzie 1979).

Table 2.1 shows the lithology of the sediments and their grouping into the main hydrogeological features of the Willunga Basin. Many of the sedimentary layers are not continuous in their extent across the basin as described by Cooper and McKenzie (1979).

The sea floor off the coast of South Australia has a very low topographic gradient until it reaches the continental shelf located 200 km offshore. At the continental shelf the sea floor then dips steeply from -100 mAHD to -2000 mAHD. The coastal basin of Gulf St Vincent has a maximum depth of -40 mAHD but is bounded by shallower sections across Investigator Strait and Backstairs passage of -34 mAHD (Figure 2.1).

A deep drill core 45 km from the coast within the Gulf St Vincent confirms the offshore depths of the geological units of the Willunga Basin (Canyon 1998). The geological units are assumed to extend offshore to a distance of ~ 90 km, to Investigator Strait and Backstairs Passage, the two straits that connect the waters of the Gulf St Vincent to the Southern Ocean on either side of Kangaroo Island (Figure 2.1 inset). The basement outcrops at the surface of the ocean floor across these openings, possibly the limit of the sedimentary deposits of the Willunga Basin (Bourman and Alley 1999).

Table 2.1: Hydro-stratigraphy of the Willunga Basin (Cooper and McKenzie 1979)

Age	Stratigraphy	Lithology	Hydrostatigraphy
Quaternary	Christies Beach Formation	Reddish brown to chocolate-brown fluvial clay, containing lenses of gravel composed mainly of flat-lying pebbles of quartzite	Aquifers/ aquitards Confining bed over much of the basin. Thin shallow sandy and gravel unconfined and semi-confined aquifers.
	Ngaltinga Formation	Clayey sand and clay with occasional sandy interbeds and grey to olive-green massive clay	
	Pirramimma Sandstone	Buff coloured, fine-grained, well-sorted and poorly consolidated sandstone	
	Ochre Cove Formation	Horizontally bedded sequence of alluvial sandstone, gravel and conglomerate	
Tertiary	Port Willunga Formation	Calcarenite, bryozoal, calcrudite, glauconitic, silt and sand	Aquifer (Port Willunga Formation) Confined aquifer in southern half of basin; unconfined elsewhere
	Chinaman Gully Formation*	Regressive non marine to marginal marine carbonaceous silts, sands and clay; dark, carbonaceous and pyritic where fresh. Thin unit that thickens to the east.	Aquitard (Blanche Point Formation)
	Blanche Point Formation*	Glauconitic, spicular and calcareous silts and clays. Western half calcareous and rich in clay, moving eastward less calcareous and rich in clay.	
	Tortachilla Limestone*	Bioclastic limestone, calcareous and richly fossiliferous, rich in brown goethite pellets.	
	North and South Maslin Sands	North MS: quartz sand and gravel South MS: marginal marine sand, glauconitic, carbonaceous and pyritic at depth	Aquifer (Maslin Sands) Confined aquifer over most of basin. Unconfined in northern most part
	Cape Jervis Beds	Pockets of discontinuous Permian sands between the basement and Maslin Sands.	
Precambrian/ Cambrian		Slates, quartzites, dolomites, tillites, shales and limestone	Fractured Rock Aquifer Confined or semi-confined aquifer beneath sediments. Unconfined where outcropping in Hills east of the Willunga Fault and along the Onkaparinga Gorge.
*The Blanche Point aquitard also refers to the Chinaman Gully Formation, Blanche Point Formation and Tortachilla Limestone lithologies.			

2.3 Hydrogeology

The hydrogeological features of interest in this system are two regional aquifers, the Port Willunga Formation (PWF) is a calcareous silty sand, and Maslin Sands (MS) is a quartz and marine sands ranging in thickness from 20 m to up to 150 m. The surface outcropping extent of the aquifers is shown in Figure 2.2, and cross sections are shown in Figure 2.3 and Figure 2.4. The aquifers are hydraulically connected to the shallow waters of the Gulf St Vincent where they outcrop to the surface along the coastline (Cooper and McKenzie 1979). These aquifers are separated by an aquitard, the Blanche Point Formation (BPF), which is a thickness ranging from 20 m to 90 m (Photo 9).

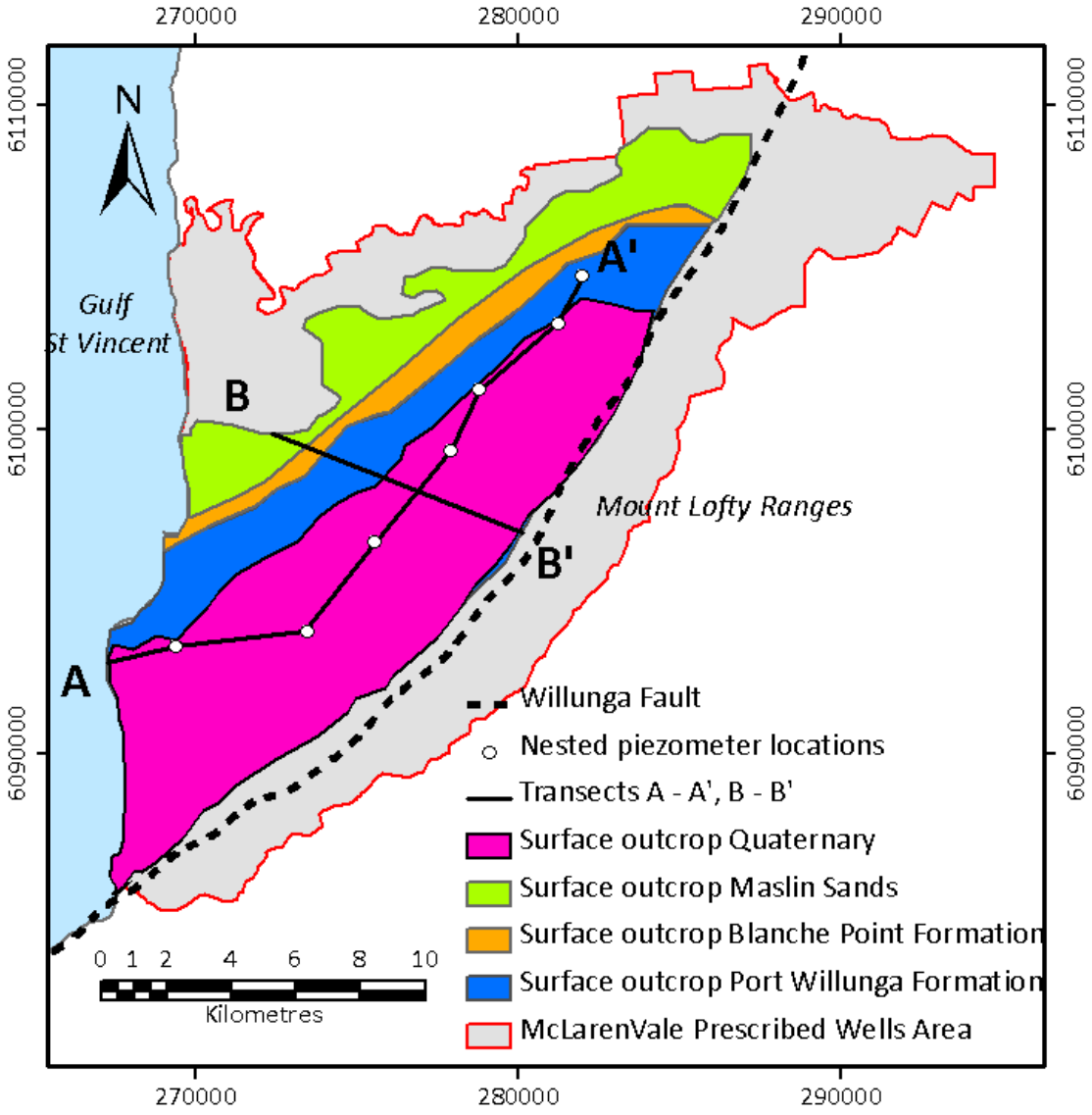

Figure 2.2: Map showing the surface outcropping of the geological features of the Willunga Basin.

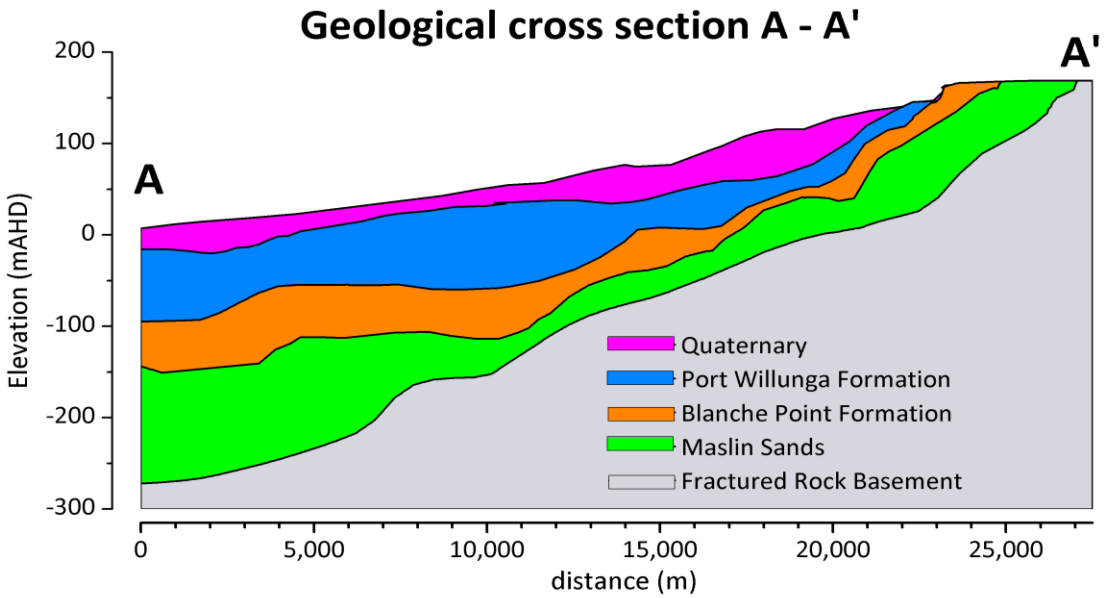

Figure 2.3: Cross section A to A- of the Willunga Basin showing main aquifers

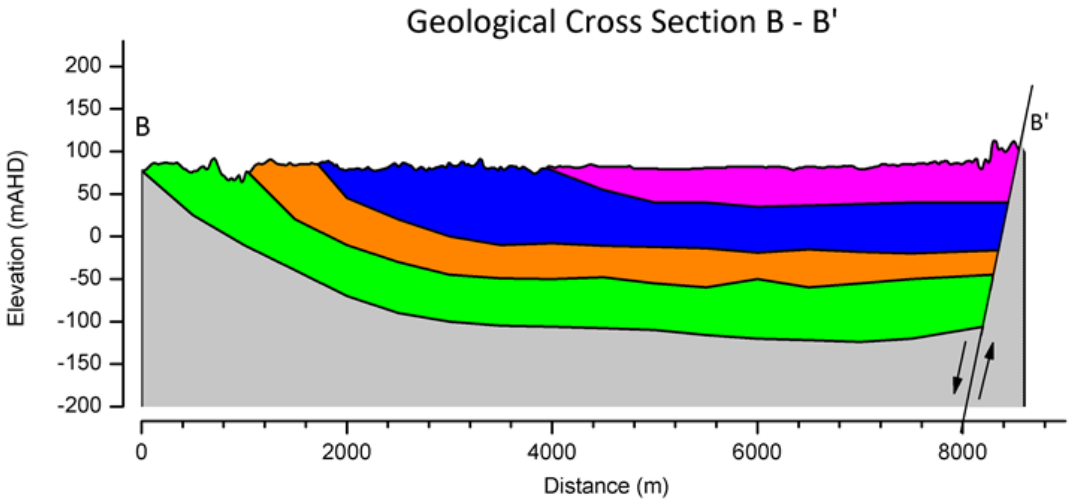

Figure 2.4: Cross Section B - B' showing major aquifer formations of the Willunga Basin, showing the location of the Willunga Fault. See Figure 2.3 for legend.

Groundwater flow in both aquifers is from north-east to south west. The hydraulic head of the Port Willunga Formation ranges from 134.84 mAHD at 19.5 km from the coast, to 0.75 mAHD at 800m from the coast (measured along the direction of the flowpath). The hydraulic heads of the Maslin Sands range from 174.1 mAHD at a distance of 25 km from the coast, to 3.89 mAHD at 2km from the coast (measured along the direction of the flowpath).

A steeper hydraulic gradient exists in the upper portion of the Maslin Sands aquifer at a distance of 18km to 25 km from the coast, refer to Figure 2.6. The vertical hydraulic gradient between the Port Willunga Formation and Maslin Sands aquifers, as measured across the aquitard, changes direction along the flowpath. In the upgradient section of the basin, the vertical gradient direction is upwards from the deeper to shallower aquifer, and it changes direction to a downwards gradient towards the centre of the basin. Further down the flowpath toward the coast, the vertical hydraulic gradient again becomes upwards.

Groundwater extraction began in the 1970s in the Willunga Basin, and significantly increased in the 1990s with the conversion to a grape growing region. Limited head data is available from the 1970s to develop a potentiometric map of the aquifers, but sufficient data exists from the late 1980s to now to make a comparison of the head change induced by groundwater extraction. Figure 2.5 and Figure 2.6 show the potentiometric heads of the Port Willunga Formation and Maslin Sands aquifers in 1998 and 2011. The head in both aquifers declined between 1998 and 2011, up to 10 m near the coast.

Groundwater salinity is mostly less than 1500 mg/L in both of the aquifers and groundwater is generally considered suitable for irrigation purposes, despite some individual monitoring locations recording significantly higher salinities (Department for Water, 2011).

Current literature estimates of the hydraulic conductivity of the aquifers range from 0.2 to 10 m/d for the Port Willunga Formation, and 0.4 to 1 m/d for the deeper Maslin Sands aquifer (Aldam

1990, Martin 1998, Martin 2006). Current recharge estimates in the literature range from 21 mm/yr to 34 mm/yr (Aldam 1990, Martin 1998, Martin 2006).

Aldam (1990) reports fourteen pump tests conducted in the 1990s, 9 in the Port Willunga Formation with a hydraulic conductivity of 2 to 10 m/d, and 5 in the northern section of the Maslin Sands around 1 m/d. Martin (1998) reports transmissivity from pumping tests of 150 – 200 m^2/d in the Port Willunga Formation, and 35 – 50 m^2/d in the Maslin Sands. The details of the pump tests are not provided, and are possibly the same as reported by Aldam (1990) . Martin (1998) in a numerical model of the system used parameter values for hydraulic conductivity of 0.2 to 8 m/d for the Port Willunga Formation and 1 m/d for the Maslin Sands. A series of pump test data on 7 wells obtained from SA Water Corporation from investigations into a local Managed Aquifer Recharge scheme at Aldinga estimate a hydraulic conductivity of the Port Willunga Formation at 0.74 to 7 m/d.

Drilling and permeability testing of three sites of the aquitard estimated vertical permeabilities of $1.12x10^{-5}$ m/d and $4.41x10^{-3}$ m/d (Aldam 1990).

Table 2.2: Literature estimates of hydraulic conductivity in the Willunga Basin

	Port Willunga Formation	**Blanche Point Formation**	**Maslin Sands**
	K (m/d)	**K (m/d)**	**K (m/d)**
Aldam (1990)	2 – 10 *	$1.12x10^{-5}$- $4.41x10^{-3}$ ***	1 *
Aldinga ASR investigation	0.74 – 7 *		
Martin (1998)	1.8 – 2.5*		0.4 – 0.6*
Martin (2006)	0.2 – 8**		1**

* Pump tests ** numerical model *** permeability tests on samples

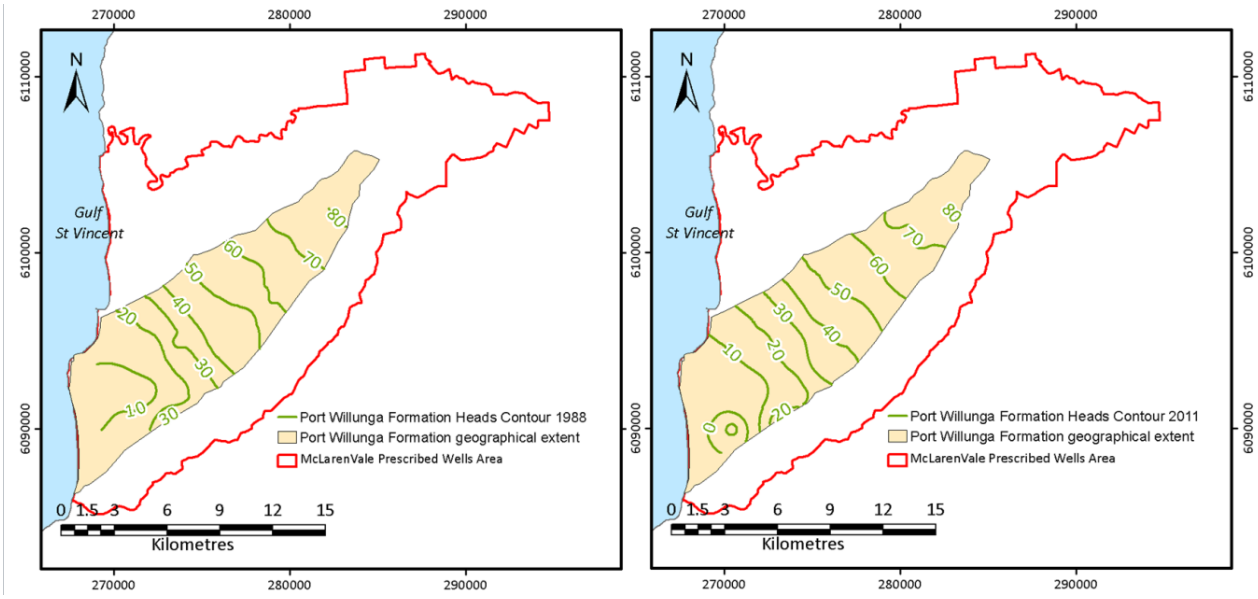

Figure 2.5: Hydraulic head contours of the Port Willunga Formation in 1988 and 2011. Groundwater extraction began in the 1970s but insufficient data exist to create an accurate contour plot.

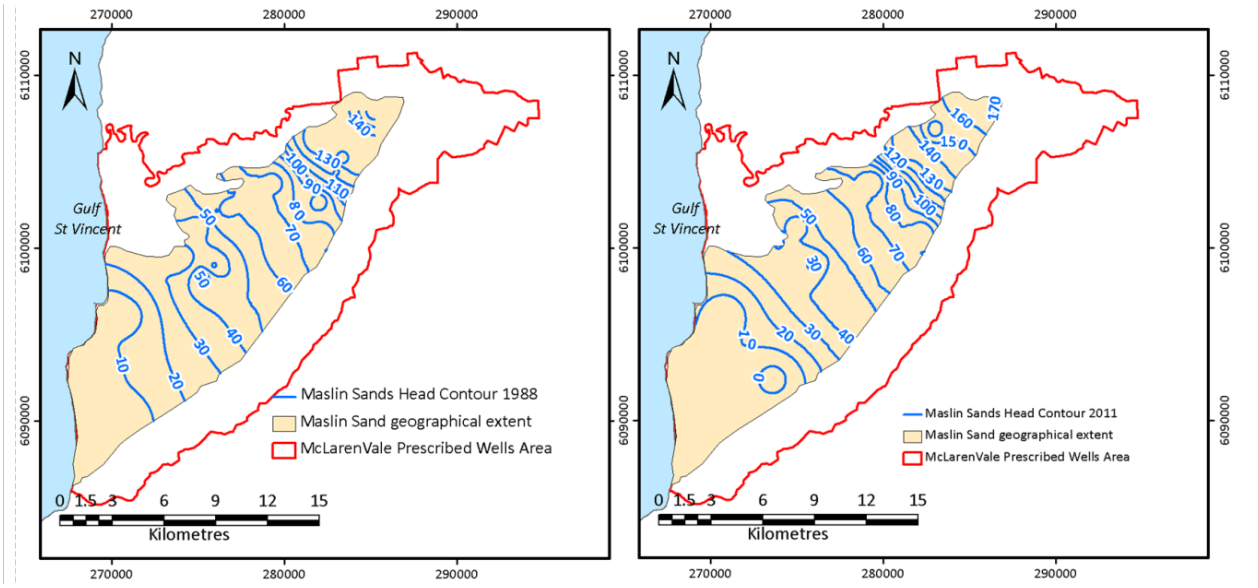

Figure 2.6: Hydraulic head contours of the Maslin Sands in 1988 and 2011. Groundwater extraction began in the 1970s but insufficient data exist to create an accurate contour plot.

2.4 Vegetation and land use

Prior to European settlement the Willunga Plains was open woodlands dominated by Eucalyptus spp. and Casuarina spp. trees, with a herbaceous understory of perennial grasses, Acacia spp. and Melaleuca spp. The uplands supported sclerophylls forests of Eucalyptus, and understory of Myrtacea, Protacea and Xanthorrhoeacea families (Denham, Lentfer et al. 2012). The area was first surveyed in 1839, and development and large scale clearing commenced from this time. Early crops were cereals and wheat, which were supplemented with fruit and vegetable crops in the late 1880s. Wine grape production commenced in the 1860s but was not a major economic activity until the 1980s. A boom in the 1990s resulted in grape vines being the dominant crop in the region (Denham, Lentfer et al. 2012).

2.5 Climate and paleoclimate

The current mean annual rainfall in the basin ranges from 641 mm at Willunga (station 23753) to 717 mm at Mt Bold Reservoir (station 23734), with 65% of this concentrated in the winter and early spring months (June to September). Pan evaporation ranges from 200mm in winter to 600mm in summer. Mean summer maximum and minimum temperatures are 28.7˚C and 17.1˚C, mean winter maximum and minimum temperatures are 14.8˚C and 8.6˚C at Noarlunga (station 23885).

The last glacial maxima occurred around 21 kyr BP in Australia, associated with a colder drier climate with increasing ocean $\delta^{18}O$ values. This was followed by deglacial warming periods associated with warmer sea surface temperatures and periods of increased precipitation. The period of warming occurred in two rapid stages, interrupted by a cooling phase, with further cooling during the late Holocene (6 kyr BP to now) (Calvo, Pelejero et al. 2007, Petherick, Bostock et al. 2013, Reeves, Barrows et al. 2013). Climate trends from 10 kyr BP to the present show decreasing ocean $\delta^{18}O$ values, and a progressive decrease in sea surface temperature from 6.5 kyr to modern times (Calvo, Pelejero et al. 2007), with a period of increased precipitation between 6 and 8 kyr (Petherick, Bostock et al. 2013).

Sea level variation in South Australia has been described as a series of recessions of up to -150 mAHD from the current 0 mAHD (Cann, Belperio et al. 1988). Sea level change is a direct result of climate change, with the last major decline in sea level at the last glacial maxima being -130 mAHD, and the current sea level has been in place from 7000 years BP shown in Figure 2.7 (Cann, Belperio et al. 1988).

The groundwater is hydraulically connected to the coast, so a declining sea level changes the hydraulic conditions of the groundwater by decreasing the head level at the coast. This pressure decline can change (or increase) the average velocity of the groundwater. Conversely a rising sea level will increase the groundwater heads at the coast, this pressure is then propagated inland, the magnitude and distance of this pressure change are determined by the aquifer properties.

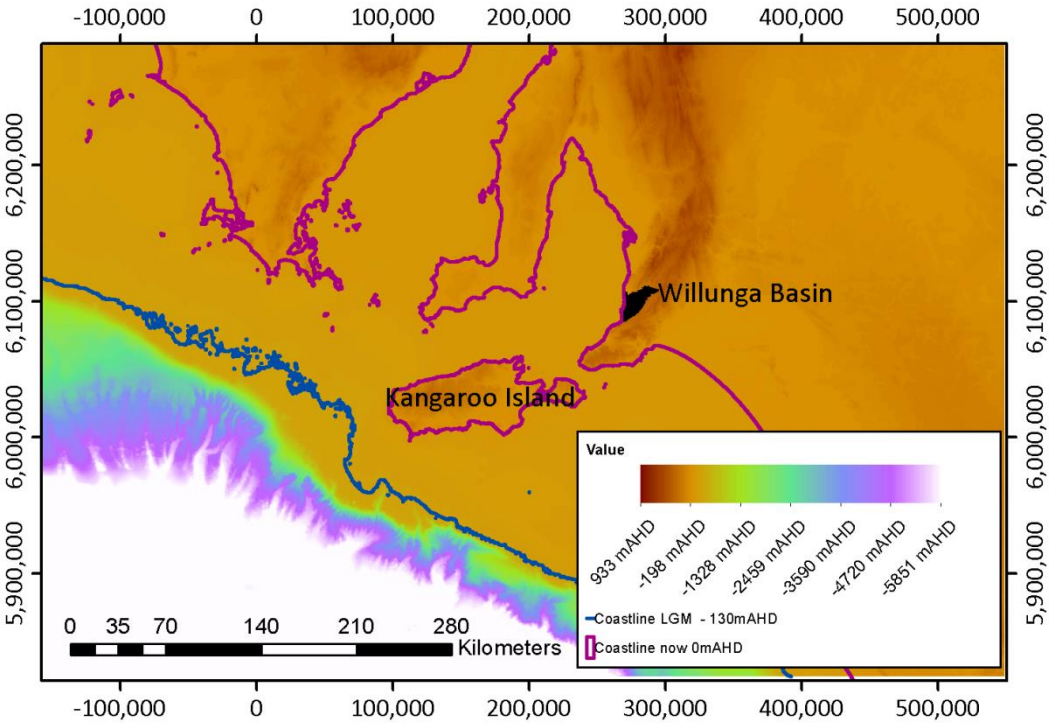

Figure 2.7: Bathymetry of South Australian Coastline. The current coastline at 0 mAHD and presumed coastline in the last glacial maxima (-130mAHD) are shown.

2.6 Conceptual Model

Figure 2.8 shows a conceptualisation of groundwater flow in the Willunga Basin. The majority of recharge to the aquifers is assumed to occur via precipitation infiltration where the aquifers outcrop at the ground surface. Both infiltration and groundwater discharge occur along Pedlar, Kangarilla and Willunga Creek (see Figure 2.1) but the quantities are difficult to characterise because this is dependent on both time varying groundwater levels and creek levels.

Recharge estimates for the Willunga Basin have only been made using chloride mass balance or inverse modelling methods, both of which provide an estimate of the diffuse recharge.

Some groundwater inflow to the basin is assumed to occur from the fractured rock basement and in particular flow across the Willunga Fault which forms the southern and eastern boundary of the basin sediments. The overall contribution from the fractured rock is thought to be smaller than that of diffuse recharge.

Groundwater discharge occurs to creeks, through submarine discharge, and groundwater extraction for irrigation and domestic supplies. Submarine discharge has been measured to occur at specific seep locations rather than diffuse recharge along the whole coastline. Volumes of submarine discharge have not been estimated (Short 2011, Short, Lamontagne et al. 2014).

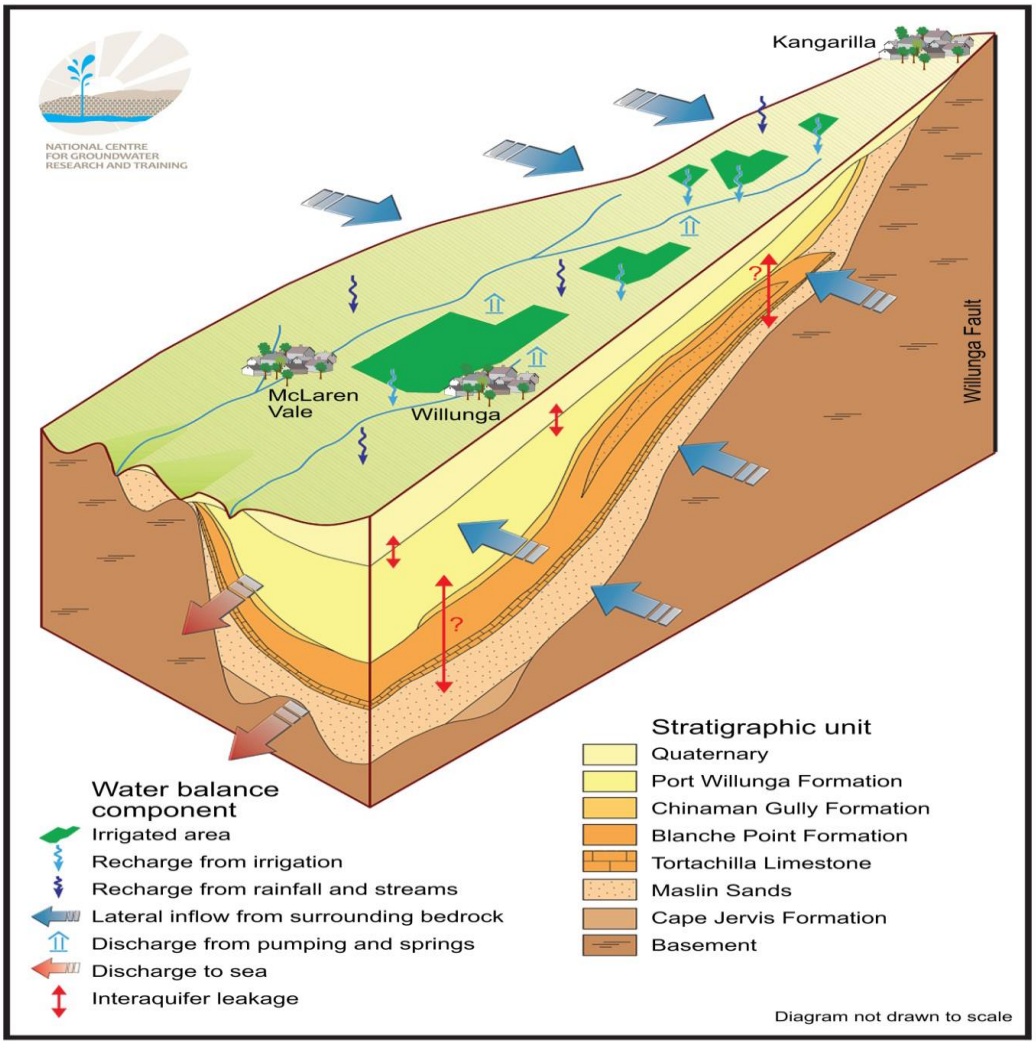

Figure 2.8: Conceptual model of the Willunga Basin

2.7 Recharge & Discharge

The main sources of recharge to the aquifers are diffuse flow from rainfall, infiltration from ephemeral streams, and flow across the Willunga fault from the fractured rock aquifer. Discharge occurs through pumping for irrigation, to the coast (submarine discharge), and to springs and ephemeral streams.

2.7.1 Flow across the fault

Martin (1998) considered the southern margin of the Willunga Fault to be closed and to act as a barrier to lateral inflow from the basement rocks. Martin (1998) estimates that a 2km distance near Kangarilla, the northern section of the Willunga Fault contributes to lateral inflow based on hydraulic gradients. Using the measured gradient across the fault and an assumed hydraulic conductivity based on pump tests annual flow volumes across the fault are estimated at 440 ML/yr to the Port Willunga Formation and 100 ML/yr to the Maslin Sands. The values used for the parameters are not defined in report. These volumes are about a tenth of the volume estimated by Herczeg and Leaney (2002) for recharge from rainfall.

2.7.2 Surface water

Twenty three surface water features (creeks) originate at the high point of the Willunga Basin above the Willunga Fault in the bedrock, and converge to discharge at three points on the coast, Pedlar, Kangarilla and Willunga Creeks (Figure 2.1). Brown (2004) estimated the surface water discharge to the ocean outflow from a survey in Sept 2003 to be 21.6 ML/d, with 40% of the flow originating in Kangarilla Creek. A second survey on March 2004 estimated total surface water flow to the coast to be 1.55 ML/d with Kangarilla Creek not flowing at the time of this survey. The ephemeral streams that discharge to the coast are both gaining and losing groundwater along their lengths, depending on rainfall and groundwater levels.

Harrington (2002) concluded in a study of Pedlar Creek that the creek was receiving groundwater more often than it discharges except in large weather events. Whether the stream is losing or gaining at any location also changes through time, dependent on groundwater levels and creek levels (Harrington 2002, Brown 2004). Batlle-Aguilar and Cook (2012) also demonstrated that infiltration rates vary over time as river levels change.

The spatial and temporal variability of the connection between surface water and groundwater in the Willunga Basin means that estimations of recharge rates can only be made for short periods of time. The variability means that upscaling these estimates to mean annual recharge would be erroneous.

An estimate of flux from streams to groundwater has not been made in the literature. Herczeg and Leaney (2002) and Martin (1998) used chloride mass balance methods to account for all recharge to the aquifers.

2.7.3 Diffuse recharge

Current recharge estimates in the literature range from 20 mm/yr to 34 mm/yr, based on chloride mass balance. Chloride mass balance is a simple tracer mass balance for a steady state system assumed to account for evaporation, recharge and surface runoff, and measures recharge over the long term (Allison, Cook et al. 1990). See Section 3.2.1 Chloride Mass Balance.

Herczeg and Leaney (2002) using a chloride mass balance approach to estimate recharge rates between 16 – 30 mm/yr (median of 22 mm/yr) in the Port Willunga Formation and Maslin Sands aquifers, equating to an annual volume of 1120 – 2240 ML/yr. Martin (1998) used a chloride mass balance to estimate annual recharge volumes of 1050 ML/yr to the Port Willunga Formation and 900 ML/yr to the Maslin Sands. These equate to recharge rates of 20 and 24 mm/yr respectively. Aldam (1990) used a chloride mass balance on three groundwater bores to estimate recharge rates of 21 to 34 mm/yr.

2.8 Groundwater extraction

Groundwater extraction from the basin for irrigation of crops was noticeably increased in the 1970- 80's due to a boom in economic activity and grape production (Denham, Lentfer et al. 2012). The current annual allowable allocation of groundwater extraction in the McLaren Vale Prescribed Wells Area (PWA) is 6,000 ML. Extraction from the aquifers peaked in 1994/95 with 9,000 ML recorded (Figure 2.9). An extraction limit of 6,000 ML/yr was implemented in 2000, and extraction has been below this value and declining since. Most of this extraction is from the Port Willunga Formation Aquifer (65%), with 18% taken from the Maslin Sands and 17% from the Fractured Rock Aquifer.

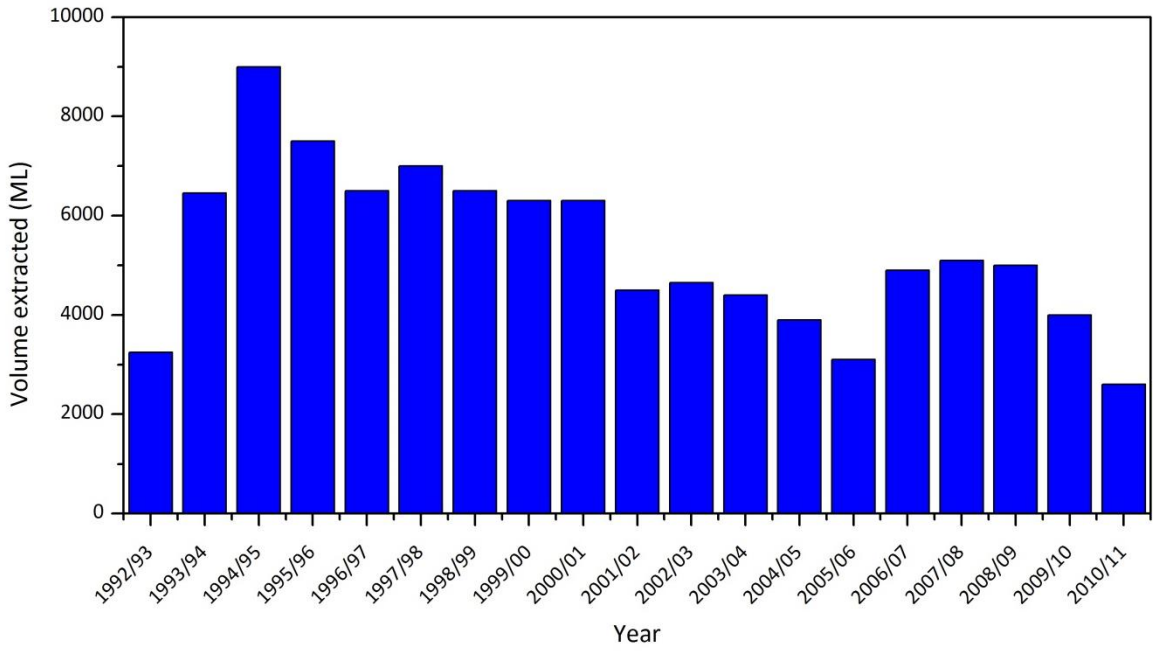

Figure 2.9: Extraction rates by aquifer in the Willunga Basin. Data sourced from 2000 and 2007 Water Allocation Plans, www.waterconnect.sa.gov.au

2.9 Submarine discharge

Short, Lamontagne et al. (2014) used Radon and EC in a series of coastal surveys to determine that submarine discharges from the aquifers of the Willunga Basin occur at specific seep sites, and not along the whole length of the coast as previously thought. They found that discharges occur

where the head of the aquifers is above sea level and the confined aquifers outcrop at the surface. Seeps were identified at the southern end of Maslin Sands beach, at the southern end of Port Willunga and the Ruawarang Springs at the southern junction of the quaternary sediments and the Willunga Fault. An estimate of discharge rate was not made.

Chapter 3 Time varying recharge in a coastal groundwater system estimated using geochemical methods and a numerical model

3.1 Introduction

Recharge, the amount of water that reaches the aquifer, is a critical component of the water balance that is difficult to quantify. Recharge can be dependent on climate, rainfall, soil and vegetation characteristics, all of which change over time. Resource management relies on balancing the recharge, storage, consumption and discharge from aquifers to estimate a sustainable yield which aims to protect use of the resource over the long term (Cook and Herczeg 2000, Mazor 2004). Direct methods to estimate recharge include seepage measurements, and indirect methods include stream flow separation methods, and water table fluctuations (Healy and Cook 2002, Seiler and Gat 2007, Batlle-Aguilar and Cook 2012). However these methods only measure recharge over short periods of time. Recharge will vary over time and a long term value is required for water resource management.

Geochemical methods have been widely used for understanding flow systems and estimating recharge rates (Cook and Herczeg 2000, Fetter 2001, McCallum, Engdahl et al. 2014, Turnadge and Smerdon 2014). These methods provide large scale estimates of recharge over long time scales. Methods of estimating recharge explored in this paper include Chloride Mass Balance (CMB) and age tracers. CMB provides an estimate of recharge based on a mass balance between rainfall and aquifer chloride concentrations, and age tracers are used to constrain the travel time of groundwater in a system, as a measure of average velocity.

Using age tracers to calculate groundwater velocity requires an appropriate tracer to measure the travel time of the system. For aquifers with short travel times of up to 50 years, CFC's, SF_6 and tritium are commonly used (Reilly, Plummer et al. 1994, Cook and Solomon 1997). Carbon-14 is useful in regional systems with travel times up to 50,000 years (Kloppmann, Dever et al. 1998, Sanford, Plummer et al. 2004), and helium-4 and chloride-36 have been used in aquifer systems with travel times greater than 50 kyrs (Solomon 2000, Mahara, Habermehl et al. 2009). Methods for calculating groundwater velocity from apparent age estimates include analytical solutions which calculate advective age based on the position of the sample and aquifer dimensions, and more complex methods utilising numerical models (Vogel 1967, Cook and Herczeg 2000, Appelo and Postma 2005).

Age tracers can be used as calibration targets in numerical models to estimate recharge (Cook and Herczeg 2000, Hill and Tiedeman 2007, Seiler and Gat 2007). When groundwater models are calibrated to hydraulic head data, estimates of groundwater recharge are highly sensitive to values of hydraulic conductivity that are usually not well known. Using an additional target of an age tracer should better constrain the estimate of recharge (Sanford 2011, Turnadge and Smerdon 2014).

Groundwater age can be simulated in numerical models using either particle tracking or solute transport simulations. Particle tracking models calculate the advective age, whereas solute transport modelling can account for processes such as diffusion/dispersion and mixing (Castro and Goblet 2005, Bethke and Johnson 2008, Ginn, Haeri et al. 2009, Mahara, Habermehl et al. 2009, Massoudieh and Ginn 2011, Sanford 2011, Zuber, Rozanski et al. 2011, Engdahl, Ginn et al. 2013, McCallum, Cook et al. 2013, Turnadge and Smerdon 2014).

The use of age tracers to estimate recharge by model calibration can be influenced by changing hydraulic conditions, several of which are investigated in this paper. Firstly, changing aquifer hydraulic gradients from sea level change are presumed to impact on age tracer distributions in the aquifer by changing average velocities. Secondly, using both age tracers and heads as joint model

calibration targets could be a problem because they are not measuring recharge over the same timescale. In the past, dual calibrations have usually assumed steady state hydraulic conditions (Reilly, Plummer et al. 1994, Sanford, Plummer et al. 2004, Sanford 2011). To determine if changing hydraulic conditions influence age tracer distributions and derived recharge estimates, transient models are required.

In this paper, geochemical methods and numerical modelling are used to estimate groundwater recharge to a coastal aquifer system in south eastern Australia. Groundwater in this aquifer system is up to 35,000 years old (Herczeg and Leaney 2002) and two important hydrological changes have occurred over this timescale. The first is the sea level decline during the last glacial maxima, which should have influenced aquifer conditions and hydraulic gradients over the same timeframe as tracers such as carbon-14. The last major decline in sea level globally occurred 20,000 years before present (Cann, Belperio et al. 1988, Drexel and Preiss 1995); sea levels have only been at their current levels during the last 7000 years. The second major hydrological change resulted from land clearing following European settlement in Australia, which has increased recharge rates within the last 200 years (Allison, Cook et al. 1990). In the Willunga Basin land was cleared approximately 150 years ago (Allison, Cook et al. 1990, Denham, Lentfer et al. 2012).

Large scale irrigation also will have changed aquifer hydraulics, however the influence of irrigation in this system has occurred since the 1970s, with large scale extraction commencing in the 1980s, peaking in the 1990s and declining since this time (Denham, Lentfer et al. 2012). The longevity of this impact of only 30 years is much shorter in comparison to land clearing and sea level change.

We installed a series of new bores along the length of the basin to measured heads, carbon-14, helium-4 and chloride in several depths of each of the main aquifers. The spatial distribution of heads, carbon-14, helium-4 and chloride in groundwater is used to make inference on groundwater flow and spatial variability of recharge. The influence of sea level change from the last glacial

maxima on groundwater ages was tested by comparing head and carbon-14 predictions from numerical models with differing coastal boundary conditions. An estimate of recharge to the aquifers is made using both chloride mass balance, and groundwater age. Time varying recharge estimates for pre and post-land clearing are tested using calibration of a regional groundwater flow and solute transport model with heads alone, and heads and carbon-14.

3.2 Background

3.2.1 Chloride Mass Balance

Chloride mass balance is a common method for determining long term recharge (Allison and Hughes 1978). Chloride is a useful tracer of groundwater movement because of its conservative nature, and high solubility. It is not involved in most of the common geochemical reactions that occur in aquifers, except in high temperature minerals (Herczeg and Edmunds 2000). When rainfall reaches the soil zone and is evaporated chloride remains behind in the soil water in increased concentrations. A simple mass balance can be used for a steady state system that balances evaporation, recharge and surface runoff:

$$P[Cl]_p = R[Cl]_{gw} + Q[Cl]_{riv} \quad (1)$$

where P is precipitation (vol), R is recharge (vol), Q is discharge to streams/surface runoff (vol), $[Cl]_{gw,}$ $[Cl]_{riv}$, and $[Cl]_p$ are the mean chloride concentrations of groundwater, runoff and precipitation (mass/volume).

Assuming that runoff is small, the equation to calculate recharge becomes

$$R = \frac{(P)(Cl_p)}{Cl_{gw}} \quad (2)$$

3.2.2 Carbon-14

Carbon- 14 (^{14}C) with a half-life of 5730 years is a widely used tracer for groundwater dating in the 1,000 to 50,000 years range (Cook and Herczeg 2000, Kalin 2000, Mazor 2004). Carbon-14 is

produced in the atmosphere when nitrogen interacts with cosmic rays producing thermal neutrons that react with nitrogen to form carbon-14. The carbon-14 is oxidised to CO_2 and mixes into the lower atmosphere. Atmospheric CO_2 dissolves in rain and infiltrates the ground (Clark and Fritz 1997, Cook and Herczeg 2000, Kalin 2000). Carbon-14 of Dissolved Inorganic Carbon (DIC) can be measured using a mass spectrometer (Kalin 2000).

The radiocarbon age (t) of groundwater is calculated by

$$A = A_0 e^{-\lambda t} \tag{3}$$

where λ is the decay constant ($1.209 \times 10^{-4} yr^{-1}$), A_0 is initial activity of carbon-14, and A is the measured carbon-14 activity. λ is related to the half-life $T_{1/2}$ by

$$T_{1/2} = \frac{\ln 2}{\lambda} \tag{4}$$

Equation 3 assumes that carbon-14 behaves conservatively within groundwater and is only lost by radioactive decay, however carbon-14 is a reactive tracer so a correction scheme may be required to account for these reactions. Carbon-14 activity in the atmosphere is not constant, and post 1950 has increased from thermonuclear testing, hence groundwater carbon-14 activities are often greater than 100 pmC if recharged in the last 70 years. Thus the initial activity (A_0) varies over time.

Carbon-14 activities can be diluted once the water enters the subsurface through carbonate dissolution and breakdown of organic material in soil, making groundwater samples appear older. Numerous correction schemes have been developed that modify A_0 to account for geochemical reactions such as calcite dissolution, dolomite dissolution and oxidation of organics (Pearson 1965, Tamers 1975, Fontes and Garnier 1979, Maloszewski and Zuber 1991, Clark and Fritz 1999).

The carbon-13 composition of dissolved inorganic carbon in groundwater is influenced by carbonate dissolution and precipitation, plant respiration and oxidation of organic matter. Carbon-

13 can indicate the dominant processes that may have affected the carbon-14 to carbon-12 ratio of groundwater that can influence age calculations.

3.2.3 Helium-4

Helium-4 is produced in the earth by decay of Uranium 238, Uranium 235 and Thorium 232 (Solomon 2000). This radioactive decay was originally thought to be a useful tool for the dating of rocks, but it was shown that the helium-4 produced was not retained within the U and Th bearing minerals (Solomon 2000). This meant that helium-4 is accumulated by waters, and can be used as a groundwater tracer. Helium-4 (^{4}He) can be used to calculate water ages in systems from approximately 10,000 years and upwards when the helium-4 concentration exceeds the natural recharge concentration of groundwater. Helium-4 is useful for groundwater flow paths with travel times longer than 50 kyrs where carbon-14 is limited (Reilly, Plummer et al. 1994, Cook and Solomon 1997, Kloppmann, Dever et al. 1998, Solomon 2000, Sanford, Plummer et al. 2004, Mahara, Habermehl et al. 2009).

The quantity of helium-4 in the atmosphere is almost constant, and shown to be 5.239 ± 0.005 ppm to an altitude of 100 km (Solomon 2000). As precipitation infiltrates the soil surface it equilibrates with the soil gas which generally has the same helium-4 concentration as the atmosphere. After infiltration, the water moves through the subsurface and accumulates the radiogenic helium-4 from decay of U and Th. The longer the groundwater residence time, the higher the quantity of helium-4.

If the production and release rate of helium-4 in aquifer solids is at a steady state, then the helium-4 release into groundwater is given by

$$G = \rho\, N_L \left\{ 8\left[{}^{238}U\right]\left(\frac{\lambda_{238}}{M_{238}}\right) + 7\left[{}^{235}U\right]\left(\frac{\lambda_{235}}{M_{235}}\right) + 6\left[{}^{232}Th\right]\left(\frac{\lambda_{232}}{M_{232}}\right)\right\} \quad (5)$$

where G is release rate of helium-4 per unit volume of solids per unit time, ρ is density of solids, N_L is Avogadro's number (6.022×10^{23} atoms mol^{-1}), λ_{238}, λ_{235}, and λ_{232} are the decay constants for ^{238}U, ^{235}U and ^{232}Th, and M represents the molecular weights (Solomon 2000).

3.3 Field Methods

3.3.1 Drilling and piezometer construction

Thirty seven observation piezometers were installed along transect A'-A (Figure 3.1, Figure 3.2 and Photo 3). At each site a primary drill hole was drilled to a target depth, and this informed the construction of all remaining well completions. Between 4 and 7 piezometers were installed at each site to target several depths in each aquifer. Each piezometer was installed with a single drill hole which was 200mm in diameter. Drilling was done by rotary mud with either a pick or roller bit. The drilling was logged by a hydrogeologist and this information was also used to inform and update the geological cross sections from (Cooper and McKenzie 1979).

Wells were constructed with a 100mm diameter PVC casing and uPVC 0.5 mm slotted casing or wirewound stainless steel 304 grade screen in high salinity wells. Screens were a maximum of 3 m in length. Gravel pack was nominal 7 mm rounded quartz gravel blended with 8/16 sand. The gravel pack extended 1 m above screens, and above this the annulus was grouted to surface. All wells were developed for a minimum of three hours through a 2 inch drill stem. All wells were surveyed to allow for accurate measurement of head. The locations of the drill sites are shown in Figure 3.1, Table 3.5 contains details of the wells, and Figure 3.2 shows the relative depths of wells in transect A-A'.

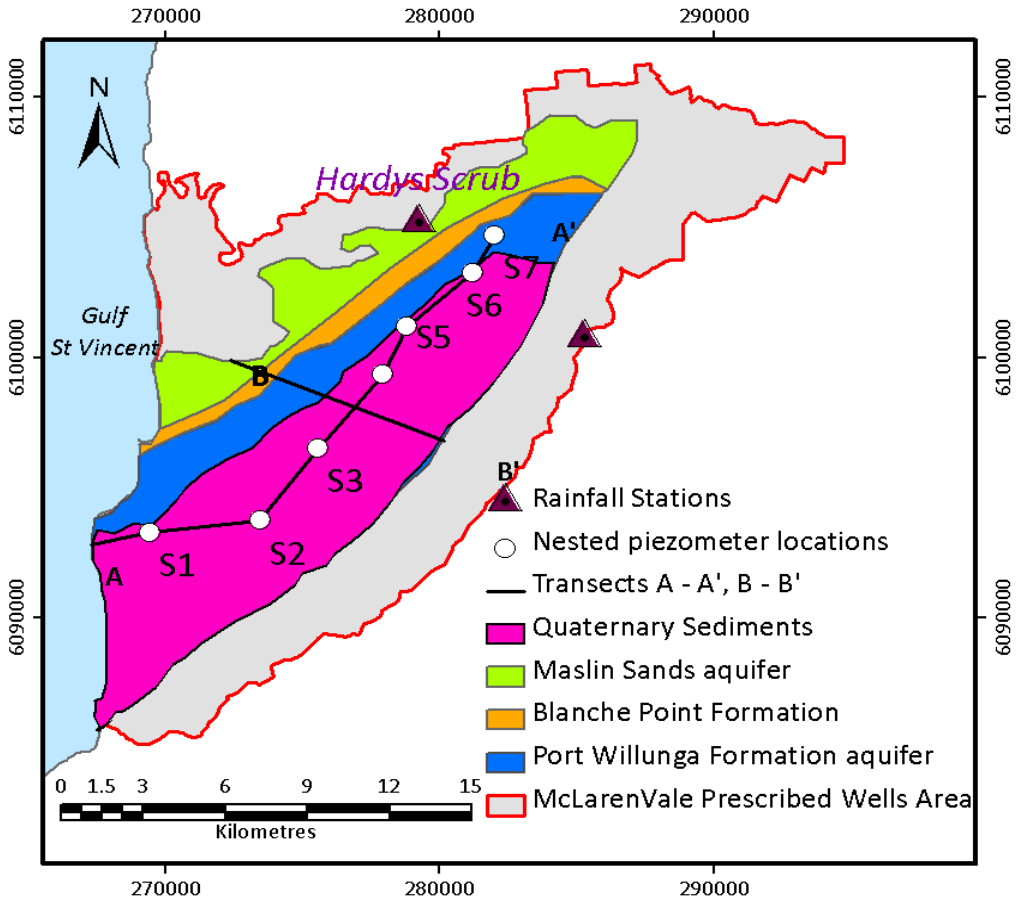

Figure 3.1: Map of Willunga Basin showing the location of the nested piezometers.

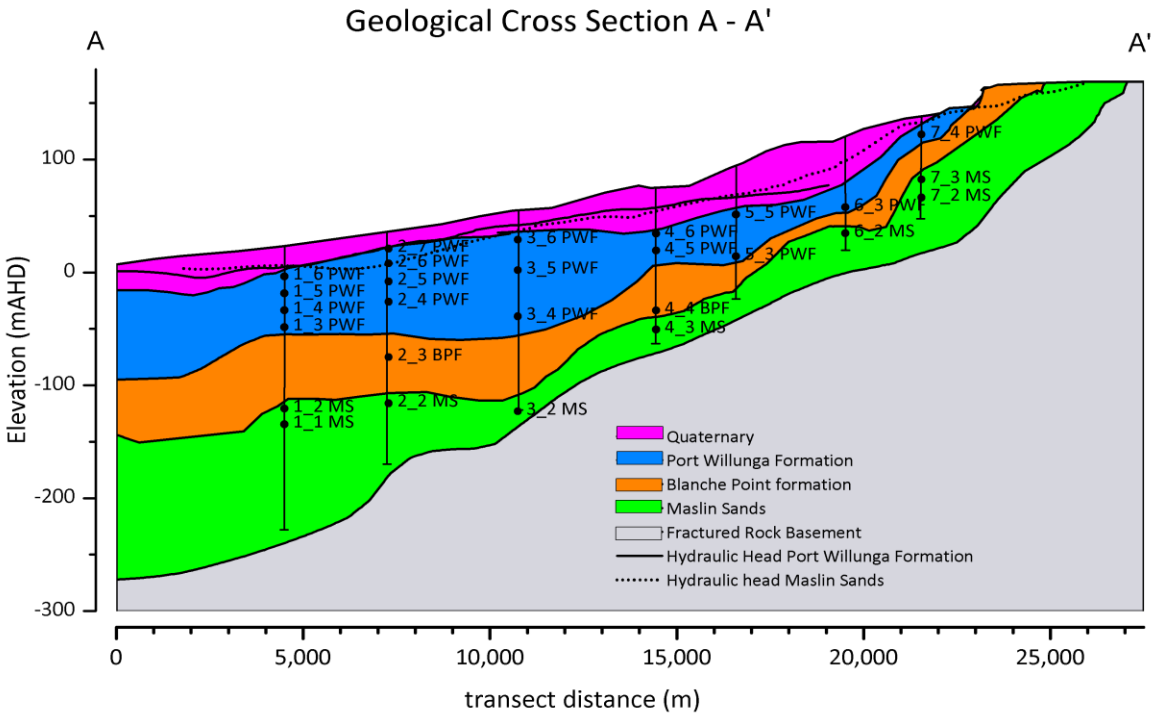

Figure 3.2: Cross section along Transect A-A', showing locations of nested monitoring piezometers and screen depths. The surface location of Transect A-A' is shown in Figure 3.1.

3.3.2 Groundwater sampling and analysis

In addition to the 37 drilled piezometers, 95 groundwater bores were sampled from the State government network for anion and cation analysis (Table 3.6). These bores were selected based on their known construction details and screen lengths of less than 10m.

All wells were purged for a minimum of three casing volumes and only sampled when water quality parameters had stabilised for pH, EC and temperature (Photo 4). pH, EC and temperature were measured continuously using a HACH Multimeter, calibrated weekly for pH and EC. Purging and sampling was undertaken with a GRUNDFOS SQ1 submersible pump.

27 samples for carbon isotope analysis were collected in 500 mL HDPE containers, and analysed by Rafter Radiocarbon Laboratories in New Zealand using Accelerated Mass Spectrometry (AMS).

Samples were treated with phosphoric acid, CO_2 was generated by water CO_2 evolution, and the sample was converted to graphite by reduction with hydrogen over ion catalyst.

15 groundwater samples for noble gas analysis (helium-4) were collected with passive diffusion samplers (Gardner and Solomon 2009) installed at screen depth for a minimum of 7 days, and measured directly using a quadropole mass spectrometer with cryogenic separation (Poole, McNeill et al. 1997) at CSIRO, Land and Water, Adelaide.

Anion and cation samples were collected in 50mL HDPE containers, hydrochloric acid was added to cation sample bottles prior to collecting samples. Cations and anions were analysed by ion chromatography using a Dionex ICS-2500 system at CSIRO Land and Water, Adelaide. Only the chloride analyses are reported in this paper.

3.3.3 Rainfall station construction

Rainfall stations were installed at two elevations in the Willunga Basin at Hardys Scrub, 177 mAHD and Mount Wilson at 408 mAHD (Figure 2.1 and Photo 1). An Adcon rain gauge with a 200 cm^2 opening and 0.1 mm resolution stainless steel double tipping bucket was used to measure rainfall. Water from the gauge was piped to a buried, sealed chamber for sample collection (Photo 2).

3.3.4 Rainfall sampling and analysis

A monthly sample at each rainfall station was collected during 2012. A 2.5L HDPE sample container was installed with a film of parrafin oil to prevent evaporation of the sample. Chloride concentrations were analysed by ion chromatography using a Dionex ICS-2500 system at CSIRO Land and Water, Adelaide. Rainfall quantities at the stations were recorded automatically in hourly intervals and accessed via telemetry (Photo 1 & 2).

3.4 Numerical Modelling methods

A three dimensional groundwater flow and solute transport model was developed to represent the two regional aquifers, the aquitard, and Quaternary sediments of Willunga Basin from the known geology on shore to the offshore extent bounded by Backstairs passage and Investigator Strait, that connect the shallow waters of the Gulf St Vincent to the Southern Ocean (Figure 3.1, Figure 3.2 and Figure 3.3). Flow across the fault and from the underlying fractured rock basement are not included in the model. The contribution of flow across the fault is assumed to occur primarily at the northern end of the basin and is believed to be small (Martin 1998).

Creek recharge is thought to be small and occurs throughout the basin. The process of recharge from creeks has not been specifically included, but it is assumed to be included in the diffuse recharge.

Recharge was applied uniformly to the top layer on shore (Figure 3.4), with the exception of the outcropping area of the aquitard. The lateral boundaries and lower boundary are all no-flow. A constant head boundary condition was applied to the Layer 1. For the constant sea level model a boundary condition of 0m was applied at the current coast. For the transient sea level model, constant head boundary conditions were applied for the relevant periods of time and locations as shown in Figure 3.1Figure 3.3, Figure 3.4 and Table 3.1.

The model was designed to simulate conditions before widespread pumping. Pumping for irrigation is therefore not included in the model. Early head data was used as a calibration target, and it is assumed that chemistry has not changed. The model was used to examine how sea level change influences heads and carbon-14 distributions by comparing models with constant coastal boundary conditions (CSL) and a transient sea level change boundary condition (ΔSL). Second, the constant coastal condition model was used to test if calibrations to carbon-14 are able to better estimate post-clearing recharge than using heads alone as a calibration target. This was done with a

series of calibrations using single and dual target calibrations to predict recharge both prior to and post land clearing. Calibrations were performed using PEST (Doherty 2010).

3.4.1 Model construction

Constant sea level and transient sea level approach

In the first component of this study, both a constant sea level model and transient sea level model of groundwater flow and solute transport were constructed. The constant sea level model has a constant head boundary condition at the current sea level of 0 mAHD. In the transient sea level model the sea level changes over 30,000 years to replicate the sea level change that occurred during the last glacial maxima. Both models are identical in all other respects, and are transient in respect to recharge, with two recharge rates being applied. A pre-land clearing recharge is applied for 29,850 years of both models, and a second recharge rate is applied for 150 years to represent post-land clearing recharge rates. These models are compared to determine if sea level change has a significant impact on the head and carbon-14 distribution results. An initial calibration of the constant sea level model was used to produced initial head and carbon-14 activities distributions to use in all model calibrations.

The second modelling component in this study used the constant sea level model (0 mAHD) to compare how calibration to heads alone, or dual calibration to both heads and carbon-14 compare. The post-land clearing recharge (last 150 years) was fixed at different values across a large range, and PEST was run allowing each model to fit the parameters of hydraulic conductivity and pre-land clearing recharge to determine if the calibration target of carbon-14 improves predictions of recharge.

The best calibration results for hydraulic conductivity and recharge were then used within the transient sea level change model to analyse how the vertical aquifer hydraulic gradients between aquifers changed over time during the last glacial maxima. Head gradients are required at five drill

sites within the basin where aquitard core samples had been obtained. The head data (as it changed over time) from the transient sea level change model was extracted at the location of the bore screen in both major aquifers. From this head data, the vertical gradient across the aquitard at each drill site was calculated using the measured aquitard thickness at that site. This vertical gradient analysis was then utilised in the aquitard research and modelling presented in Chapter 4.

3.4.1.1 Model and convergence

The model was developed in Groundwater Vistas using MODFLOW Newton Solver (Niswonger, Panday et al. 2011), and coupled with MT3DMS (Zheng and Wang 1999) to simulate the transport and radioactive decay of carbon-14. The Newton solver enables the drying and wetting of nodes without inactivating and activating nodes (Niswonger, Panday et al. 2011).

Modflow NWT automatically calculates time steps for each model until convergence is reached, so this is variable for each model (Niswonger, Panday et al. 2011). The time taken for a model to reach convergence is rapidly improved when the initial heads and carbon-14 activities are closer to those of the final solution. The initial head and carbon-14 activities used in all the calibration runs were taken from the solution of the initial calibrated coastal sea level model.

3.4.1.2 Hydrogeologic Units & discretisation

The model dimensions are based on geological data from Cooper and McKenzie (1979), the drilling data from this project, and data from the South Australian Government Drillhole database. Offshore aquifer dimensions were extrapolated using drilling data for Enchilada, a deep exploratory bore drilled to 1.3 km in depth and 45 km off the coastline. The preserved drilling cuttings from Enchilada drill hole were viewed at the South Australia State Government Core Library, located at Glenside South Australia, to confirm that stratigraphic units were consistent with the onshore drilling findings.

The model grid is 136 rows x 132 columns x 16 layers. Grid discretisation onshore is 200 x 200 m, and increases offshore until the largest grid size is 7500 x 7500 m (Figure 3.3 and Figure 3.4). The total surface area of the active component of the grid is 2,392.2 km^2 and the number of active cells is 94,405.

Layer depth varied across the model domain, each aquifer comprised 5 layers, the aquitard comprised 4 layers, and Quaternary sediments were represented by 2 layers, 16 layers in total. The model was constructed initially with four units to represent Quaternary, Port Willunga Formation, Blanche Point Formation and the Maslin Sands. Fractured rock basement is not simulated. Data used to prepare the top and bottom levels of each of these units were taken from geological drilling data from Cooper and McKenzie (1979) and the drilling program. The topography of the upper unit (Quaternary and outcropping areas) was established using the current surface raster from the South Australian Government, converted using ARC GIS. The grids for the top of the initial four groundwater units were created in Groundwater Vistas using data by importing text files for x, y and z co-ordinates. The data for text files were generated by using X and Y as the easting and northing coordinates of each drill location and z the depth in mAHD of the top of the formation.

Once the initial four units were constructed to the interpreted geological elevations the layer split function was used to split the upper unit into two layers (Quaternary and outcropping), the second and fourth units (Port Willunga Formation and Maslin Sands aquifers) into 5 layers each and the third unit (Blanche Point formation) into four layers.

The large grid size offshore was considered suitable given that there are no target data available in this section of the model, but it still allowed for sea level change to be simulated. The density difference between sea water and fresh water was not included in the model because the nearest onshore calibration target to the coast was 4.5 km and all calibration wells have a low salinity.

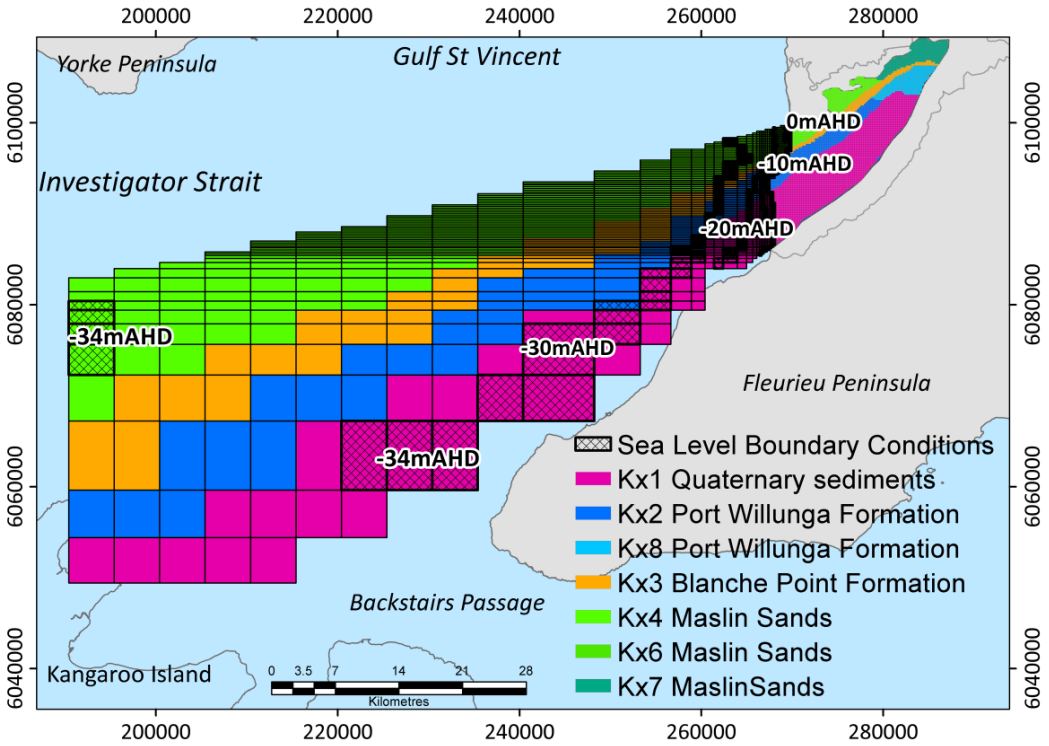

Figure 3.3: Layer 1, showing outcropping hydraulic conductivity zones. Sea level boundary conditions are applied to nodes in Layer 1.

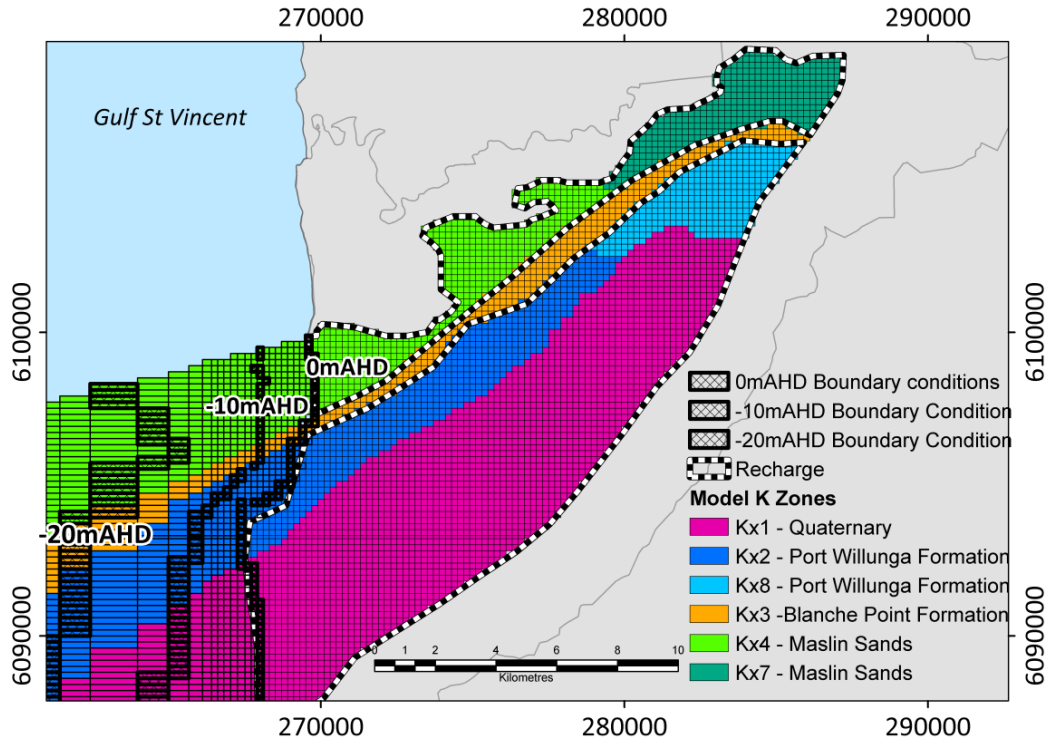

Figure 3.4: On-shore grid domain, layer 1 Model hydraulic conductivity zones. Sea level boundary conditions are applied to nodes in Layer 1

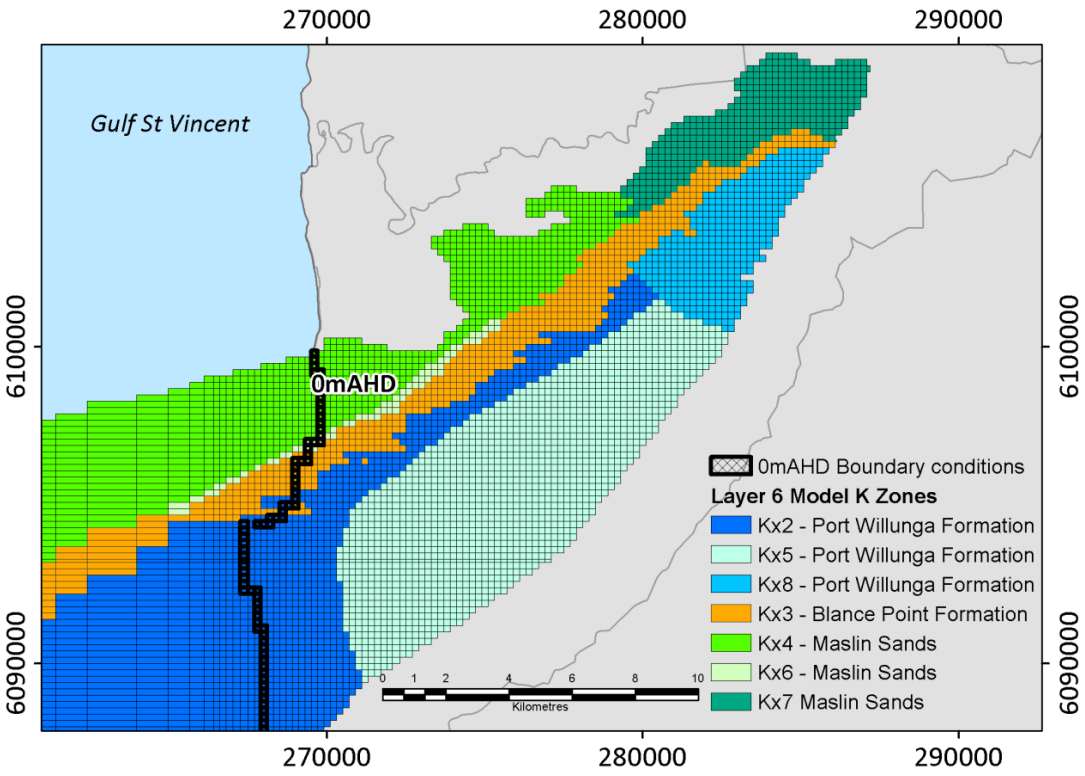

Figure 3.5: Layer 6 Model hydraulic conductivity zones

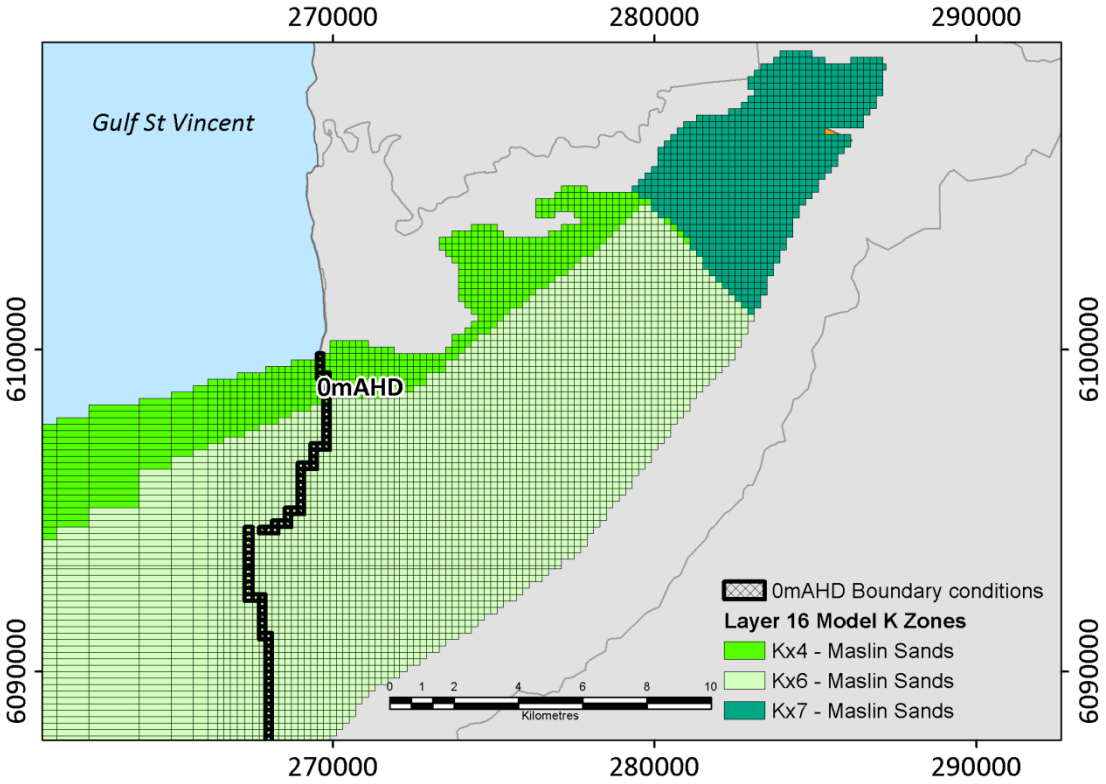

Figure 3.6: Layer 16 Model hydraulic conductivity zones

The model domain has a specific storage of 0.0001, specific yield of 0.1, and porosity of 0.3. These values were taken from the model developed by Martin (2006) and used for the water allocation plan by the government authority to determine sustainable yields.

The porosity measurements on the aquitard described in Chapter 4 were not generated until after the modelling was underway. The range of porosity was 0.3 to 0.5, with a mean of 0.4.

The effective diffusion coefficient of carbon-14 was set at 0.0603 m^2/yr, the effective diffusion coefficient of CO_2 in water (Jahne, Heinz et al. 1987) . Layer properties were set to unconfined for Layer 1, and for layers 2 to 16 convertible, using the upstream weighted package in Modflow NWT. Using convertible properties in the layers enable the model to determine if the node is confined or unconfined based on the properties of the units.

3.4.1.3 Hydraulic Conductivity

The model grid consists of 8 hydraulic conductivity zones. The upper aquifer (Port Willunga Formation) was divided into three K zones (Figure 3.4 and Figure 3.5).

The lower aquifer (Maslin Sands) is represented by three hydraulic conductivity zones (Figure 3.6). Two zones are used to represent the horizontal distribution of the North Maslin Sand and South Maslin Sand geological units, as defined by Cooper and McKenzie (1979). A further zone was used to represent the recharge area to the north east, where a steep head gradient in both aquifers is present. The aquitard is a single hydraulic conductivity zone, as are the Quaternary sediments.

Initial hydraulic conductivity values are shown in Table 3.2, and PEST was used to calculate final hydraulic conductivity values.

3.4.1.4 Recharge

The model was run for a period of 30,000 years, with time varying recharge zones. Recharge 1 represented pre-land clearing recharge (29,850 years), and Recharge 2 was applied for the final 150 years and represents post-clearing recharge. The recharge rates were determined during model calibration. Recharge is applied to the Quaternary and outcropping areas of the Port Willunga Formation and the Maslin Sands aquifers. The carbon-14 activity of all active recharge was set at 100 pmC.

Recharge was not varied spatially in the model, because there is insufficient information to determine such variations.

3.4.1.5 Coastal Boundary conditions (constant sea level and transient sea level change)

To test how sea level influenced carbon-14 distributions in the aquifers two different models with differing coastal head boundaries were constructed.

In the first model the constant sea level boundary (CSL) was applied as a constant head at 0 mAHD in Layer 1 for 30,000 years (Figure 3.3). In the transient sea level change model (ΔSL)

constant head boundaries were applied at different locations for each stress period to 'offshore' cells in Layer 1, where the current bathymetry/surface elevation corresponds with the depth of the sea level (Figure 3.3). The sea level low stand of -34 mAHD in Stress Period 2 is used to represent the predicted sea level of -130 mAHD , the last glacial maxima (Cann, Belperio et al. 1988). The sea floor has a depth of -34 mAHD where the boundary condition is applied, this is where the basement outcrops at Backstairs Passage and Investigator Strait.

The run time of the transient sea level change model was up to 3 days. To calibrate this model with PEST where the model runs up to 150 times before finding a preferred solution was therefore not possible. Instead, the results of the transient sea level change model were compared with the constant sea level change model by using the parameters from the calibrated coastal sea level change model.

Table 3.1: Stress periods and recharge times for the sea level change model (ΔSL). Modflow NWT calculates time steps until convergence is reached.

Stress Period	Time (years BP)	Sea Level (mAHD)
1	30,000 – 20,000	0
2	20,000 – 11,750	-34
3	11,750 – 10,500	-30
4	10,00 – 9,250	-20
5	9250 – 8,000	-10
6	8,000 - 150	0
7	150 - 0	0

3.4.2 Calibration method

Constant sea level model: calibration approach

Two series of calibrations on the coastal sea level model were conducted using PEST. The first calibrations were to a single target of head (Øh), and the second to a dual target of heads and carbon-14 (Øh+ØC). The post-land clearing recharge (last 150 years) was fixed at different values between 15 and 140 mm/yr, and PEST was run allowing each model to fit the parameters of

hydraulic conductivity for all aquifers and aquitard, and pre-land clearing recharge. By examining model fits to head and carbon-14 for different post clearing recharge rates we could determine if the additional calibration target of carbon-14 improved predictions of post-clearing recharge. Parameter ranges and initial parameter values were set equal to those given in Table 3.2.

Calibration was carried out using PEST (Doherty 2010) in Groundwater Vistas using BeoPEST to reduce run times. BeoPEST is software that allows the PEST procedure for optimisation to be run in parallel across more than one computer. All PEST simulations were carried out with constant sea level boundary conditions at 0 mAHD, the present position of the coastline.

Calibration programs such as PEST use inverse modelling to calculate parameter values to minimise a weighted least squares objective function, using linear regression (Hill and Tiedeman 2007). PEST uses a least squares fitting routine and a Guass Marquardt Levenberg method to minimise a user defined objective function

$$\emptyset_k = \sum_{k=1}^{N_{obs}} \left(w_k x_m^k - w_k x_x^k\right)^2$$

where Ø is the objective function value, w_k is the weight applied to the difference between the measured value (x_m^k) and simulated parameter (x_x^k) of the same type k, and N_{obs} is the total number of measured parameter values of the same type (Doherty 2010). PEST software uses the model and runs it as many times as is necessary to determine the optimal set of parameters to meet the desired targets. The parameters to be estimated by PEST are given initial values, upper and lower boundaries, and any other defining information such as tying parameters together so that increases or decreases can be scaled.

Table 3.2: Initial PEST parameter values and allowable range. In all cases vertical hydraulic conductivity (Kv) is a tenth of horizontal vertical conductivity (Kx).

Parameter	Aquifer Unit	Kx Initial Value	Kx Minimum value	Kx Maximum value
		m/yr	m/yr	m/yr
Kx1	Quaternary	500	0.0001	3650
Kx2	PWF – northern (outcrop)	500	0.0001	3650
Kx3	BPF – aquitard	$1x10^{-7}$	$1x10^{-10}$	$1x10^{-4}$
Kx4	MS – northern (outcrop)	160	0.0001	3650
Kx5	PWF – central/southern	500	0.0001	3650
Kx6	MS – southern	400	0.0001	3650
Kx7	MS – upgradient	55	0.0001	3650
Kx8	PWF – upgradient	50	0.0001	3650
R1	Pre-land clearing recharge	0.021	$1x10^{-8}$	0.5

The range of allowable hydraulic conductivity values in calibration were constrained by the range of values from the current literature (Table 3.2).

3.4.2.1 Calibration targets

120 head targets from the State Government monitoring data network were used for calibration, 66 in the Port Willunga Formation and 54 in the Maslin Sands; targets were given a weighting of 1. Head targets were calculated from the average head data over 5 years using a time period prior to major groundwater development in the region (from 1960 to 1985). Recent head data from transect bores were also used as this provided direct information on vertical head gradients. Early head targets were chosen because the model does not simulate groundwater extraction in the region.

Twenty five carbon-14 activity targets were used from the transect piezometers described in 3.3.1 Drilling and piezometer construction, and again all targets were given a weighting of 1. Carbon-14 target data was collected over a period of two years from 2011 and likely reflects long-

term recharge/hydraulic conditions. Target descriptions are provided in Table 3.5 and Table 3.7 at the end of this Chapter.

3.5 Results

3.5.1 Chloride mass balance

Chloride mass balance recharge estimates were calculated using 2012 data from both rainfall stations (Table 3.4). The mean weighted rainfall Cl^- concentration for Mount Wilson (23 km from the coast, 408 mAHD) was 8.5 mg/L, and measured annual precipitation was 516.7 mm/yr. The mean weighted rainfall Cl^- concentration for Hardy's Scrub (12.5km from the coast, 177 mAHD) was 13.1 mg/L, and the total precipitation recorded was 624.3 mm/yr.

The groundwater data in Figure 3.7 show a general trend of increasing Cl- concentration toward the coast as measured along the assumed flowpath, consistent with increased Cl- fallout recorded in the rainfall station closer to the coast. For example, the mean Cl- in the PWF more than 5 km from the coast is 414 mg/L, between 2 and 5km from the coast is 774 mg/L, and within 2km of the coast is 14,477 mg/L. Very high values within 2km of the coast probably reflect mixing with seawater.

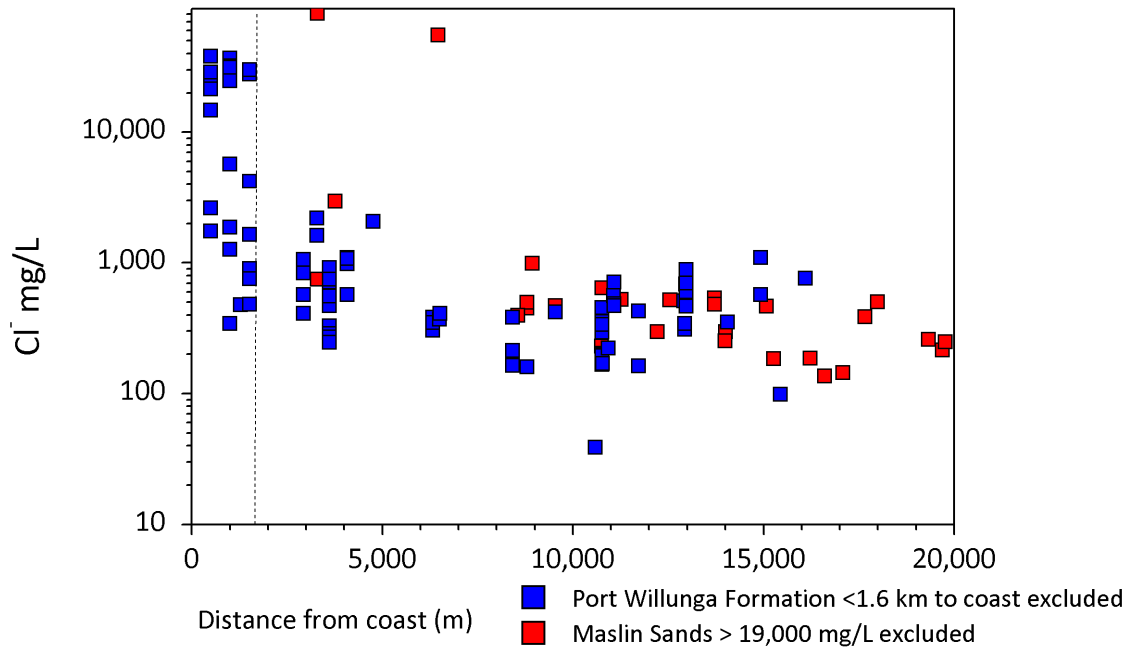

Figure 3.7: Groundwater chloride concentrations by distance from the coast. The vertical dotted line is 1.6 km from the coast, all samples to the left of the line were excluded.

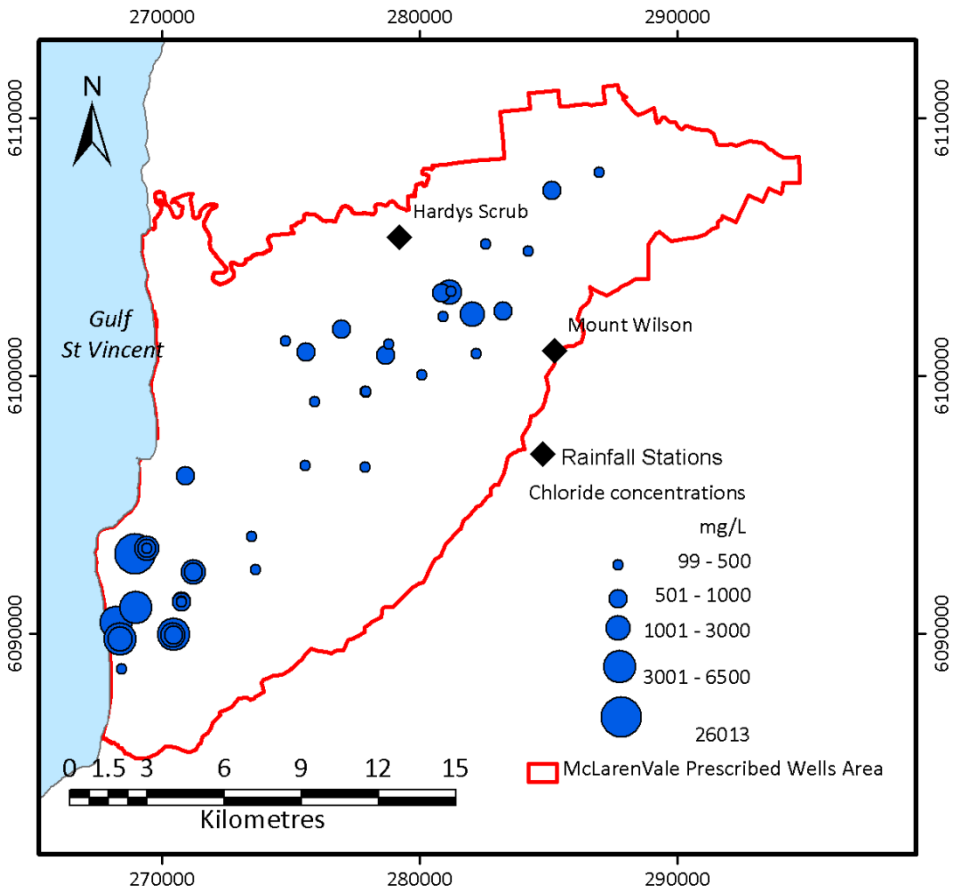

Figure 3.8: Groundwater chloride concentrations plotted spatially. Locations of rainfall stations at Mount Wilson (408mAHD) and Hardy's Scrub (177 mAHD) shown.

In calculating the chloride mass balance, groundwater data with high concentrations was excluded. Samples within 1.6 km of the coast in the Port Willunga Formation were excluded (23 of the 95 total samples taken) due to the possibility that seawater intrusion contributes to higher chloride concentrations in these samples. Two samples were excluded from 30 taken in the Maslin Sands. These two samples exceeded seawater concentrations of chloride, and are assumed to be hypersaline groundwater that have undergone evaporation (Post and Banks in press). From the remaining samples (72 in the Port Willunga Formation, and 28 in the Maslin Sands) the mean Cl^- concentration of the Port Willunga Formation was 536 mg/L, and the Maslin Sands was 501 mg/L.

The average chloride mass balance recharge estimates for Port Willunga Formation are 8 mm/yr using the Mount Wilson rainfall station data, and 15 mm/yr using Hardys Scrub rainfall station. The

chloride mass balance estimate of recharge to the Maslin Sands is 9 mm/yr using Mount Wilson rainfall data, and 16 mm/yr using Hardys Scrub rainfall station.

Alternatively, using the Cl- values of all groundwater samples (including those within 2km of the coast) results in a mean groundwater Cl- of 2675 mg/L for the Maslin Sands, and 3947 mg/L for the Port Willunga Formation, equating to a recharge estimate of 1-2 mm/yr for both aquifers.

The Hardys Scrub rainfall station predicts almost double the recharge of the Mount Wilson rainfall station. Mount Wilson station is located a distance of 5km east of Willunga Basin and at double the altitude. The Hardy's Scrub rainfall station is located within the recharge zone of the Maslin Sands where it outcrops to the surface, the adopted recharge rate for this study as estimated by CMB is 15-16 mm/yr.

3.5.2 Groundwater age

3.5.2.1 Carbon-14 and carbon-13

Carbon-14 activities in the Port Willunga Formation are in the range 86.7 to 37.59 pmC with the exception of a low value close to the coast and adjacent to the aquitard of 5.93 pmC (S1-3) (Figure 3.9 and Figure 3.10). Carbon-14 activities in the Maslin Sands range from 40.20 to 6.23 pmC.

Groundwater samples of the Willunga basin have a $\delta^{13}C$ in the range of -12.88 to -8.31 $^{0}/_{00}$, across the full range of carbon-14 activity from 5.9 to 86.7 pmC (Figure 3.7). Correction schemes aim to estimate the initial carbon-14 activity (A_0) at the time of recharge to account for dilution from oxidation of old organic matter or dissolution of carbonate material, which can make ages appear older.

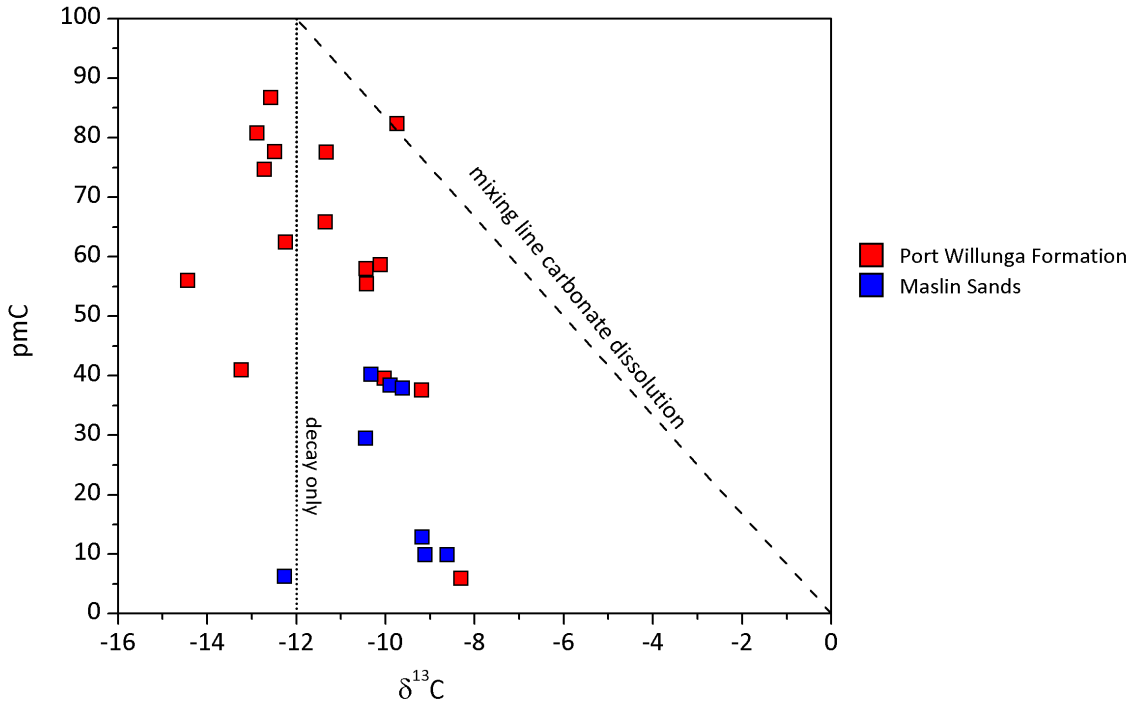

Figure 3.9: Plot of $\delta^{13}C$ vs carbon-14 activity of groundwater samples. Dashed line is a potential groundwater mixing line for carbonate dissolution increasing $\delta^{13}C$ as groundwater age increases, the vertical line is assumes no carbonate dissolution so $\delta^{13}C$ remains constant.

The dashed line in Figure 3.9 shows where samples would be expected to plot if carbonate dissolution and exchange were the only processes affecting carbon-14. Atmospheric CO_2 has a $\delta^{13}C$ ~ -7 $^{0}/_{00}$. As water infiltrates the subsurface this water equilibrates with soil gas CO_2 which is modified through plant respiration. Soil gas CO_2 from plant respiration of C3 vegetation in Willunga Basin is assumed to have $\delta^{13}C$ signature of between – 18 to -22 $^{0}/_{00}$, and the resulting soil gas $\delta^{13}C$ assumed to be ~ -16 $^{0}/_{00.}$ (Clark and Fritz 1999). Carbonate rock is assumed to have $\delta^{13}C$ values close to 0 to -2 $^{0}/_{00}$ (Kalin 2000). Carbonate dissolution could have the effect of making carbon-14 activity of groundwater appear 'older' than the actual time since recharge. $\delta^{13}C$ can vary spatially, and can also vary temporally due to vegetation change. The spatial and temporal variability of A_0 means initial values are difficult to estimate in a regional system.

Correction of A_0 for the observed change in $\delta^{13}C$ in groundwater from carbonate dissolution using the Pearson scheme using an initial $\delta^{13}C$ of -12 $^{0}/_{00}$ resulted in little changes overall to the data. 15 samples were within 5% of the measured pmC, 7 were within 10%, and three were within 15%. We decided not to correct because the correction provided minimal change to the data. A potential impact of not correcting the data is that groundwater ages are overestimated, which in turn predicts a slower velocity and recharge predictions from calibration.

3.5.2.2 Carbon-14 and helium-4

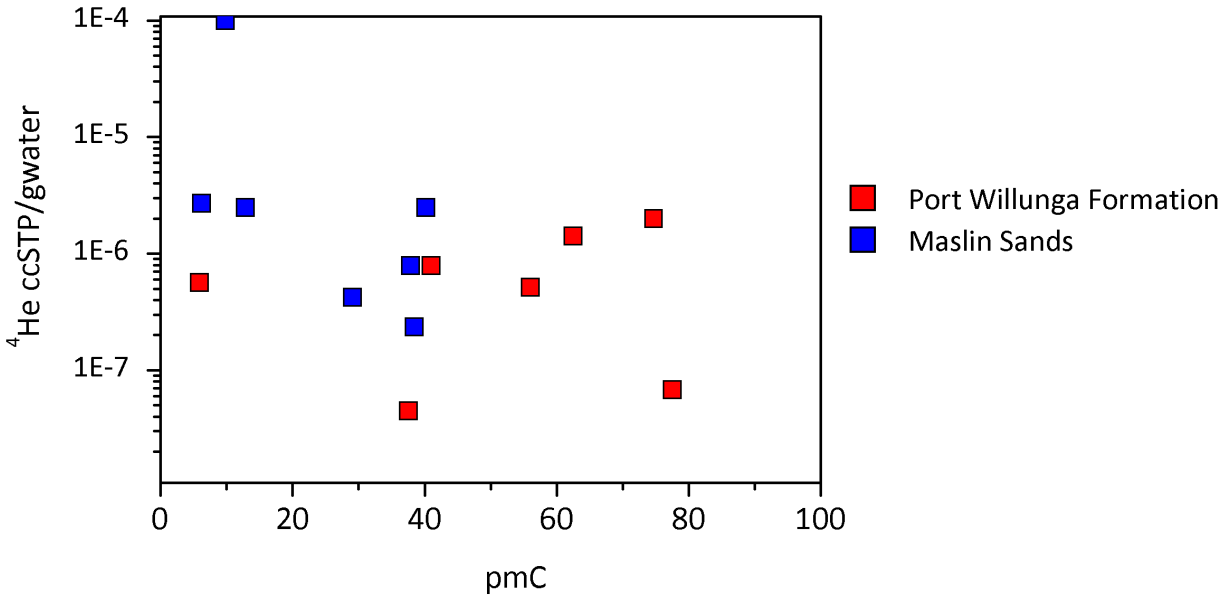

Figure 3.10: Carbon-14 vs helium-4. Port Willunga Formation (red markers) show lower carbon-14 activities and helium-4 concentrations than the Maslin Sands (blue markers), indicating a shorter residence time in this aquifer.

A comparison of carbon-14 and helium-4 data show that groundwater in the Port Willunga Formation has higher carbon-14 activities than the Maslin Sands, consistent with the shorter flow distance. As water ages, helium-4 concentrations should increase as carbon-14 activities decrease. In the Maslin sands helium-4 concentrations increase as carbon-14 activities decrease but this expected relationship is not evident in the Port Willunga Formation (Figure 3.10). It is possible that converging flow paths, or the contribution of helium-4 diffusive flux from the porewaters in the aquitard complicate this comparison by increasing helium-4 values.

Helium-4 concentrations of groundwater in the Port Willunga Formation range from 4.46 x 10^{-8} to 1.98 x 10^{-6} ccSTP/gwater, and in the Maslin sands from 2.34 x 10^{-7} to 9.92 x 10^{-5} ccSTP/gwater (Figure 3.11b). Assuming that recharge has a helium-4 concentration of 4.35 x 10^{-8} ccSTP/gwater, the Port Willunga Formation groundwater has concentrations of helium-4 that are 1 to 45 times greater than recharge, and the Maslin Sands groundwater is 5 to 2000 times greater. Viewing this data spatially (Figure 3.11) can give an indication of how carbon-14 activities and helium-4 concentrations evolve along the predominant direction of flow. Figure 3.11 is constructed using the data from the drilled transect, and is oriented in the general direction of groundwater flow from the north east of the basin to the coast. Whilst this is the predominant flow path, vertical flow is assumed across the aquitard, and also converging flowpaths andlateral flow within the aquifers. Despite the converging flow paths the transect data as presented is useful because it contains discrete vertical solute data within both the aquifers and the aquitard which can inform the conceptual model of the system. This data can provide information on how the vertical and lateral flows are influencing groundwater as it moves along the predominant flow path.

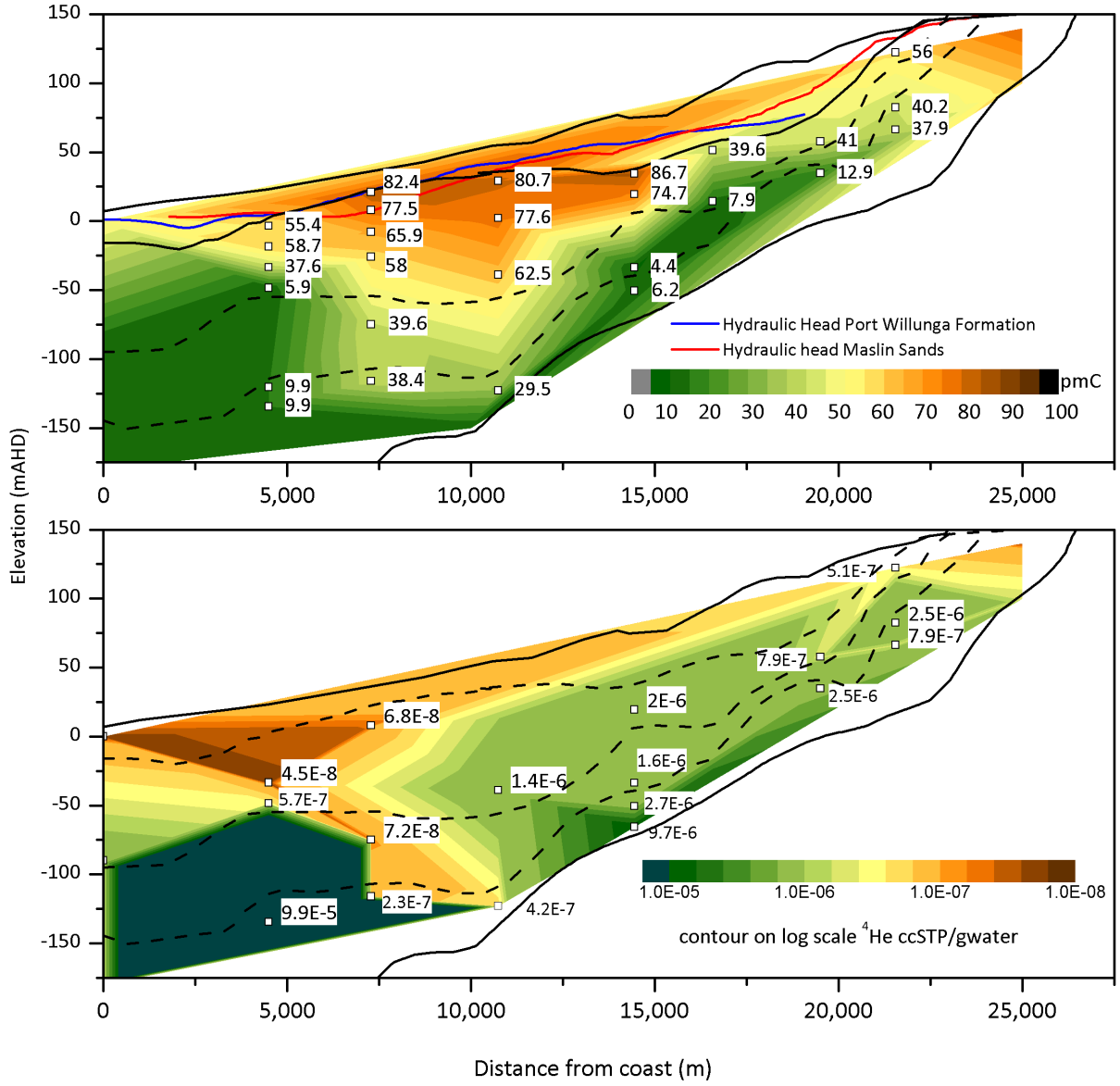

Figure 3.11: a) Transect A–A' groundwater carbon-14 activities. b) Transect A-A' groundwater helium-4 concentrations in log contours. The location of the aquifers and aquitard are delineated by dashed lines. The brown/orange contour indicates water of shorter residence times, and the green contours indicate longer residence times.

The transect shown of the Port Willunga Formation is from 25km to 4km from the coast. Carbon-14 activities decline over the distance from 25 km to 18 km as is expected. This rapid decline in carbon-14 activities also coincides with a steep head gradient. Between 18km to 5 km carbon-14 activities then increase (Figure 3.11). This increase in carbon-14 activity indicates recharge is

occurring through the overlying Quaternary sediments. This area also coincides with the low chloride concentrations in Figure 3.7. In the Maslin Sands aquifer, an increase in carbon-14 activities with depth in the middle of the Maslin Sands aquifer may indicate either leakage through the aquitard from the Port Willunga Formation, converging flowpaths from the northern outcropping region of the aquifer, or flux from the fractured rock aquifer via the Willunga Fault.

Helium-4 in the Port Willunga Formation is low upgradient, and values increase moving shoreward. Helium-4 concentrations then decrease nearest the coast, which may indicate some recharge of younger waters through the Quaternary sediments. At the top of the flowpath helium-4 concentrations in the Maslin Sands are higher than in the Port Willunga Formation. An anomaly in the Maslin Sands is a section of relatively low helium-4 concentration between 7,500 and 12,000 m, potentially a flux of younger waters through the aquitard or from the basement rocks. At the deepest point in the Maslin Sands aquifer, the highest helium-4 concentration is observed as anticipated.

3.5.3 Groundwater modelling

The modelling result consists of two sections; first, a comparison of the coastal sea level model (CSL) and the transient sea level change model (ΔSL). This includes an analysis of the head response in the aquifers from the transient sea level change model.

Second, the results of the calibrations of the coastal sea level model to head only calibration (Øh) and dual target calibrations (Øh+ØC) to both heads and carbon-14 to predict recharge post-land clearing.

3.5.3.1 Sea level change, influence on heads and carbon-14 activities

This section compares an identical model run with two different coastal boundary conditions; the coastal sea level boundary condition constant at 0 mAHD for all time (CSL), and the transient sea level change through the last glacial maxima (ΔSL). In all other aspects, model parameters and

geometry are identical. The transient sea level change model is not calibrated due to long run times, but the model outputs were tested with several models with different parameters. The results shown are using the parameters of hydraulic conductivity and recharge from the calibrated CSL model in Section 3.5.3.2.

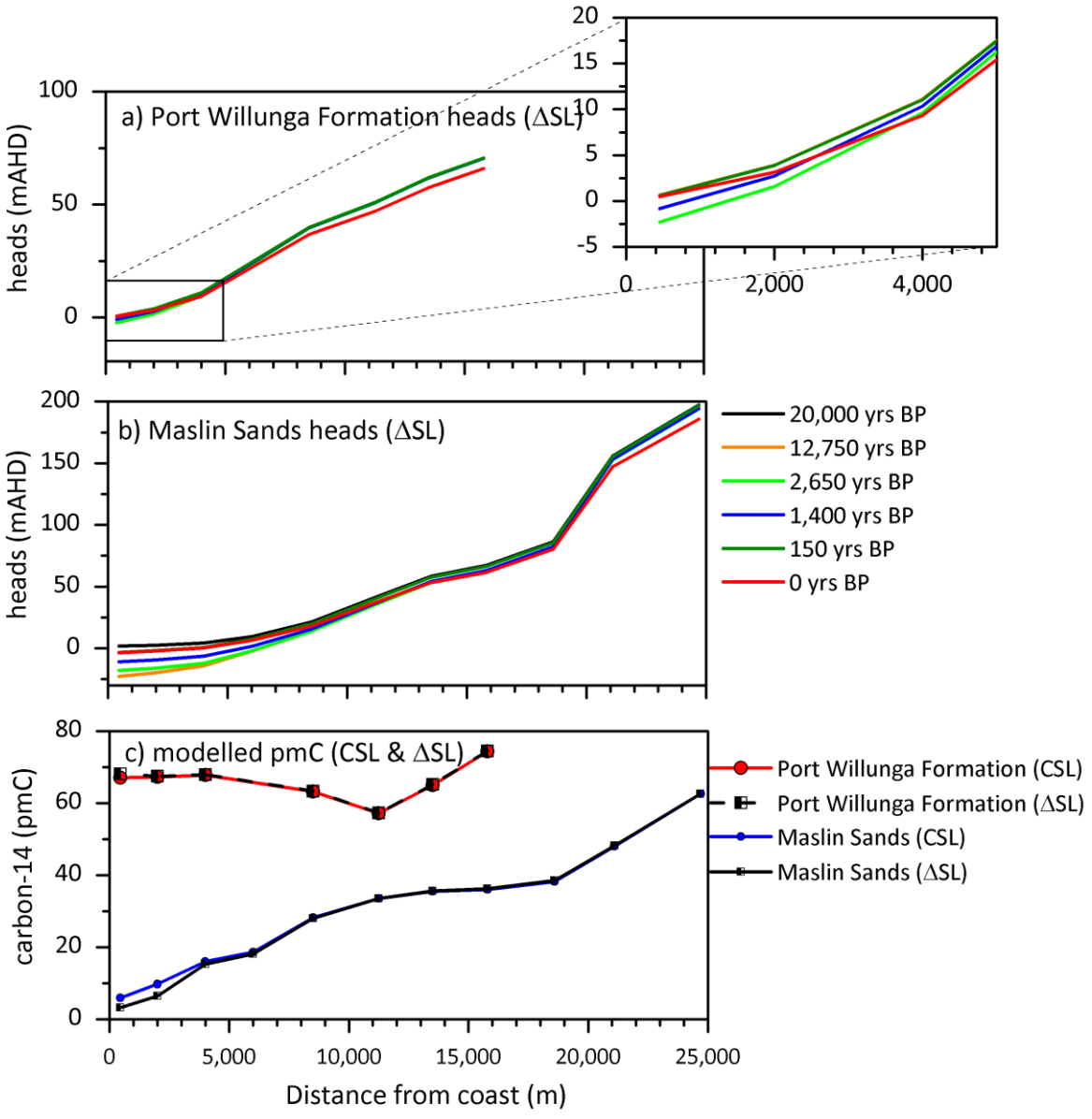

Figure 3.12: Head profile change with time for Δ sea level change model in a) Port Willunga Formation, and b) Maslin Sands aquifer, and c) modelled carbon-14 activities from Δ sea level model and SS models at 30,000 years.

Figure 3.12 demonstrates how heads change over time in both aquifers in the transient sea level change model (ΔSL). In the Port Willunga Formation, the head difference between 20,000 and 150 years BP is 3 m, and the propagation distance of the head change through the aquifer is approximately 3000 m inland. The largest head change in the Port Willunga Formation is caused when the recharge rate changes from 36 mm/yr to 25 mm/yr in the last 150 years of the model (red line).

In the Maslin Sands aquifer the model predicts a head decline of up to 20 m close to the coast during the last glacial maxima, and this propagates through the full length of the aquifer. The maximum head difference between 20,000 and 150 years at 20 km is 2.5 m. However, the most significant change in heads in the north east section of the Maslin Sands aquifer is caused by the decline in recharge rate from 36 mm/yr to 25 mm/yr applied in the last 150 years of the model. The pressure response of sea level change is more significant in the Maslin Sands aquifer than the Port Willunga Formation. The head response and time taken is a function of hydraulic conductivity and storage, so the confined aquifer responds quicker than the unconfined aquifer because the storage is four orders of magnitude lower.

The head changes in the aquifers over time as they translate to vertical hydraulic gradient changes across the aquitard are shown in Figure 3.13. The head profile change over time from the Maslin Sands and Port Willunga Formation of each site was taken from the model at a series of times to represent 6 time steps. These head gradients were divided by the distance between each screen to calculate the vertical hydraulic gradient at each time step. The resulting vertical hydraulic gradients across the aquitard during the sea level low stand of -130 mAHD are; (i) increasing downward gradient across the aquitard closer to the coast, and (ii) increasing upwards in gradient in the upper portion of the system relative to the current hydraulic gradients. The change is greatest at Site A, farthest from the coast, where the relative head difference between the Port Willunga and Maslin Sands aquifers is largest and the aquitard thickness is smallest, 30 m.

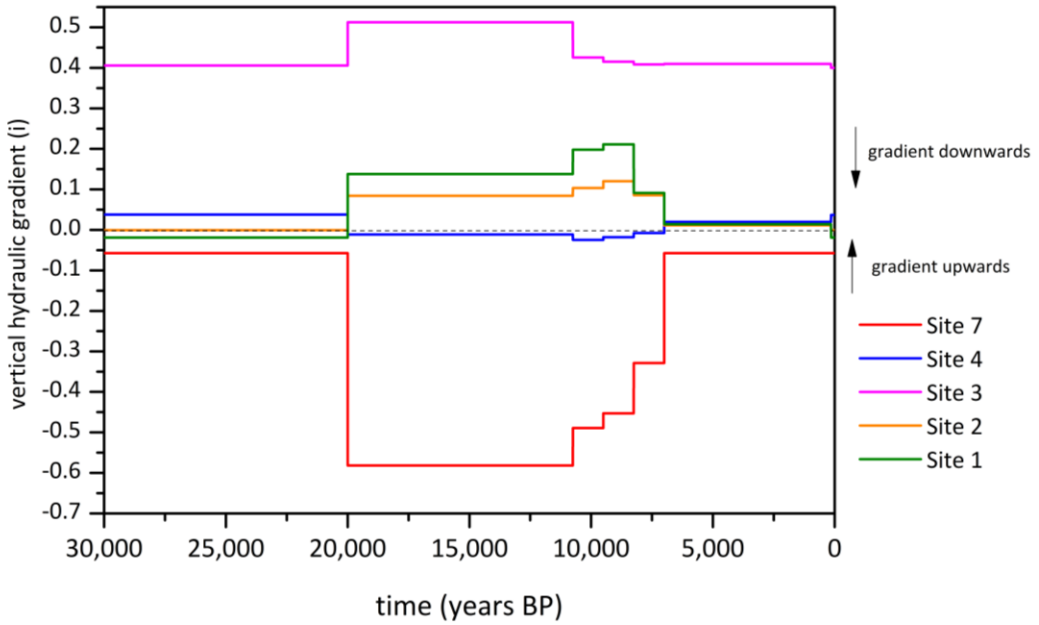

Figure 3.13: Vertical hydraulic gradient boundary conditions across the aquitard from the

Along this transect, the difference in the final model predictions for carbon-14 activities in each of the aquifers between the models with differing sea level boundary conditions is very small (Figure 3.12c), despite a change in heads of up to 20 m. The concentration difference is greatest closest to the coast in the Maslin Sands aquifer but the difference is less than 3 pmC.

The similarity of the heads and carbon-14 predictions from the differing sea level boundary condition models also can be seen in Figure 3.14, showing a statistically similar outcome for heads and carbon-14 predictions when compared to the target observation data.

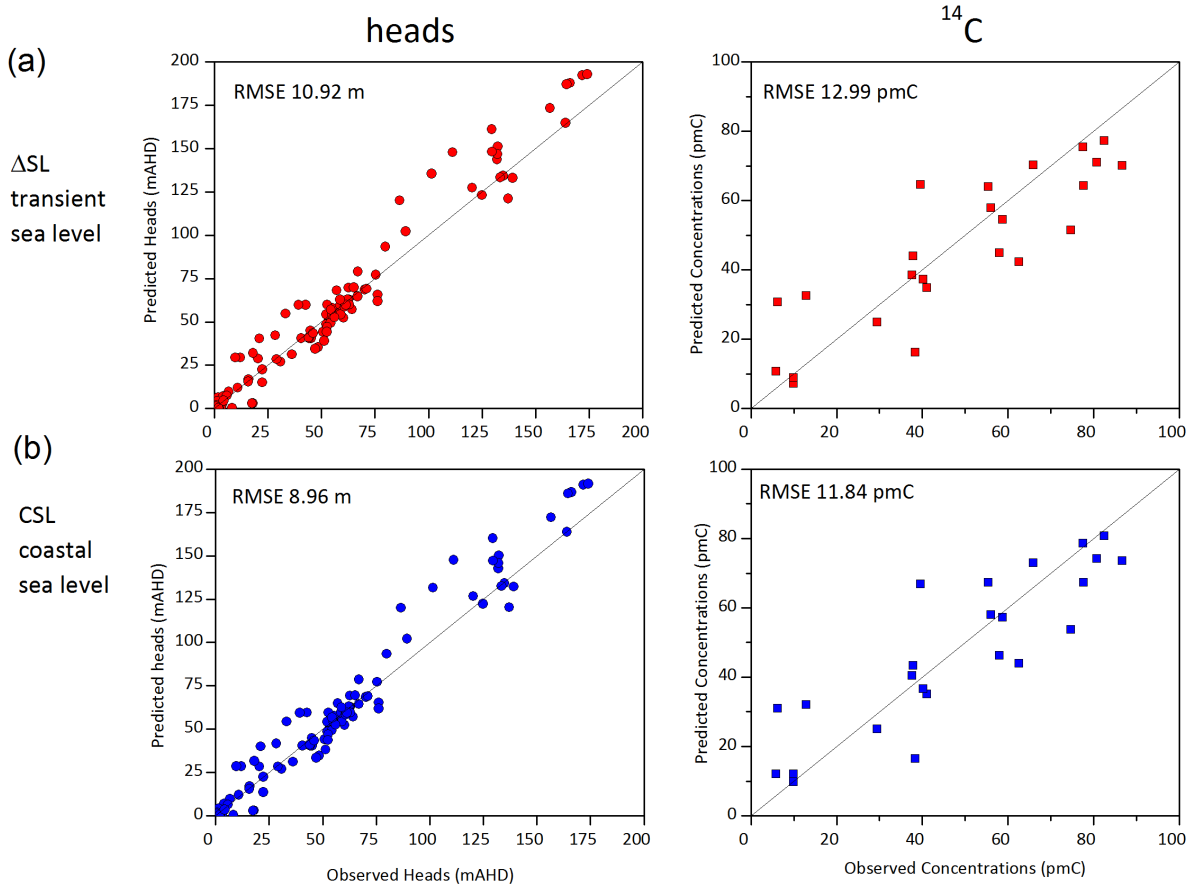

Figure 3.14: Predicted vs observed heads and carbon-14 activities a) Δ Sea level boundary condition b) no change in sea level

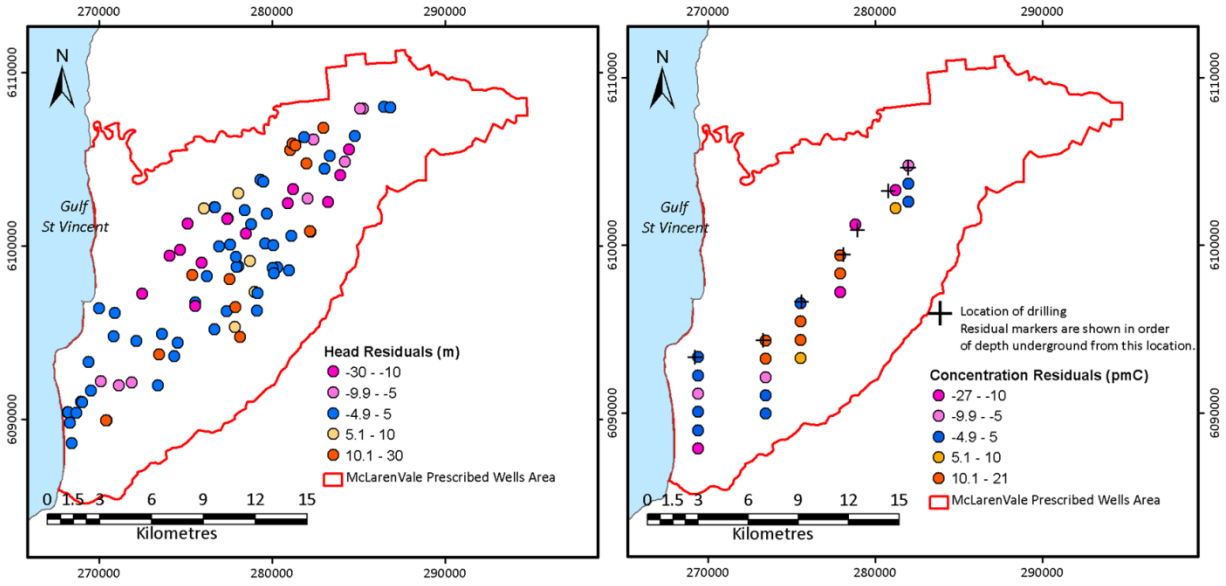

Figure 3.15: Head and carbon-14 residuals from the calibrated model with no sea level change (Figure 3.14b)

The head RMSE and carbon-14 RMSE of the models with different coastal boundary conditions are within 3% of each other (Figure 3.14). The coastal sea level model is a calibration output, so this model has the better result. The RMSE difference between the models is very small despite a change in aquifer heads of up to 20 m in the transient sea level change model, so the coastal sea level boundary condition model (SLC) was able to be used for modelling purposes. The run times for a model with transient sea level change are long, and limit its usefulness with PEST which can run a model up to 150 times before finding a preferred solution.

The residuals of the coastal sea level model are shown in Figure 3.15. The best results are in blue, with pink and blue showing further deviations of the model results from the measured samples. The head residuals have over or under predicted results at all locations, even in near proximity to each other. Model fit could potentially be improved by increasing parameterisation, particularly by increasing the number of hydraulic conductivity and recharge zones. This adds more complexity to the model and would increase PEST run times significantly, but with over and under predictions in close proximity it could be difficult to improve the calibration result without very fine

spatial discretisation of these parameters. The pmC residuals also do not show an obvious pattern of over or under prediction that could be modified without greatly increased parameterisation.

3.5.3.2 Single target vs dual target calibration

The results of the single and dual target series of calibrations are shown in Figure 3.16. For each calibration, the post-land clearing recharge rate was held at a specific value, and the model optimised pre-land clearing recharge and the hydraulic conductivities within the ranges set. All results are presented with the x-axis as the fixed post-land clearing recharge from 150 yrs BP to present with values increasing from left to right.

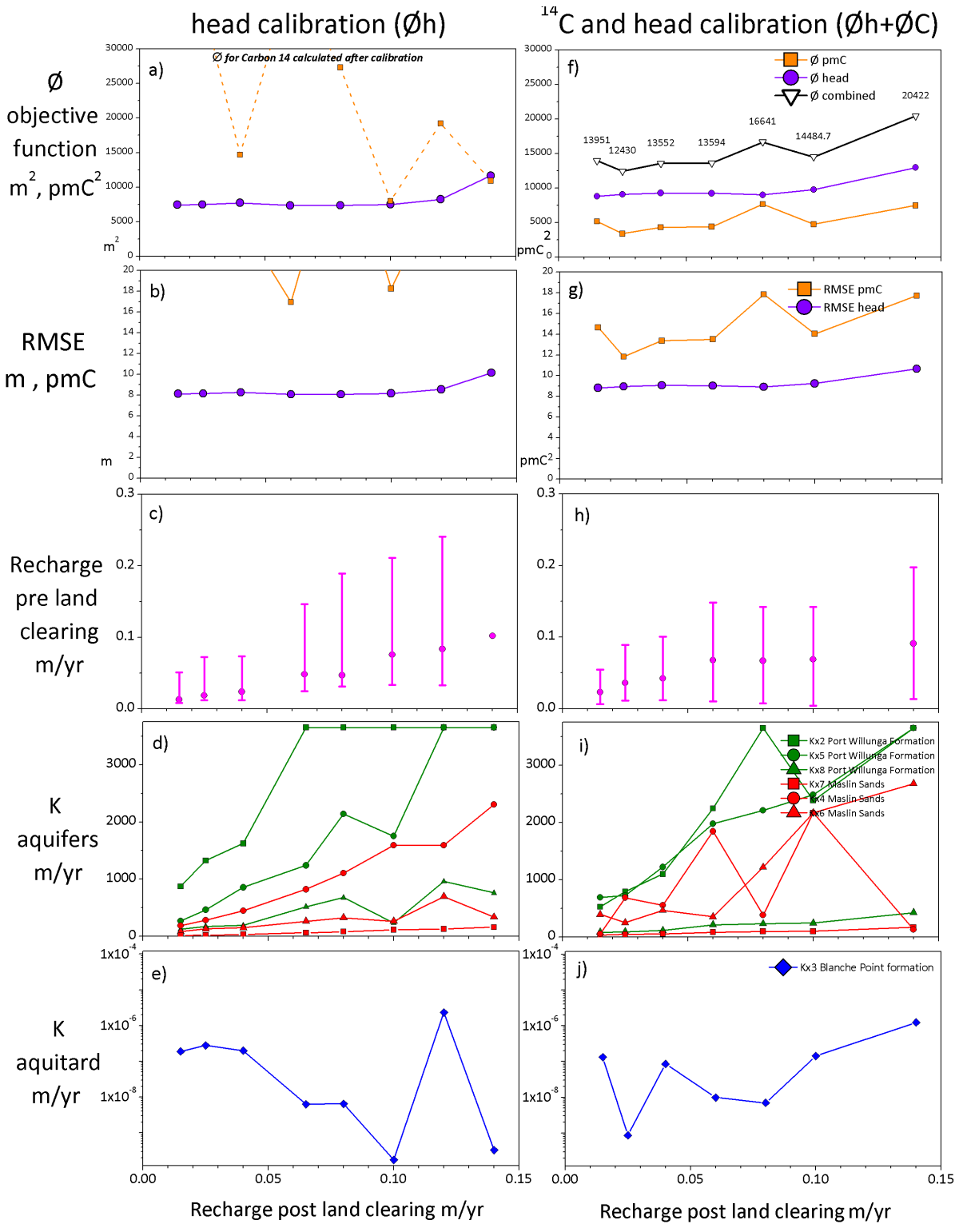

Figure 3.16: PEST calibration results. a) to e) are the model predictions for the single calibration to head (Øh). Plots f) to j) are the predictions of the dual calibration to head and pmC (Øh+ØC). a) and f) are the objective function results for each model, the lower the value the closer the model fit to data. c) to j) show the predicted parameters of pre-land clearing recharge and hydraulic conductivities.

The total range of objective functions for the head only calibrations was 7354 to 11,665 m^2 (Figure 3.16 a). Generally in calibration the lowest Ø is considered to be the best fit, in this case 7354 m^2. For these results the range of post land clearing recharge between 15 and 100 mm/yr are within 5% of the lowest value, and up to 120 mm/yr within 12%, these are all considered acceptable results. These results demonstrate the non-uniqueness of the calibration result.

For head calibrations, a poorer calibration fit was achieved when post-land clearing recharge was 140 mm/yr with an objective function result 58 % higher than the best calibration result.

For the dual calibration results (Øh+ØC), the overall objective function range was higher than the head calibrations because the model adds the two objective functions of head and pmC. The Ø total ranged from 12,480 to 20,422 (Figure 3.16 b). The $Ø_{head}$ component of the objective function ranged between 8795 and 12,832 m^2, and the $Ø^{14}C$ component was between 5156 and 7546 pmC^2.

The lowest Ø was 12480 at a post clearing recharge of 25 mm/yr. The objective function results where post clearing recharge was between 15 and 60 mm/yr were within 12% of the lowest result, and are all acceptable fits. For post land clearing recharge between 80 and 140 mm/yr the objective functions were 17 to 64% higher. Therefore, the model calibration predicts a post-land clearing (0-150 yrs BP) recharge between 15 and 60 mm/yr, with pre-land clearing recharge of 15 to 55 mm/yr.

The hydraulic conductivity values predicted from the model calibrations are at the lower range of values predicted through previous modelling and pump test predictions described in

Table 3.3 and equate to between 0.1 and 2.2 m/d for the aquifers. In the optimisations where recharge was set at 60 mm/year or higher, the K values of the Port Willunga Formation reached the 10 m/d range, however the calibration residuals for head and carbon-14 were poorer.

Table 3.3: Comparison of literature values and optimised model parameter estimates

Parameter	Aquifer Unit	Kx Literature values m/d	Kx Optimised values m/d
R2	Post land clearing recharge (mm/yr)	21 - 34	25
R1	Pre-land clearing recharge (mm/yr)	-	36
Kx1	Quaternary	-	10
Kx2	PWF – Northern (outcrop)	0.2 - 10	2.16
Kx3	BPF – aquitard	$6x10^{-13}$ – $1.5x10^{-13}$	$2.36x10^{-12}$
Kx4	MS – northern (outcrop)	0.4 - 1	1.8
Kx5	PWF – central/southern	0.2 - 10	1.9
LKx6	MS – southern	0.4 - 1	0.67
Kx7	MS – upgradient	0.4 - 1	0.11
Kx8	PWF – upgradient	0.2 - 10	0.24

3.6 Discussion

The carbon-14, helium-4 and chloride data plotted spatially provides several insights into the conceptual model of the Willunga basin:

1) The upgradient section of both the Maslin Sands and Port Willunga aquifers is a lower velocity flow region compared to the portion of the aquifers nearer the coast. This is based on the rapid decline in carbon-14 activities and the steeper hydraulic gradient. It is also supported by the lower hydraulic conductivity values predicted in the up gradient regions in the calibrated model.
2) Recharge to the Port Willunga Formation aquifer is occurring at a distance between 5 and 15 km inland through the Quaternary sediments, resulting in increased carbon-14 activities and lower chloride concentrations.
3) Mixing with younger waters appears to be occurring at the centre of the Maslin Sands aquifer, either from the Port Willunga Formation through the aquitard, or lateral flow from the northern outcropping region. This is based on the increased carbon-14 activities and reduced helium-4 concentrations at this location. Caution needs to be taken with this observation because it is made using a 2 dimensional transect of a 3 dimensional flow system.

The geochemistry data show that recharge varies spatially with a higher recharge zone in the Port Willunga Formation at a distance between 5 and 15 km inland. This was not accounted for in the model prediction or calibration, and should be explored further to refine estimates of recharge for current basin management.

The process of sea level change as modelled does not have a significant influence on carbon-14 activities in the Willunga Basin. Sea level change was shown in the Maslin Sands aquifer to have induced a head change of 20 m close to the coast, the head change was propagated the full distance into the aquifer. Despite this significant head change, the head and carbon-14 model predictions of

the sea level change model are within 3% of the predictions from the same model with no change in coastal boundary condition.

In addition to refining our understanding of the hydrogeology of the basin, the study provides estimates of recharge in the basin. The chloride mass balance predicts a recharge rate of 15-16 mm/yr to the aquifers. The model calibration predicts a post-land clearing (0-150 yrs BP) recharge between 15 and 60 mm/yr, with pre-land clearing recharge of 15 to 55 mm/yr. The chloride mass balance result is at the lower range of the model calibration prediction. These results compare with the previous recharge estimates in the literature which range from 21 mm/yr to 34 mm/yr, based on chloride mass balances and modelling estimates (Aldam 1990, Martin 1998, Martin 2006).

Chloride Mass Balance provides an estimate of recharge based on a mass balance between rainfall and aquifer chloride concentrations, and in this case only a year of recent annual rainfall data used as average chloride deposition rate, whilst the aquifer residence time is around 35,000 years

Allison, Cook et al. (1990) in the Murray Darling basin found that recharge rates increased by up to two orders of magnitude as a result of land clearing, yet the Willunga Basin model using carbon-14 predicts recharge post-land clearing in the same range, or only marginally higher (up to 10 mm/yr) than pre land clearing. The climate and vegetation of these two systems is different, the Murray Darling is an arid basin, and pre land clearing recharge rates were below 1 mm/yr, whereas the Willunga Basin has a temperate climate close to the coast.

This model was given two recharge time steps, to represent pre land clearing and post land clearing (the last 150 years). The use of a single recharge rate over 29,850 years to represent pre-land clearing recharge may have oversimplified the climate of the time. This time scale represents a range of different climates from the last glacial maxima through to the Holocene and present. Reeves, Barrows et al. (2013) modelled local temperatures as warmer than the current temperature during the period 9 – 20 kyr. Precipitation was lower than current conditions between 2 – 5 kyr, and

higher between 9 and 20 kyr, with lower precipitation during the last glacial maxima at 20-25kyr (Reeves, Barrows et al. 2013). Further work should explore this.

The model calibration results demonstrate the non-uniqueness of head as a target in this regional groundwater model, that head is relatively easy to fit within a range of recharge and hydraulic conductivity combinations. The dual calibration to carbon-14 and heads (Øh+ØC) performed better overall than the single head calibration (Øh) in decreasing uncertainty around recharge prediction. The carbon-14 target provides us with ability to narrow down the best result, where the heads targets presents a broad range of acceptable calibration results.

An attempt was made to include the flow across fault as part of the overall water balance in the model. A model (not shown in results) was constructed with three equal distance sections of general head boundary along the length of the Willunga Fault. The effect of these boundary conditions were that the flux of water from the fault was much larger than seems reasonable and much larger than the recharge to the aquifer, and head and carbon-14 calibration was not improved. Without an estimate of flux from the fault it was difficult to constrain the boundary conditions. Whilst flux across the fault is thought to have an influence on head and carbon-14 activities it is difficult to constrain without a reasonable estimate and did not add value to the component of the study being investigated, which is changing recharge rates and sea level change. A transect of bores perpendicular to the fault would assist in determining the flux contribution across this interface.

3.7 Conclusions

The model calibration predicts a post-land clearing (0-150 yrs BP) recharge between 15 and 60 mm/yr (the best calibration result at 25 mm/yr) with pre-land clearing recharge of 15 to 55 mm/yr. A chloride mass balance assessment of recharge is also made using local rainfall data, this estimate is 15-16 mm/yr. Previous literature estimates for the Willunga Basin are 21 to 34 mm/yr, within the range of the calibration results.

The use of carbon-14 as an additional calibration target was shown to improve the estimate of recharge by providing a definite calibration result with a best fit, while the model fit to heads was shown to be non-unique and not able to reliably predict recharge. The process of sea level change as modelled did not have a significant influence on carbon-14 activities in the Willunga Basin, despite a significant change in aquifer heads in the Maslin Sands, so steady state coastal boundary conditions were sufficient for the modelling of carbon-14.

The model estimated hydraulic conductivities of the aquifers all to be close to the lower range of previous literature estimates, between 0.11 and 2.61 m/d, whereas pump tests have measured hydraulic conductivities up to 10 m/d in some locations.

Table 3.4: Rainfall Station data used in Chloride Mass Balance

	Hardys Scrub		Mount Wilson	
Month (2012)	**Rainfall (mm)**	**Cl- (mg/L)**	**Rainfall (mm)**	**Cl- (mg/L)**
January	10.6	8.42	16.6	7.23
February	67.8	5.82	28.1	2.45
March	47	4.19	46.9	28.8
April	26	5.54	0.3	8.07
May	64.4	NA*	48.2	NA
June	113.5	NA	141.4	NA
July	38.1	NA	13.5	NA
August	53.5	9.457	103.3	10.84
September	38.5	15.51	97	17.77
October	29.9	10.78	51	12.34
November	15.1	15.28	43	7.349
December	12.3	6.107	35	5.515
Total	**516.7**	**9.01 (mean)**	**624.3**	**11.15 (mean)**

*NA not available

Table 3.5: Transect environmental tracer data

	Name	Easting	Northing	Ground level mAHD	Top of Screen mAHD	Aquifer	^{14}C pmC	$\delta^{14}C$ $^{0}/_{00}$	$\delta^{13}C$	Target weight (^{14}C)	^{4}He ccSTP/gwater	Cl^- mg/L
1	S1-6	269409.5	6093309.4	23.384	-3.616	PWF	55.43	-445.71	-10.418	1		1058
2	S1-5	269409.5	6093309.4	23.384	-18.616	PWF	58.69	-413.08	-10.11	1		839
3	S1-4	269409.5	6093309.4	23.384	-33.616	PWF	37.59	-624.06	-9.19	1	4.46e-08	409
4	S1-3	269409.5	6093309.4	23.384	-48.616	PWF	5.93	-940.72	-8.31	1	5.64e-07	570
5	S1-2	269409.5	6093309.4	23.384	-120.616	MS	9.92	-900.77	-8.62	1		
6	S1-1	269409.5	6093309.4	23.384	-134.616	MS	9.87	-901.31	-9.11	1	9.2e-05	
7	S2-7	273464.3	6093756.8	39.918	20.918	PWF	82.39	-176.1	-9.74	1		350
8	S2-6	273464.3	6093756.8	39.918	7.918	PWF	77.52	-224.8	-11.33	1	6.8e-08	382
9	S2-5	273464.3	6093756.8	39.918	-8.082	PWF	65.86	-341.4	-11.35	1		365
10	S2-4	273464.3	6093756.8	39.918	-26.082	PWF	57.95	-420.55	-10.43	1		304
11	S2-3	273464.3	6093756.8	39.918	-75.082	BPF	39.63	-603.68	-9.195	0	7.17e-08	
12	S2-2	273464.3	6093756.8	39.918	-116.082	MS	38.43	-615.66	-9.8932	1	2.34e-07	
13	S3-6	275554.8	6096528.7	60.992	28.992	PWF	80.74	-192.6	-12.88	1		382
14	S3-5	275554.8	6096528.7	60.992	1.992	PWF	77.63	-223.72	-12.48	1		164
15	S3-4	275554.8	6096528.7	60.992	-39.008	PWF	62.47	-375.29	-12.24	1	1.42e-06	214
16	S3-2	275554.8	6096528.7	60.992	-123.008	MS	29.52	-704.8	-10.45	1		
17	S4-6	277917.2	6099378.7	63.267	34.267	PWF	86.7	-132.97	-12.57	1		194
18	S4-5	277917.2	6099378.7	63.267	19.267	PWF	74.67	-253.26	-12.72	1	1.98e-06	170
19	S4-4	277917.2	6099378.7	63.267	-33.733	BPF	4.45	-955.54	-11.59	0	1.6e-06	

	Name	Easting	Northing	Ground level mAHD	Top of Screen mAHD	Aquifer	^{14}C pmC	$\delta^{14}C$ $^{0}/_{00}$	$\delta^{13}C$	Target weight (^{14}C)	^{4}He ccSTP/gwater	Cl^- mg/L
20	S4-3	277917.2	6099378.7	63.267	-50.733	MS	6.23	-937.72	-12.26	1	2.7e-06	
21	S5-5	278811.27	6101234	67.235	51.235	PWF	39.61	-603.9	-10.03	1		428
22	S5-3	278811.27	6101234	67.235	14.235	BPF	7.89	-921.1	-8.51	0		
23	S6-3	281222	6103279	93.657	57.657	PWF	40.98	-590.2	-13.23	1	7.89e-07	351
24	S6-2	281222	6103279	93.657	34.657	MS	12.87	-871.3	-9.18	1	2.48e-06	
25	S7-4	282551.2	6105131.9	146.24	122.24	PWF	56.01	-439.9	-14.44	1	5.13e-07	99
26	S7-3	282551.2	6105131.9	146.24	82.24	MS	40.21	-597.94	-10.32	1	2.48e-06	
27	S7-2	282551.2	6105131.9	146.24	66.24	MS	37.9	-621.07	-9.62	1	7.89e-07	

Table 3.6: Groundwater environmental tracer data

Name	Easting	Northing	Aquifer	$\delta^{2}H$ permil	$\delta^{18}O$ permil	Cl- mg/L
51350_A	277895.8	6099395	PWF	-26.3	-5.2	167
51350_B	277895.8	6099395	PWF	-25.0	-5.0	192
51350_C	277895.8	6099395	PWF	-24.3	-5.0	294
51350_D	277895.8	6099395	PWF	-24.2	-4.9	354
51351_A	277906.4	6099395	PWF	-25.7	-5.3	171
51351_B	277906.4	6099395	PWF	-24.4	-5.1	203
51351_C	277906.4	6099395	PWF	-22.2	-4.8	454
51352_A	277911.5	6099394	PWF	-25.8	-5.3	167
51352_B	277911.5	6099394	PWF	-25.7	-5.1	197
51352_C	277911.5	6099394	PWF	-23.5	-4.9	337
KTP024	285135	610720	MS	-19.1	-3.9	501
KTP029	286977	6107900	MS	-24.5	-5.2	321
WLG038	270434.5	6089951	PWF	-23.2	-4.8	750
WLG040	268941	6093082	MS	-24.3	-4.2	26013
WLG044	270906	6096135	MS	-18.0	-3.9	970
WLG057	270437.7	6089953	PWF	-23.1	-4.2	4600
WLG061	283239	6102518	PWF	-23.3	-4.7	760
WLG065	277893.3	6096457	MS	-21.7	-4.8	230
WLG071	275931.7	6099014	PWF	-26.1	-5.3	160
WLG072	275931.7	6099014	MS	-27.4	-5.1	450

Name	Easting	Northing	Aquifer	$\delta^{2}H$ permil	$\delta^{18}O$ permil	Cl- mg/L
WLG079	284218.7	6104841	MS	-22.6	-5.1	144
WLG092	282211	6100861	MS	-27.6	-5.4	464
WLG097	280856.6	6103227	MS	-25.5	-4.9	537
WLG099	282057.9	6102404.9	PWF	-26.1	-5.1	1100
WLG100	280074	6100036	PWF	-25.7	-5.0	310
WLG101	270423.8	6089951	PWF	-22.9	-4.1	2200
WLG102	273639	6092480	PWF	-24.0	-4.9	370
WLG127	268211	6090419	PWF	-21.3	-4.6	6400
WLG132	268342	6089792	PWF	-21.7	-4.7	1300
WLG133	268342	6089792	PWF	-20.7	-4.3	4300
WLG135	268979.3	6091010	PWF	-21.6	-4.6	5300
WLG136	268422	6088615	PWF	-23.0	-5.0	480
WLG155	276960.9	6101806.6	MS	-26.2	-5.1	520
WSS001_B	271220	6092385	PWF	-22.1	-4.5	1100
WSS001_C	271220	6092385	PWF	-19.2	-4.0	980
WSS001_D	271220	6092385	PWF	-22.0	-4.6	1100
WSS001_E	271220	6092385	PWF	-22.5	-4.6	1100
WSS002_A	270746	6091241	PWF	-20.4	-4.4	870
WSS002_B	270746	6091241	PWF	-20.9	-4.4	710
WSS002_C	270746	6091241	PWF	-23.8	-4.8	470
WSS002_E	270746	6091241	PWF	-21.3	-4.6	290
WSS002_F	270746	6091241	PWF	-21.2	-4.6	330

Name	Easting	Northing	Aquifer	$\delta^{2}H$ permil	$\delta^{18}O$ permil	Cl- mg/L
WSS003_A	270750	6091229	PWF	-15.5	-3.4	734
WSS003_B	270750	6091229	PWF	-20.1	-4.1	701
WSS003_C	270750	6091229	PWF	-20.1	-4.5	530
WSS003_D	270750	6091229	PWF	-21.0	-4.6	248
WSS003_E	270750	6091229	PWF	-21.4	-4.7	262
WSS003_F	270750	6091229	PWF	-21.9	-4.7	291
WSS-CHR-1	275598.1	6100941	PWF	-19.3	-4.1	740
WSS-DGR-1	281148	6103245	PWF	-23.4	-4.8	1500
WSS-DGR-2	281148	6103246	PWF	-23.7	-4.6	1100
WSS-FR-1	278683.8	6100821	PWF	-25.1	-4.8	900
WSS-FR-2	278685	6100821	PWF	-25.2	-4.8	1000
WSS-IR-1	280916.9	6102297	PWF	-23.9	-4.6	430
WSS-SHR-1	274796.7	6101343	MS	-18.7	-3.9	160
WSS-SHR-2	274797.1	6101345	MS	-17.2	-3.6	170

Table 3.7: Hydraulic head target data

Name	Easting	Northing	Aquifer	Head mAHD
S1-6	269409.5	6093309.4	PWF	1.854
S1-5	269409.5	6093309.4	PWF	1.837
S1-4	269409.5	6093309.4	PWF	1.801
S1-2	269409.5	6093309.4	MS	3.897
S1-1	269409.5	6093309.4	MS	1.721
S2-7	273464.28	6093756.81	PWF	22.398
S2-6	273464.28	6093756.81	PWF	22.393
S2-5	273464.28	6093756.81	PWF	22.391
S2-4	273464.28	6093756.81	PWF	22.384
S2-2	273464.28	6093756.81	MS	22.388
S3-6	275554.81	6096528.68	PWF	40.541
S3-5	275554.81	6096528.68	PWF	40.576
S3-4	275554.81	6096528.68	PWF	45.15
S3-2	275554.81	6096528.68	MS	12.135
S4-6	277917.19	6099378.65	PWF	56.355
S4-5	277917.19	6099378.65	PWF	56.528
S4-3	277917.19	6099378.65	MS	53.744
S4-2	277917.19	6099378.65	MS	53.45
S5-5	278811.27	6101234.04	PWF	62.822
S5-4	278811.27	6101234.04	PWF	62.775
S5-2	278811.27	6101234.04	MS	59.042
S6-3	281222	6103279	PWF	89.396
S7-4	282000	6104750	PWF	134.84
S7-2	282000	6104750	MS	137.12
WLG038	270434.52	6089951.25	PWF	3.1
WLG131	268207	6090418	PWF	8.33
WLG133	268342	6089792	PWF	3.23
WLG006	279695.72	6101839.25	PWF	70.21
WLG007	280933.06	6102469.59	PWF	79.87
WLG014	277578.9	6100054.99	PWF	55.13
WLG016	278740	6099120	PWF	64.26
WLG019	272505.63	6097254.26	PWF	20.42
WLG020	274553.91	6094418.94	PWF	36.21
WLG022	270852.2	6094794.02	PWF	10.9

Name	Easting	Northing	Aquifer	Head mAHD
WLG057	270437.7	6089953.17	PWF	18.03
WLG064	276962.24	6099956.37	PWF	52.25
WLG135	268979.29	6091009.56	PWF	1.3
WLG125	269531.35	6091665.6	PWF	1.82
WLG127	268211	6090419	PWF	2.07
WLG132	268342	6089792	PWF	1.7
WLG071	275943	6099023	PWF	52.17
WLG008	278501.19	6100725.6	PWF	57.1
WLG015	280316.68	6098746.26	PWF	62.45
WLG018	277863	6095321	PWF	50.811
WLG021	279120.69	6096260.18	PWF	54.31
WLG039	270429.09	6089951.45	PWF	17.56
WLG045	279006.5	6097345.78	PWF	60.26
WLG047	272155	6094518	PWF	15.94
WLG049	271898	6092140	PWF	6.71
WLG051	280043.85	6098726.98	PWF	58.66
WLG052	273414	6091955	PWF	15.83
WLG053	274348.18	6093642.71	PWF	30.89
WLG055	278071	6098811	PWF	59.01
WLG058	276241	6098261	PWF	52.61
WLG059	277944	6098803	PWF	55.06
WLG060	279613	6100152	PWF	62.2
WLG067	280116	6098417	PWF	60.8
WLG068	276681	6095172	PWF	44.255
WLG069	277400.09	6096220.77	PWF	44.93
WLG070	275570	6096736	PWF	44.06
WLG073	279158	6097277	PWF	56.07
WLG084	281108.67	6100576.23	PWF	71.08
WLG085	273655	6094917	PWF	29.116
WLG086	271169	6091942	PWF	4.0327
WLG087	270110	6092190	PWF	1.44
WLG088	269039	6090979	PWF	0.87
WLG090	282223	6100817	PWF	75.4
WLG134	268692	6090380	PWF	0.75
WLG136	268422	6088615	PWF	1.97
WLG061	283239	6102518	PWF	86.51

Name	Easting	Northing	Aquifer	Head mAHD
WLG011	275127.67	6101287.28	MS	33.2
WLG023	276081.67	6102168.25	MS	60.85
KTP006	285246.74	6107930.26	MS	166.12
KTP015	285077.74	6107906.27	MS	164.47
KTP016	286469.68	6108007.23	MS	171.7
KTP017	286838.67	6107993.17	MS	174.05
KTP018	284799.72	6106329.21	MS	156.66
KTP021	284453.31	6105561.16	MS	129.44
KTP022	282988	6106805	MS	163.99
WLG002	281063.71	6105519.23	MS	124.92
WLG009	278047	6103035	MS	66.88
WLG042	275394.71	6098305.24	MS	48.43
WLG043	283359.7	6105182.23	MS	132
WLG044	270906.03	6096134.99	MS	5.82
WLG046	270022	6096414	MS	4.33
WLG048	276687.66	6102230.22	MS	63.03
WLG050	279352	6103801	MS	62.69
WLG054	274090.34	6099419.14	MS	18.1
WLG056	280090	6100023	MS	61.39
WLG062	278416.02	6102044.81	MS	58.72
WLG063	279503.39	6103714.96	MS	65.16
WLG065	277893.26	6096456.55	MS	51.3
WLG072	275931.65	6099013.68	MS	28.41
WLG074	282409	6106126	MS	132.31
WLG075	281857	6106257	MS	132.21
WLG078	277437.68	6101576.26	MS	42.67
WLG079	284218.68	6104841.25	MS	129.58
WLG080	283039.38	6104445.03	MS	120.31
WLG083	282057	6102736	MS	66.97
WLG092	282211	6100861	MS	76.25
WLG093	277537	6098075	MS	52.48
WLG094	281194	6105906	MS	133.5
WLG104	274708	6099758	MS	21.05
WLG108	277426	6101568	MS	39.36
WLG111	276697	6102229	MS	52.66

Name	Easting	Northing	Aquifer	Head mAHD
WLG140	281354.4	6105780.98	MS	139.2
FAF_2	278165	6094759	PWF	46.107
FAF_5	278165	6094759	MS	47.043
FAF_8	280990	6098604	MS	54.445
FAF_9b	280990	6098604	PWF	76.203
FAF_13a	283945	6104070	MS	101.49
FAF_15	283945	6104070	PWF	111.14

Photo Gallery

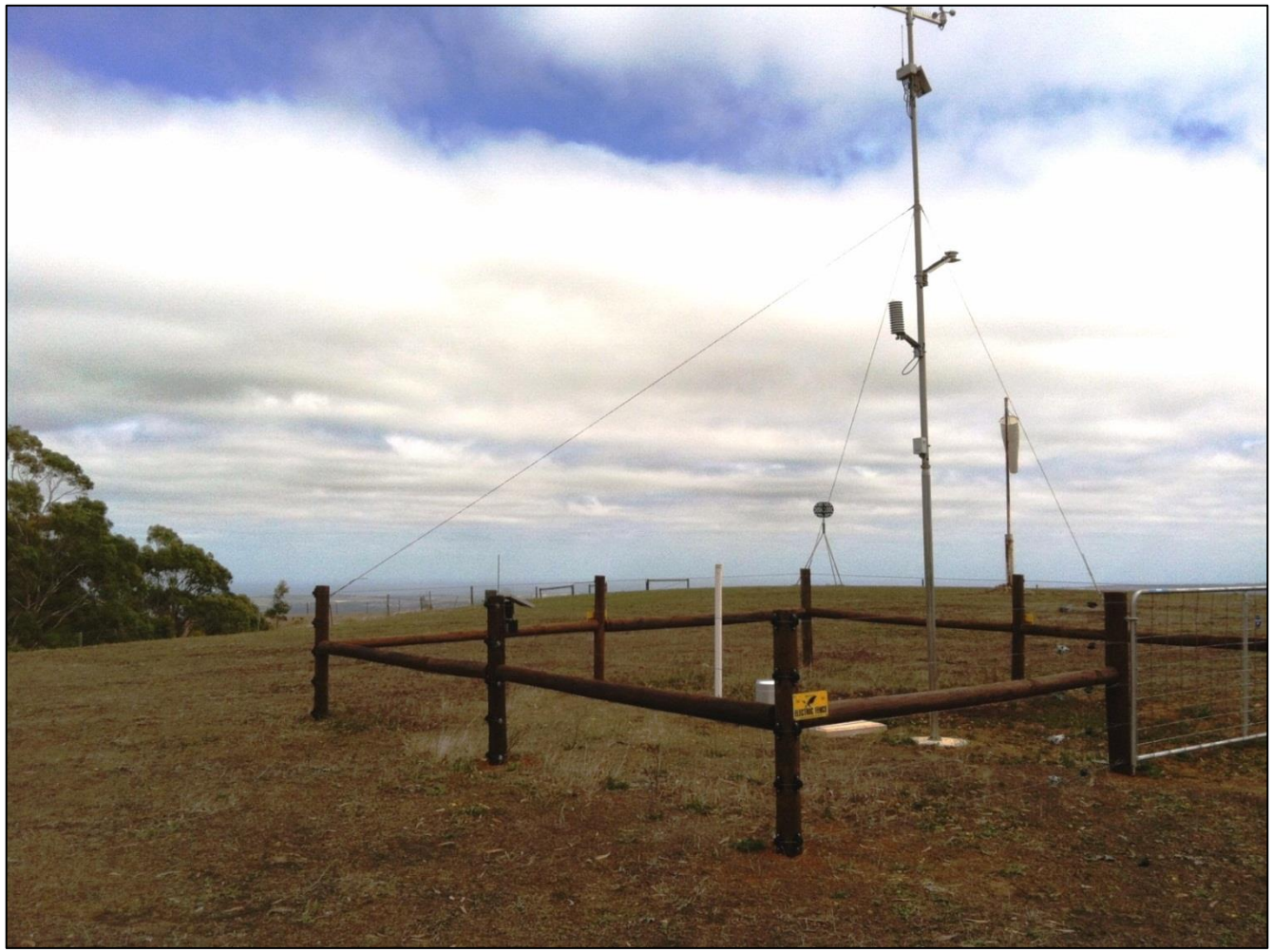

Photo 1: Rainfall station at Mount Wilson, 408 mAHD.

Photo 2: Some of the local wildlife, a redback spider waiting near the handle of the buried rainfall station sampler.

Photo 3: Two drill rigs working at the same time at Site 4. Triple barrel core - rotary diamond drill rig on left for the aquitard coring, and a mud rotary auger on the right for drilling of groundwater bores.

Photo 4: Groundwater sampling near the vineyards, this pump and winch was constructed to reach a depth of 200m.

Photo 5: Aquitard coring and sampling at Site 1 (Aldinga) on a 40°C day.

Photo 6: Core at Site 1. Core was placed in the jig by the drillers, we recorded the measurements, lithology and collected cores for scraping (shown), and sealing by vacuum sealing or for noble gas analysis.

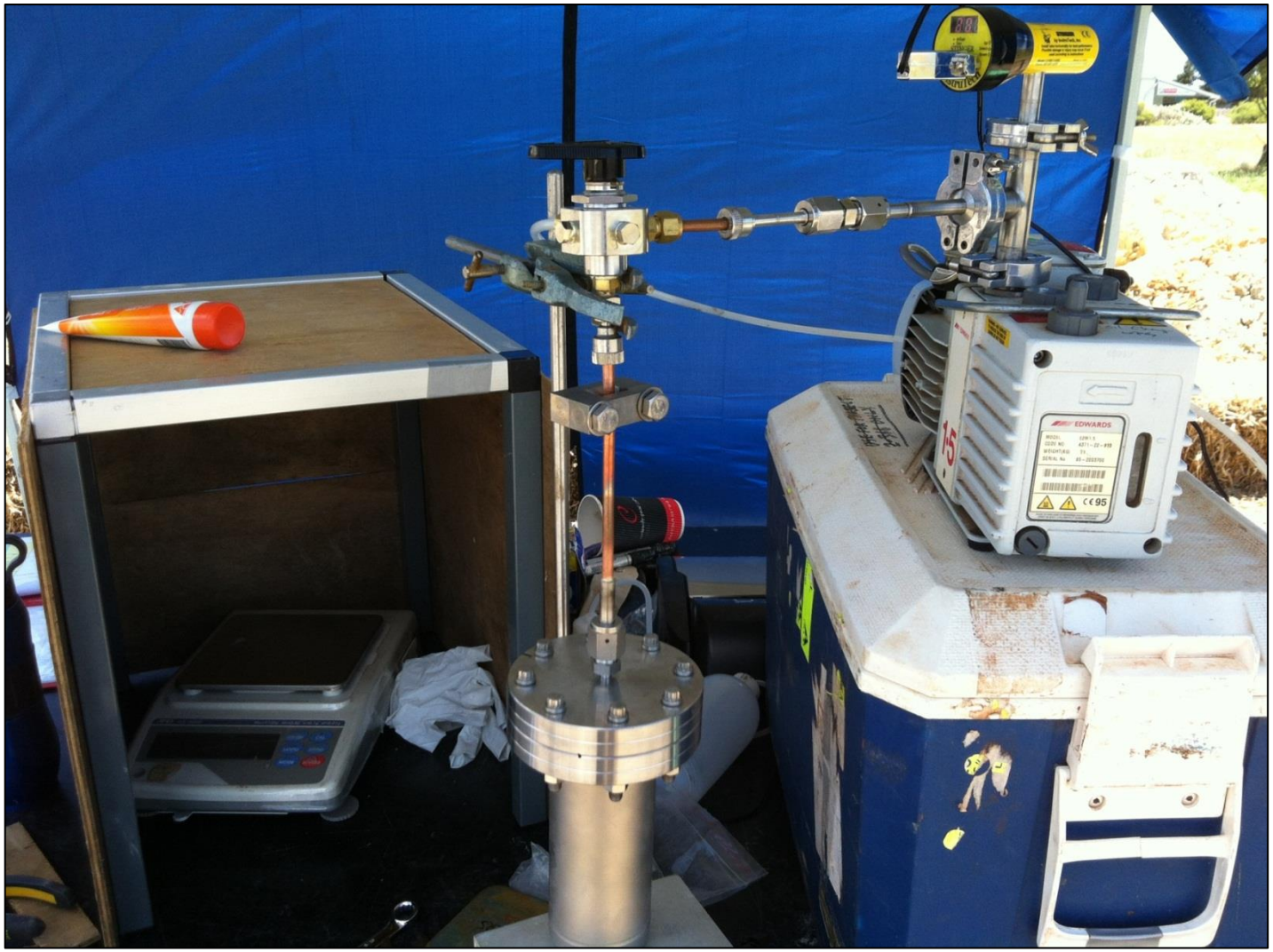

Photo 7: Core sampling for noble gases. Core is placed in the stainless steel canister, which is vacuum extracted and flushed with Nitrogen gas several times until sealed under vacuum by clamping the copper tube.

Photo 8: Fossils in the aquitard core.

Photo 9: View of Blanche Point looking south from Maslins Beach. Maslins Beach is the outcrop of the aquifer, overlain by the layers of the Blanche Point Formation (outcrop of the aquitard).

Chapter 4 Using aquitard porewater chemistry to reveal long-term changes in regional groundwater chemistry

4.1 Introduction

Aquitards control the hydraulics of many aquifer systems, and can allow leakage between aquifers (Timms, Acworth et al. 2001, Timms, Hendry et al. 2009, Mazurek, Alt-Epping et al. 2011). While regional models used for groundwater management usually include aquitards, the hydraulic parameters or flux across the aquitard is rarely measured.

Physical methods of determining hydraulic properties of aquitards include slug tests and physical measurements of cores in a laboratory using centrifuge or triaxial methods (Van Der Kamp 2001). The problem with these physical methods is the small scale and that the cores are measured after the cores have been extracted from the ground when the significant pressure of the overburden is removed.

Environmental tracers have also been used to measure flux across a section of aquitard thickness by analysis with the advection-dispersion equation (Bredehoeft and Papadopulos 1980, Van Der Kamp, Van Stempvoort et al. 1996, Hendry and Wassenaar 2009, Mazurek, Alt-Epping et al. 2009, Gardner, Harrington et al. 2012). For example, Mazurek, Alt-Epping et al. (2011) used solute profiles to resolve downwards velocities of $2x10^{-11}$ to $6x10^{-13}$ m/s from nine core sites across the UK and Europe. Gardner, Harrington et al. (2012) used solute profiles in the Great Artesian Basin, Australia to calculate flux where the flux differed by three orders of magnitude, 3 mm/yr and less than 0.003 mm/yr for two sites. Love, Herczeg et al. (1996) used solute profiles to infer leakage in the Otway Basin in South Australia, from an aquifer system in which both upwards and downwards vertical hydraulic gradients exist.

Tracer profiles through aquitards have also been used to give insights into the long term evolution of groundwater resources (Timms, Acworth et al. 2000, Mazurek, Alt-Epping et al. 2009, Hendry and Wassenaar 2011, Harrington, Gardner et al. 2013). Hendry, Barbour et al. (2013) used stable isotope solute profiles through the Cretaceous shale (384 m thick) in Williston Basin, Canada to show recharge to the deeper aquifer occurred in glacial times, and water in the top 25 m of the aquitard was deposited in the Holocene (10 kyr). Solute profiles in the aquitard of the Great Artesian Basin, South Australia were used to infer salinity changes in the aquifer over 120 kyrs (Harrington, Gardner et al. 2013).

The above studies all assume steady state hydraulic conditions, and a vertical hydraulic gradient in a single direction and of constant magnitude at each site. Love, Herczeg et al. (1994) proposed that the interpretation of age tracers in coastal connected groundwaters should be subject to changing hydraulic gradients from sea level change since the last glacial maxima. This sea level change will also change the vertical hydraulic gradients across aquitards. The last glacial maxima occurred at 18-20 kyrs BP (Cann, Belperio et al. 1988), and would have resulted in the coastline of South Australia being 200 km farther out to sea (Chapter 2).

This study analyses vertical porewater profiles of environmental tracers in an aquitard along the full length of a regional groundwater flow system subject to both upwards and downwards hydraulic gradients that have changed over time. Solute profiles for three tracers were measured at five locations along the flowpath, from 22 km inland to 4.5 km from the coast. One dimensional numerical models were developed for each site for analysis with the advection-dispersion equation.

Head predictions over time obtained from the sea level change model presented in Chapter 3 were used to calculate transient vertical hydraulic gradients. These transient vertical hydraulic gradients were then applied to the aquitard solute profile models. Simulation of aquitard chemistry profiles then provides information on aquifer solute concentration changes over periods of thousands of years.

4.2 Theory

The flow of water in low conductivity units is assumed to be vertical, by application of the tangent law of refraction (Fetter 2001). Water moving through an aquifer at almost any angle (σ_1 between 0 - 90°) when it reaches the aquitard interface, will then refract and move at a right angles (σ_2) to the interface surface through the aquitard.

$$\frac{K_1}{K_2} = \frac{\tan\ \sigma_1}{\tan\ \sigma_2} \quad (1)$$

where K_1 is hydraulic conductivity of the aquifer (length/time), K_2 is the hydraulic conductivity of the aquitard, σ_1 is angle of water flow in the aquifer to the aquitard interface, σ_2 is angle of water from the interface into K_2 (aquitard). At almost any angle where a high K unit (K_1=aquifer) is adjacent a much lower K unit (K_2=aquitard) and σ_1 is between 1° and 90°, then $\sigma_2 \approx 90°$.

This flow through aquitards can be considered to be vertical, and the movement of solutes through the aquitard can be described by the one dimensional form of the advection-dispersion equation

$$\frac{\partial(n_e C)}{\partial t} = \frac{\partial}{\partial z}\left(n_e D_e \frac{\partial C}{\partial z}\right) - v_z \frac{\partial C}{\partial z} - \gamma n_e \quad (2)$$

where C is concentration of solute in porewater (M/L^3), D_e is effective diffusion coefficient of tracer (L^2/T), n_e is effective porosity (dimensionless), v_z is effective velocity (L/T), γ is production (M^3/T), t is time, and z is distance (L).

Van Der Kamp, Van Stempvoort et al. (1996) define effective porosity as the proportion of total volume of a porous material that is available for diffusion of water or of solutes. The diffusion of anions across an aquitard is impacted by negatively charged surfaces of minerals which reduces the available porosity (Pearson, Arcos et al. 2003). The porosity for solute transport of anions such as chloride is adjusted to an anion-effective porosity, reported as 0.4 to 0.5 of the total porosity in the literature (Mazurek, Alt-Epping et al. 2009).

Archies law is commonly used to determine effective diffusion coefficients in aquitards (D_e) (Mazurek, Alt-Epping et al. 2009)

$$D_e = D_o\, n^m \tag{4}$$

where D_o is the free solution diffusion coefficient (length^2/time), n is total porosity, and m, an empirical constant.

If solute concentrations in the aquitard are measured in a continuous vertical profile, and the upper and lower boundary conditions are known or assumed, then Equation 1 can be solved either numerically or analytically to solve for velocity, v_z.

If velocity is constant in time, and boundary conditions of aquifer concentrations are also constant, then an analytical solution for concentration of a solute tracer at a distance, z in an aquitard can be derived from Bredehoeft and Papadopulos (1980). .

$$Cz = (C_L - C_0)\frac{\left(exp\left(\frac{v_z z}{De}\right)-1\right)}{\left(exp\left(\frac{v_z L}{De}\right)-1\right)} + C_0 \tag{3}$$

where C_0 is the concentration in the upper aquifer (mass volume), C_L is the concentration in the lower aquifer (mass/volume), z is the distance of measurement where $0 \leq z \leq L$, and L is the thickness of the aquitard.

The limitation of using this analytical solution in aquitards is the assumption of steady state conditions, for both hydraulic and concentration boundary conditions (i.e., constant solute concentrations in the aquifer over time). This solution is also limited to inert tracers.

In coastal systems, vertical hydraulic gradients from sea level change in the last glacial maxima will have changed over timescales similar to the long timescales that may be taken for equilibration of solutes across aquitards. This could limit the use of analytical solutions that assume steady state hydraulic conditions.

The time that solute profiles take to develop following a change in hydraulic conditions will depend upon rates of advection and diffusion. If advection is the dominant transport process, then

$$t_s \approx \frac{L}{v_z} \quad (5)$$

where v_z is vertical velocity (length/time), L is aquitard thickness, and t_s is time to reach steady state.

If diffusion is the dominant transport process then the equilibration rate will be a function of the solute diffusion coefficient.

$$t_s = \frac{(0.5L)^2}{4D_e} \quad (6)$$

Free solution diffusion coefficients of helium, NaCl and deuterium are 2.21×10^{-2} m^2/yr, 5.1×10^{-2} m^2/yr, and 7.16×10^{-2} m^2/yr respectively (Cook and Herczeg 2000). Helium has a more rapid rate of diffusion than chloride so the rate of equilibration across an aquitard for helium is shorter than for chloride. Using equation 6, at the King site, Saskatchewan, Canada, the aquitard is 150 m thick; using the parameters from Hendry and Wassenaar (2011) the time for equilibrium diffusion to the centre of the aquitard (t_s) is ~ 200 kyrs for chloride and ~ 120 kyrs for helium-4.

Determining flux using the advection-dispersion equation requires measuring the concentration of an environmental tracer in aquitard porewaters across the full thickness of aquitard. Tracers currently being used in aquitard studies are anions (Cl-, δ^{37}Cl, Br-, I-), stable isotopes of water (δ^{18}O, δ^{2}H), and noble gases (He, ^{3}He/^{4}He, ^{40}Ar/^{36}Ar). These tracers have been used with success in both Europe and Canada (Hendry and Wassenaar 2009, Mazurek, Alt-Epping et al. 2011, Bensenouci, Michelot et al. 2014, Rebeix, Le Gal La Salle et al. 2014). Helium-4, chloride and deuterium have been used in the Australian setting. Helium-4 was used with success in the Great Artesian Basin

(Gardner, Harrington et al. 2012), and chloride in the Otway Basin (Love, Herczeg et al. 1996) and Great Artesian Basin (Harrington, Gardner et al. 2013). (Harrington, Gardner et al. 2013) found in the Great Artesian Basin that chloride is a more useful tracer than deuterium because a lack of glaciation in Australia to provide a dynamic tracer signal.

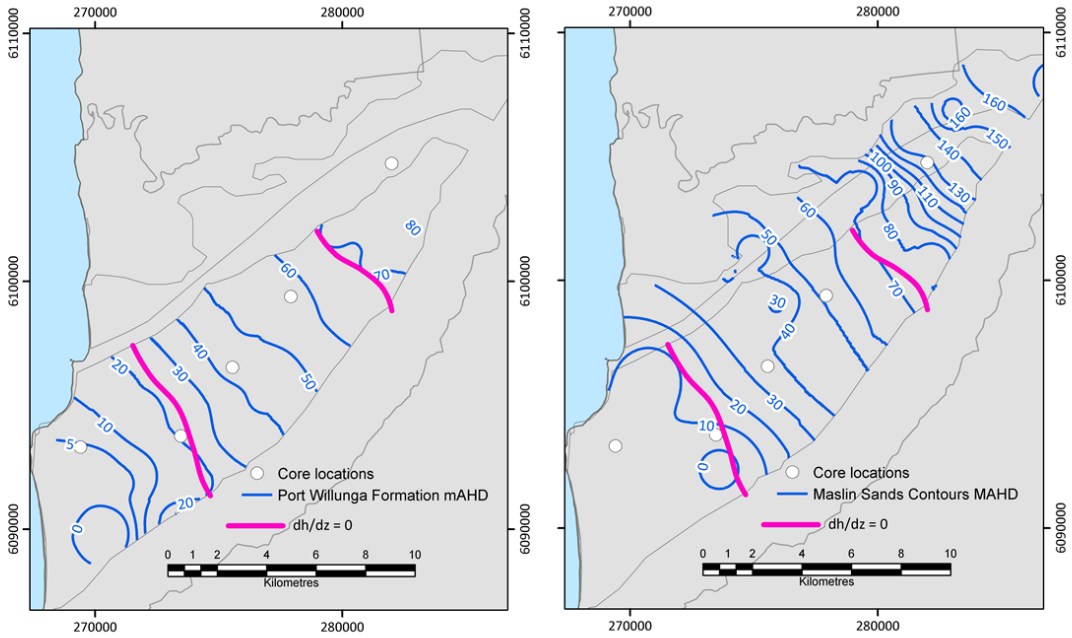

Figure 4.1: Water level of regional aquifers (a) Port Willunga Formation (b) Maslin Sands. The pink line is the point where the heads in between the aquifers are approximately equal, so the vertical gradient across the aquitard is zero. Head data sourced from www.waterconnect.gov.au

A significant feature of the Willunga Basin is that the direction of the vertical hydraulic gradient fluctuates between the two regional aquifers along the flow path (Figure 4.1). The measured vertical gradient across the aquitard is between 0.057 upwards at the top of the Willung Basin, and 0.4 downwards in the centre of the basin (Table 4.4). Groundwater in both aquifers flows from the upper north east of the basin towards the coast in the south west. The two locations where the vertical gradient between the two aquifers is zero is shown by a pink line. In the north west the vertical gradient is upwards, in the central portion the vertical hydraulic gradient is downwards, and nearing the coast the gradient again becomes upwards.

The last major sea level low in the Gulf St Vincent was in the last glacial maxima (LGM) 18 to 22 kyrs BP where the sea level fell to -130 mAHD (Cann, Belperio et al. 1988). Following the LGM, sea levels rose to their current level of 0 mAHD at 7 kyrs before present (BP). Prior to this, sea levels fluctuated and the last major sea level low stand prior to the LGM was 160 kyrs before present at -150 mAHD (Cann, Belperio et al. 1988).

Vertical hydraulic gradient fluctuations in response to the sea level change in the last glacial maxima (30 kyr) were modelled in a 3D regional groundwater model calibrated to head and carbon-14 (Chapter 3). The model showed that the head change was greatest in the Maslin Sands, with a head change of up to 20 m at the coast that propagated 5 km into the aquifer, and only a small head in the Port Willunga formation, which is unconfined. The head predictions from this model were extracted and applied in this study.

4.4 Methods

The data presented in this chapter is presented as locations Sites A to E. These cores were collected from five of the seven locations drilled and sampled in Chapter 3. The correlation of sites between these chapters is shown in Table 4.1.

Table 4.1: Corresponding site locations for Chapters 3 and 4.

Chapter 3 nested piezometers site name	**Chapter 4 corresponding aquitard core**
Site 7	A
Site 6	not cored
Site 5	not cored
Site 4	B
Site 3	C
Site 2	D
Site 1	E

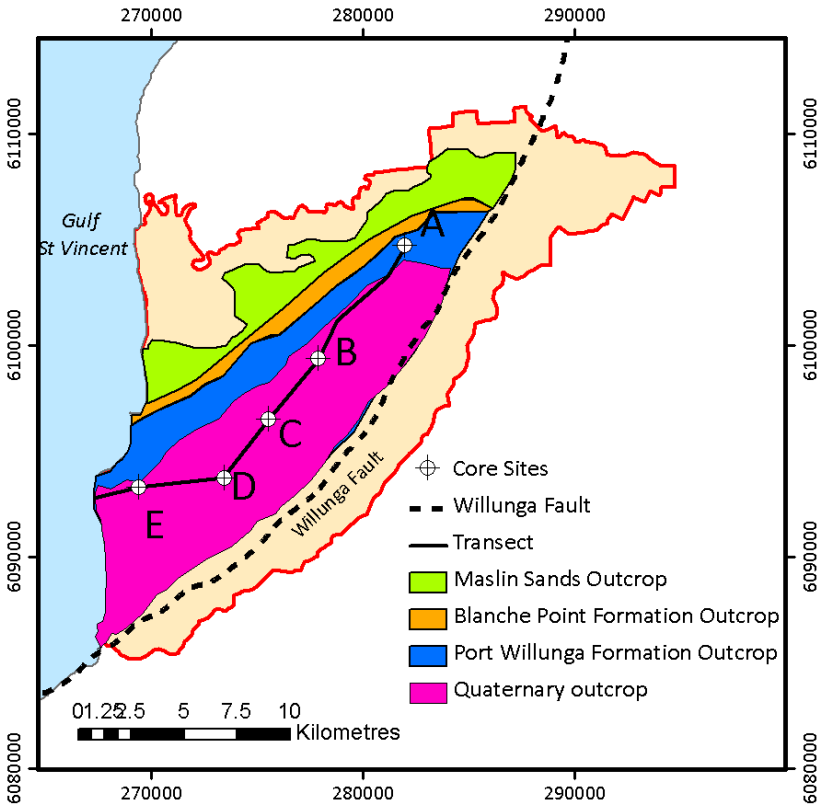

Figure 4.2: Location of sites where cores were sampled.

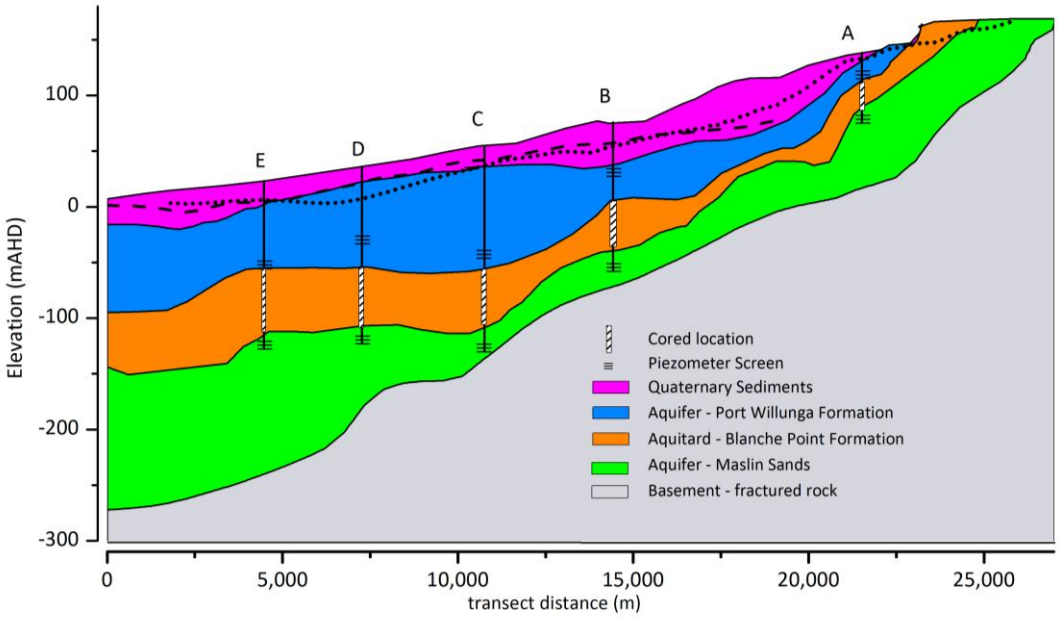

Figure 4.3: Cross section along transect showing the regional aquifers separated by the aquitard. The hatched area shows the depth of each aquitard cored, and the bore screen locations for the upper and lower aquifer boundary conditions.

4.4.1 Drilling and Coring

Solute profiles of aquitard porewater chemistry were constructed from core measurements for chloride, deuterium and helium-4 at five locations (Sites A through E; Figure 4.2). Site A is the furthest up gradient at 22 km from the coast, B through E move closer to the coast, with site E located closest to the coast at a distance of 4.5 km.

A primary drill hole was drilled to a target depth at each of the seven sites, and informed the construction of all remaining well completions. Drilling was by rotary mud, with a 200 mm diameter pick or roller bit (Photo 3, Photo 6).

Wells were constructed in the upper and lower aquifer with a 100mm diameter PVC casing and UPVC 0.5 mm slotted casing or wirewound stainless steel 304 grade screen in high salinity wells. Screens were a maximum of 3m in length. Gravel pack was nominal 7mm rounded quartz gravel blended with 8/16 sand and grouting to surface was undertaken through tremmie line displacement and multiple poly pipe strings. All wells were developed by airlifting for a minimum of three hours through a 2 inch drill stem.

Table 4.2: Drilling sites, piezometer depths and core thickness

	Easting	Northing	Distance from coast (km)	Surface elevation ground level (mAHD)	Upper Aquifer (PWF) Piezometer Screen depth (mbgl)	Lower Aquifer (MS) Piezometer Screen depth (mbgl)	Core thickness (m)
A	282551.2	6105131.9	22	146	24-27	64-67	30
B	277917.2	6099378.7	15	63	44-47	114-117	55
C	275554.8	6096528.7	11.2	60	100-103	182-185	68
D	273464.3	6093756.8	7.7	40	66-68	155-158	82
E	269409.5	6093309.4	4.5	24	77-74	144-147	72

The full thickness of the aquitard was continuously sampled using a diamond drill fitted with a triple core barrel. At 50 cm intervals samples were cut, scraped to remove drill mud, and double sealed on site in vacuum bags (Photo 5). These cores were stored under refrigeration at the end of each day, and were used for all analysis except noble gases. Core samples for noble gas analysis were cut, scraped and sealed in evacuated and nitrogen flushed stainless steel canisters, as shown in Photo 7 (Osenbrück, Lippmann et al. 1998, Gardner, Harrington et al. 2012).

4.4.2 Groundwater

Piezometers were surveyed for accurate measurement of head and calculation of vertical hydraulic gradients. A density correction was made for the head in the piezometer column screened in the lower aquifer at Site E, where the measured chloride concentration of groundwater is 20,664 mg/L. The head correction is given by

$$h_{feq} = h_{mahd} + ((h_{mahd} - L \times \rho_w) - (h_{mahd} - L)) \quad (7)$$

where h_{feq} is the head of water in the piezometer converted a freshwater equivalent, h_{mahd} is the measured head as referenced to the australian sea level (h_{mahd}), water column length is h_{mahd} minus screen depth (L), and ρ_w is density (M/L^3). Density used was 1.026 g/L, equivalent to the density of seawater. At Site E the uncorrected vertical gradient is 0.003 downwards, when corrected for density the vertical gradient is 0.019 upwards. All other groundwater samples in the study were below 670 mg/L Cl- and TDS 1500 mg/L; so density correction was not required.

Purging and sampling of overlying and underlying aquifers was undertaken with a GRUNDFOS SQ1 submersible pump for a minimum of three casing volumes and until monitored parameters had stabilised for pH and EC (Photo 4). pH, EC and temperature were measured continuously using a HACH Multimeter, which was calibrated weekly for pH and EC. Anion samples were collected in 50 mL HDPE containers and analysed by the standardised American Public Health Association (APHA) method 4110, ion chromatography using a Dionex ICS-2500 at CSIRO Land and Water, Adelaide.

Groundwater samples for stable isotopes were collected in 2mL glass vials with no headspace, and analysed by Picarro Laser Water Isotope Analyser V2 at UC Davis, California or Flinders University, Adelaide.

Groundwater samples for noble gas analysis were collected with passive diffusion samplers (Gardner and Solomon 2009) installed at screen depth for a minimum of 7 days, and measured directly using a quadropole mass spectrometer with cryogenic separation (Poole, McNeill et al. 1997) at CSIRO, Land and Water, Adelaide.

4.4.3 Cores

Core samples were sent to the University of Saskatchewan for analysis of gravimetric water content (GWC), bulk density and specific gravity. GWC was determined by drying at 90°C. Bulk density and specific gravity were measured using standard method ASTM 2009:2010. The bulk density and specific gravity were used to calculate total porosity. The ratio is given by

$$n_t = \left(1 - \frac{\rho_{bulk}}{\rho_{specific}}\right) \times 100 \quad (8)$$

where n_t is total porosity (dimensionless), ρ_{bulk} is bulk density (M/L^3), and $\rho_{specific}$ is specific density (M/L^3).

Water was extracted from cores for chloride analysis by both aqueous leaching and mechanical squeezing methods. Aqueous leaching involved drying core samples at 65°C for 24 hours, rewetting with deionised water, shaking for 48 hours, and then extracting the supernatant for analysis. Supernatant was treated with barium nitrate to remove solids, and analysed for chloride by American Public Health Association (APHA) method 4500-Cl^- E using a Lachat QuikChem 8500 series 2 at CSIRO, Land and Water, Adelaide. Porewaters were squeezed from core samples at 65 Mpa, and extracted waters were analysed using Ion Chromatography.

Chloride concentrations from leachate sampes (Cl_{leach}) are a 'diluted' sample containing both anion accessible waters that contain chloride, and water from anion excluded pore spaces that are devoid of chloride (Mazurek, Alt-Epping et al. 2011). In contrast, porewaters from squeezed samples are assumed to contain only waters that are anion accessible or free waters.

The chloride concentrations from the leached samples have therefore been corrected to account for the effect of the dilution from waters in the inaccessible pore space using Equation 8 (Mazurek, Alt-Epping et al. 2009). There are more leach samples than squeeze samples so each leach sample without a corresponding squeeze sample has been corrected with the ratio of the nearest leach and squeeze sample combination.

$$Cl_{corrected} = Cl_{leach} + Cl_{leach}\left(1 - \frac{Cl_{leach}}{Cl_{squeeze}}\right) \quad (9)$$

In addition to this correction, the ratio of these two samples can be used to correct the measured porosity of cores to an 'anion accessible porosity' using Equation 9.

$$n_{ae} = n_t\left(\frac{Cl_{leach}}{Cl_{squeeze}}\right) \quad (10)$$

where n_{ae} is anion accessible porosity, n_t is measured porosity, $Cl_{leach}/Cl_{squeeze}$ is the ratio of chloride concentration of the diluted leach sample to the squeeze sample, where samples are taken from the same depth within the core.

An attempt at analysing deuterium in the cores was made by University of Saskatchewan using the air equilibration method (Wassenaar, Hendry et al. 2008). This method resulted in very poor duplication of results, which is usually associated with high methane samples. These samples were low in methane and the cause of the poor result is uncertain. Deuterium results presented in this paper were obtained from pore waters by squeezing cores at 65 Mpa, and analysis using a Picarro Laser Water Isotope Analyser at the University of Saskatchewan, Saskatoon.

The noble gas canisters with core samples were stored for a minimum of 8 weeks to allow for porewater concentrations to equilibrate with the headspace (Osenbrück, Lippmann et al. 1998). Canisters were sealed under vacuum after several rounds of flushing with N2 gas and vacuum extraction. Headspace gases were measured directly using a quadropole mass spectrometer with cryogenic separation (Poole, McNeill et al. 1997) at CSIRO, Land and Water, Adelaide. Results of helium-4 analysis were corrected for sample loss during sample collection using the following procedure.

Sample loss and excess air from the noble gas samples was established by comparing the ratio of ^{20}Ne measured in the sample to an assumed water equilibration of ^{20}Ne. The assumption is that the concentration of neon-20 in groundwater should remain constant after recharge, as it is not affected by water-rock interactions. The process of recharge can introduce 'excess air' (Heaton and Vogel 1981, Kipfer, Aeschbach-Hertig et al. 2002), which contributes a proportionally higher quantity of neon-20 than the equilibrium, but there should be no loss of neon-20. The ratio is given by

$$R_{Ne} = \frac{^{20}Ne_m}{^{20}Ne_{eq}} \tag{11}$$

where $^{20}Ne_m$ is the concentration of neon-20 in the sample, and $^{20}Ne_{eq}$ is the assumed concentration in recharge water.

If R_{Ne} is less than 1 then the measured sample is assumed to have lost some of the gas during the vacuum sealing of the sample. Gas loss during sampling will also reduce helium-4 concentrations by the same ratio. A correction for helium-4 loss is made by multiplying the inverse of the ratio by the sample helium concentration

$$^{4}He_{corrected} = \frac{^{4}He_m}{R_{Ne}} \tag{12}$$

This correction assumes that no fractionation of gas occurs during the loss process. If R_{Ne} is greater than 1 then no correction was made to helium values. A ratio of greater than 1 assumes that

concentrations include the excess air component and production and has not been corrected. While it is possible that some gas from the porewaters is lost during the sampling process, it is difficult to correct for this loss when the initial quantity of excess air from recharge is unknown.

The basis of this correction is that in process of vacuum sealing the canister degassing of the sample could occur, resulting in the loss of neon-20 and helium-4. Core samples for noble gases will not gain significant helium-4. This correction also assumes that no loss of helium-4 through diffusion to the atmosphere occurs while cores are exposed between drilling and sample collection.

The assumed equilibrium concentrations for neon-20 and helium-4 were 1.67×10^{-7} ccSTP/gwater, and 4.36×10^{-8} ccSTP/gwater respectively, based on a recharge temperature of 15°C and altitude of 100 mAHD (Kipfer, Aeschbach-Hertig et al. 2002). Dissolved gas concentrations in groundwater are dependent on temperature, salinity and pressure (Kipfer, Aeschbach-Hertig et al. 2002). If the assumed recharge temperature was 5°C then the dissolved gas concentrations for neon-20 and helium-4 would be 1.83×10^{-7} and 4.56×10^{-8} ccSTP/gwater, and if the temperature was much warmer at 25°C the concentrations would be 1.54×10^{-5} and 4.22×10^{-8} ccSTP/gwater, so the difference across the potential 20°C temperature range is up to 7%.

4.4.4 Numerical Modelling

Numerical modelling of the solute profiles was undertaken in three steps: (i) steady state flow and concentration boundary conditions (SS), (ii) transient flow with changing vertical hydraulic gradients (Δi), and (iii) transient flow with changing concentration boundary conditions (i.e., aquifer solute concentrations) and vertical gradients (ΔC+Δi). Models with transient boundary conditions were run for 300,000 years.

1. Steady State model (SS). These models tried to match the profiles by using current measured vertical hydraulic gradients, and current aquifer solute concentrations as fixed boundary conditions.

2. Changing hydraulic gradients (Δi). This scenario attempted to match the profiles by applying a changing hydraulic gradient over a period of 20,000 years to replicate the effect of sea level change. These vertical gradients were taken from the 3D model described in Chapter 3.
3. Changing solute concentrations and hydraulic gradients (ΔC+Δi). The third model scenarios used changing solute concentration boundary conditions in both the upper and lower aquifer, as well as the changing hydraulic boundary conditions from step 2.

A 1D numerical model was developed for each core site in Visual Modflow, using Modflow 2000 (Harbaugh, Banta et al. 2000) and MT3DMS (Zheng and Wang 1999). Each model consisted of a single column and row (5 x 5 m) with between 20 and 30 layers. The maximum thickness of each layer is 2.5m. The boundary condition for the upper aquifer head and concentration is applied to the upper node, and the boundary condition for the lower aquifer head and concentration is applied to the lowest node. A uniform K_v (vertical hydraulic conductivity) and n (porosity) field were used within the model. This approach is appropriate in aquitards that are very low velocity environments and where flow is largely one dimensional.

Whilst an aquitard can have several hydraulic conductivity layers, the velocity will be determined by the lowest hydraulic conductivity. Varying hydraulic conductivity in a 1D model would have no effect on the core profile. In many cases where velocity is negligible and diffusion is the dominant solute transport process, then porosity is the significant parameter that influences the rate of solute transport. The change in porosity measured in these cores was very small.

MT3DMS was used to simulate observed distributions of chloride, deuterium and helium-4. Helium-4 was modelled using zero order decay to simulate production, and advective and diffusive transport.

Archies law (Equation 3) was used to estimate effective diffusion coefficients (D_e). Total porosity (n_e) for deuterium and helium-4 is 0.5. Anion effective porosity (n_{ae}) for chloride was 0.4. The empirical exponent, *m* used was 2 for both chloride and helium-4, and 2.5 for deuterium, from (Mazurek, Alt-Epping et al. 2009). The resulting D_e using in modelling for deuterium was 0.00419 m^2/yr, helium-4 is 0.0126 m^2/yr, and for chloride 0.0081 m^2/yr.

Helium-4 production rates in the literature range from 2.4 x 10^{-12} to 2.8 x 10^{-13} ccSTP/gwater/yr (Aeschbach Hertig, Peeters et al. 2000, Solomon 2000, Mazor 2004). A production rate of 2.4 x 10^{-12} ccSTP/gwater/yr was used in this study, in the absence of local uranium and thorium concentrations from the aquifer material to constrain the rate. At this rate of production, the helium concentration of the water in contact with the subsurface would double the assumed recharge concentration of 4.36 x 10^{-8} ccSTP/gwater in 14,000 years. This approach assumes that the rate of production is equal to the release rate of helium-4 (Solomon, Hunt et al. 1996, Smith, Solomon et al. 2013).

Model profile fits were measured using both root mean square error (RMSE) and normalised RMSE (nRMSE)

$$RMSE = \frac{\sum \left(x_m - x_x\right)^2}{N_{obs}}$$

where x_m is the value of the simulated parameter, x_x is the observed value, and N_{obs} is the total number of measured observations.

nRMSE is the RMSE is divided by the range of observed values

$$nRMSE = \frac{RMSE}{x_{max} - x_{min}}$$

In this study a nRMSE of < 30% is considered a reasonable fit.

4.4.4.1 Boundary conditions

1. Steady State model (SS).

Profiles were modelled using current measured vertical hydraulic gradients, and current aquifer solute concentrations as upper and lower boundary conditions (Table 4.4). The profiles were modelled at hydraulic conductivities of 1×10^{-5} m/d, 1×10^{-6}, 1×10^{-7} and 1×10^{-9} m/d.

2. Changing hydraulic gradients (Δi).

The next scenario considered changing hydraulic gradients over the past 20,000 years. The head profile change over time at the upper and lower well screen was taken from the sea level change model presented in Chapter 3. These head gradients were divided by the aquitard thickness to calculate the vertical gradient at each time step. These vertical gradients were then applied to the 1D aquitard models using time dependent constant head boundary conditions. The 3D model did not exactly reproduce the observed head gradients across the aquitard at the core locations, even though the calibration to head and carbon-14 for both aquifers was statistically successful. The modelled vertical gradients from the 3D model were therefore adjusted so that the gradient in the final time step was equal to the measured hydraulic gradient. The difference required to adjust the final modelled gradient output to the current measured gradient was added (or subtracted) to all the modelled gradient time steps. The profiles were modelled at hydraulic conductivities of 1×10^{-5} m/d, 1×10^{-6}, 1×10^{-7} and 1×10^{-9} m/d.

3. Changing solute concentrations and hydraulic gradients (ΔC+Δi).

The final scenarios considered changing solute concentration boundary conditions in both the upper and lower aquifer, as well as changing hydraulic boundary conditions. The concentration boundary conditions were varied manually using the method described below as a starting point to match the observed solute profiles.

This method applied assumes that the profiles are diffusion dominated, so the upper aquifer boundary conditions are modified to control the upper half of the aquitard profile, and the lower half of the profile are modelled by adjusting the lower aquifer concentrations.

The method of determining the boundary condition is by trial and error, however the starting point was chosen by making an educated estimate of the timing and concentration change of the boundary condition using the following method. The lowest and highest concentrations within the aquitard profile are where concentration changes have occurred (points a. and b. in the example given in Figure 4.4). The time for the boundary condition concentration change is calculated using Equation 6, using the depth of the sample in the aquitard to the closest aquifer. The concentration value is estimated to be a value much higher, or much lower than the concentration value in the aquitard. The resulting boundary condition for the upper aquifer is shown in the example in Figure 4.4.

After initial estimates were made using this method, the boundary condition timings and concentrations were manually adjusted to improve the model fit.

The profiles were modelled at hydraulic conductivities of 1×10^{-5} m/d, 1×10^{-6}, 1×10^{-7} and 1×10^{-9} m/d.

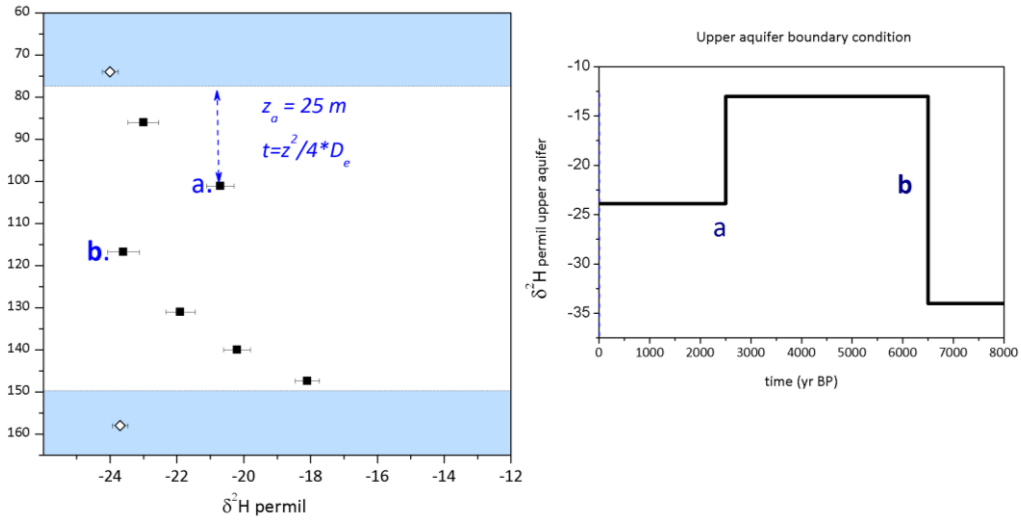

Figure 4.4: Method for determining initial aquifer boundary conditions applied in ΔC+Δi models.

4.5 Results

The lithology of the Blanche Point Formation features lignites, limestones, sandy clays, glauconite, and chert limestone bands. These layers appear laterally discontinuous between each site.

Porosity was measured on 45 samples with values ranging from 0.26 to 0.64, with a mean of 0.5. A porosity value of 0.5 was therefore used for deuterium and helium 4 modelling. Anion effective porosities are calculated from the ratio of $Cl_{leach}/Cl_{squeeze}$ ratio as defined in Equation 9.

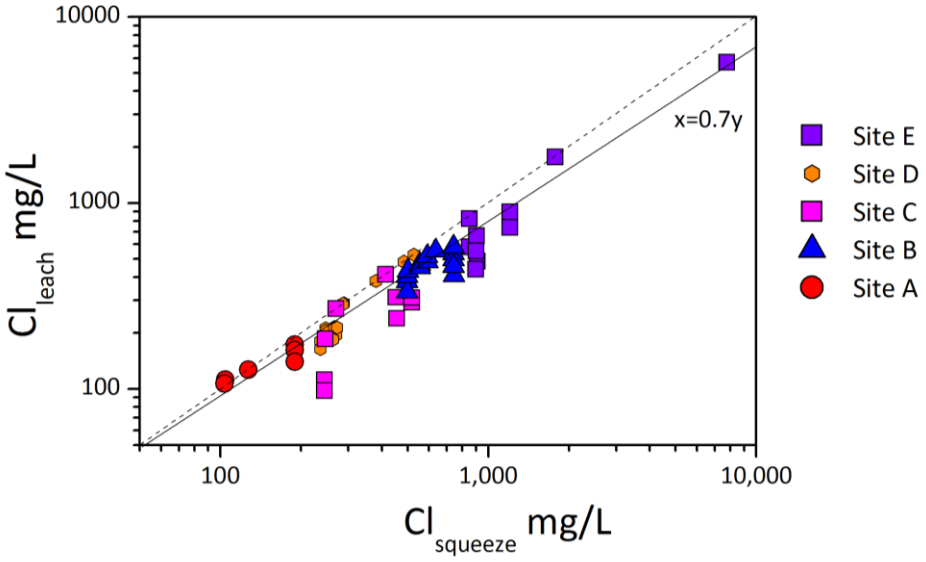

Figure 4.5: Chloride leach concentrations v chloride paste concentrations (aquitard core samples)

Figure 4.5 is a plot of the chloride leach to chloride squeeze samples. 57 leach samples were taken overall. 21 squeeze samples were extracted from cores, and 47 chloride analysis were undertaken on these samples, all duplicates and some triplicates. Corrections were made to all chloride leach samples that are presented in Figure 4.5 based on the squeeze sample results for the corresponding depths of core. 36 pf the 57 samples did not have a corresponding squeeze sample from the same depth, so the closest depth squeeze sample was used to make the correction. The mean ratio of Cl_{leach} to $Cl_{squeeze}$ was 0.7, and the range of ratios was between 0.4 and 1. The mean of 0.7 is higher than the reported literature values of 0.4 and 0.5 reported in Mazurek, Alt-Epping et al.

(2009), and it was noted during drilling that the cores were less consolidated than would be expected of an aquitard, and in some instances had a friable texture.

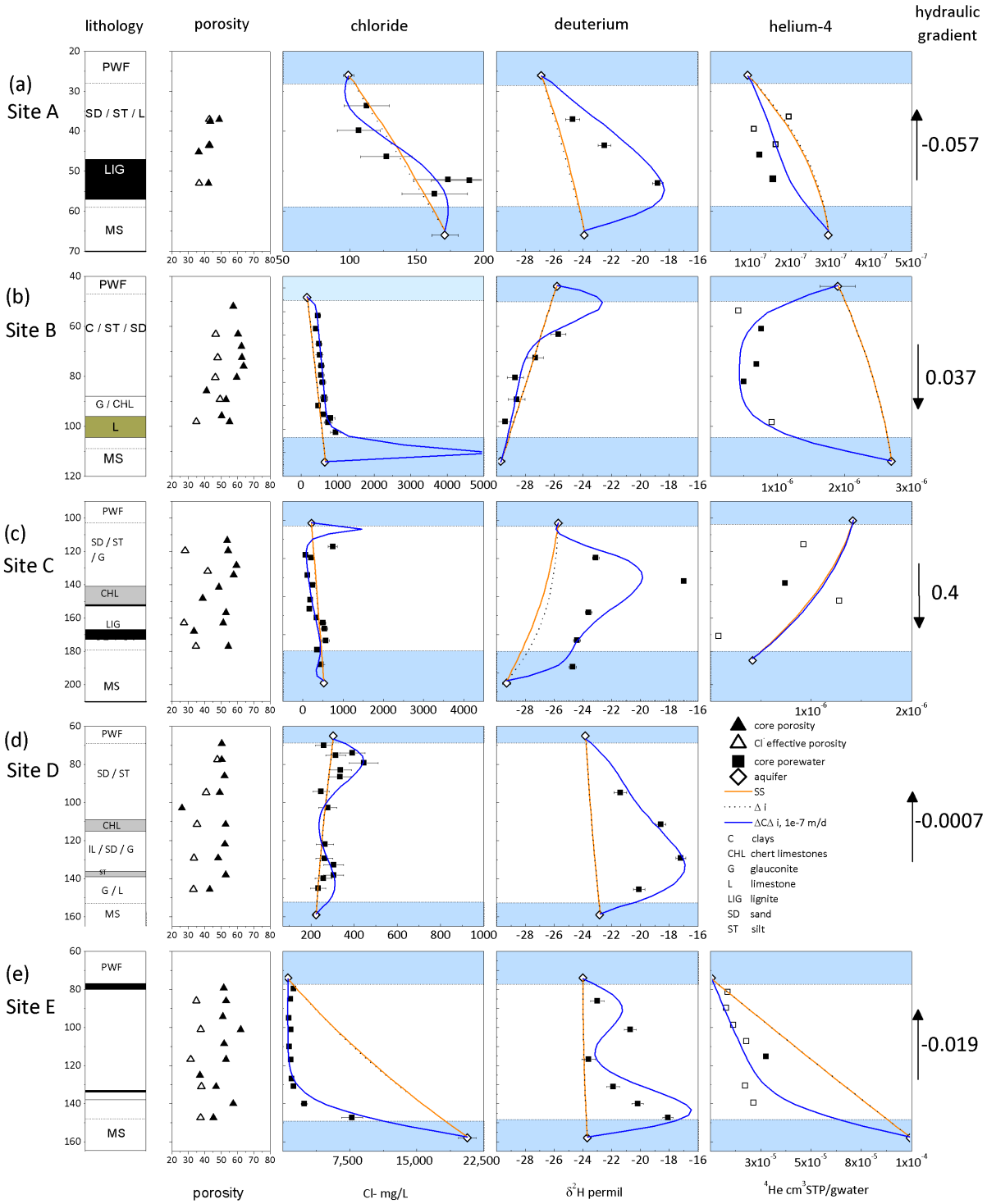

Figure 4.6: Lithology, porosity and solute profiles. All profiles are shown with x axis of tracer concentration, against the y axis of depth, mbgl. Blue shaded regions show the upper and lower aquifer. Measured groundwater samples are

diamond markers, core samples are shown with a square marker, helium corrected samples are an open square. Base case (SS) model results are shown in an orange line, changing hydraulic boundary condition (Δi) model results are a black dashed line, and changing solute concentration (Δi +ΔC) model results are blue.

4.5.1 Steady State models (SS)

In Figure 4.6 the results of the Steady State models are shown by an orange line (SS). The profiles were modelled at hydraulic conductivities of 1 x 10^{-5} m/d, 1 x 10^{-6}, 1 x 10^{-7} and 1 x 10^{-9} m/d however only K = 1 x 10^{-7} m/d are shown. These profiles are generated with the current hydraulic gradient and aquifer solute concentrations (Table 4.4). The RMSE for all steady state profiles across a range of hydraulic conductivities are shown in Figure 4.7, and normalised RMSE results shown in Figure 4.8. Normalised RMSE values are the RMSE divided by the range of observed values, and are a more useful indicator of model success when the value of observations is very large like in some of the chloride profiles. For this study a normalised RMSE of < 30% is considered a reasonable fit. For K values 1x10^{-7} m/d and lower the RMSE does not change as diffusion is the dominant transport process, for K values higher than this advective solute transport changes the fit to the observed solute profiles.

Although the model provides a reasonable fit for some solutes at some sites, there is no single site where the steady state model is a satisfactory fit for all three solute profiles. The chloride profiles at Site A, C and D provide the best model fits for SS models (where nRMSE < 30%) but the deuterium models are not a satisfactory fit to the observed data (nRMSE of 70, 65, and 163%). Even in these profiles the measured chloride concentrations fluctuate, indicating a better fit could be made by changing solute concentrations in the aquifer boundary conditions. At Site B the deuterium model is a reasonable fit for the observed concentrations (nRMSE of 22%), but the chloride and helium-4 models do not provide a satisfactory fit to the observed data (nRMSE greater than 300%).

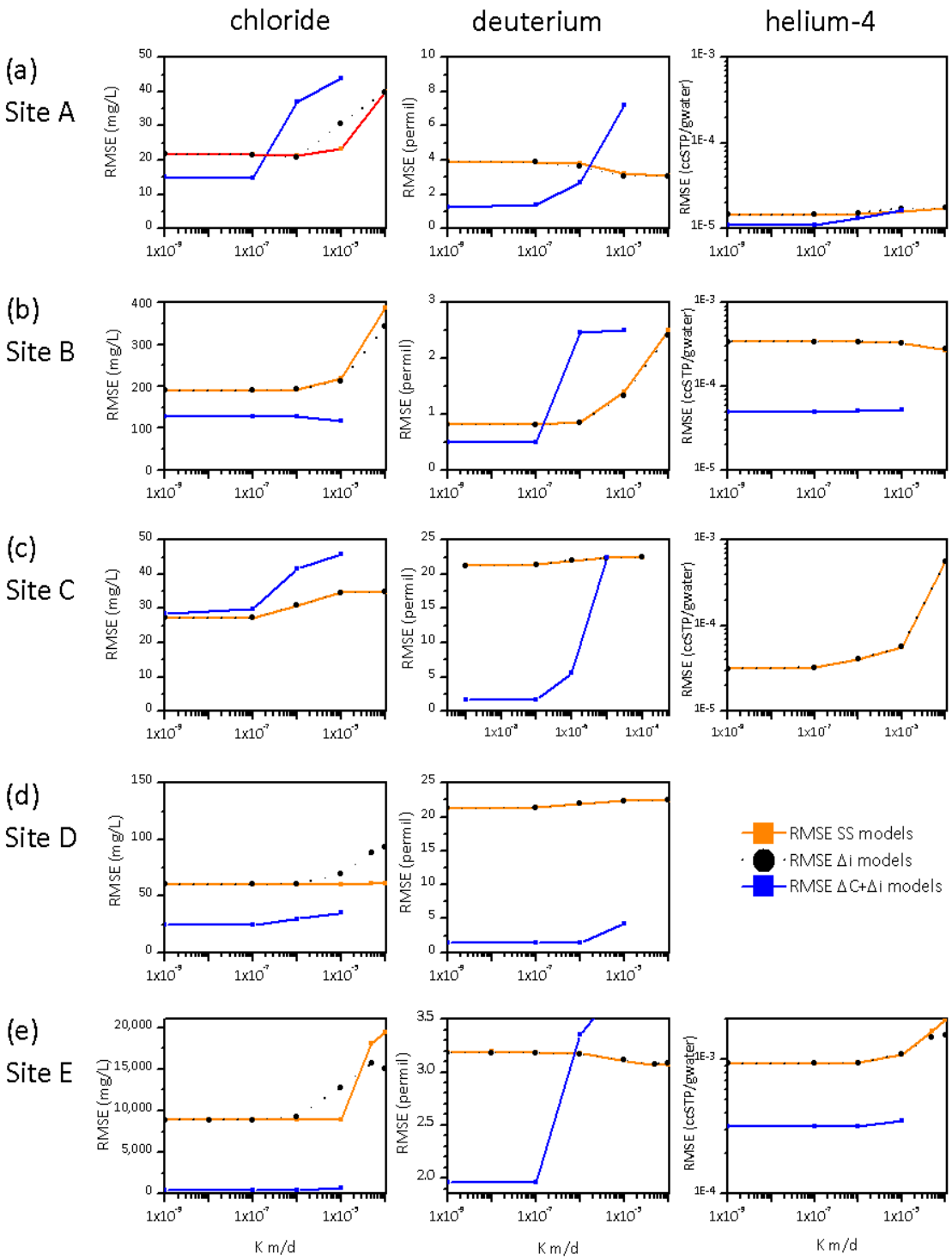

Figure 4.7: RMSE of concentrations for the SS, Δi and Δi +ΔC models (Figure 3.6) for all core profiles across the range of hydraulic conductivities from $1x10^{-4}$ to $1x10^{-9}$ m/d. SS are shown in black, and Δi is shown in orange, and Δi +ΔC in blue. Helium-4 results are presented as a normalised RMSE, where nRMSE = RMSE / $y_{max} - y_{min}$

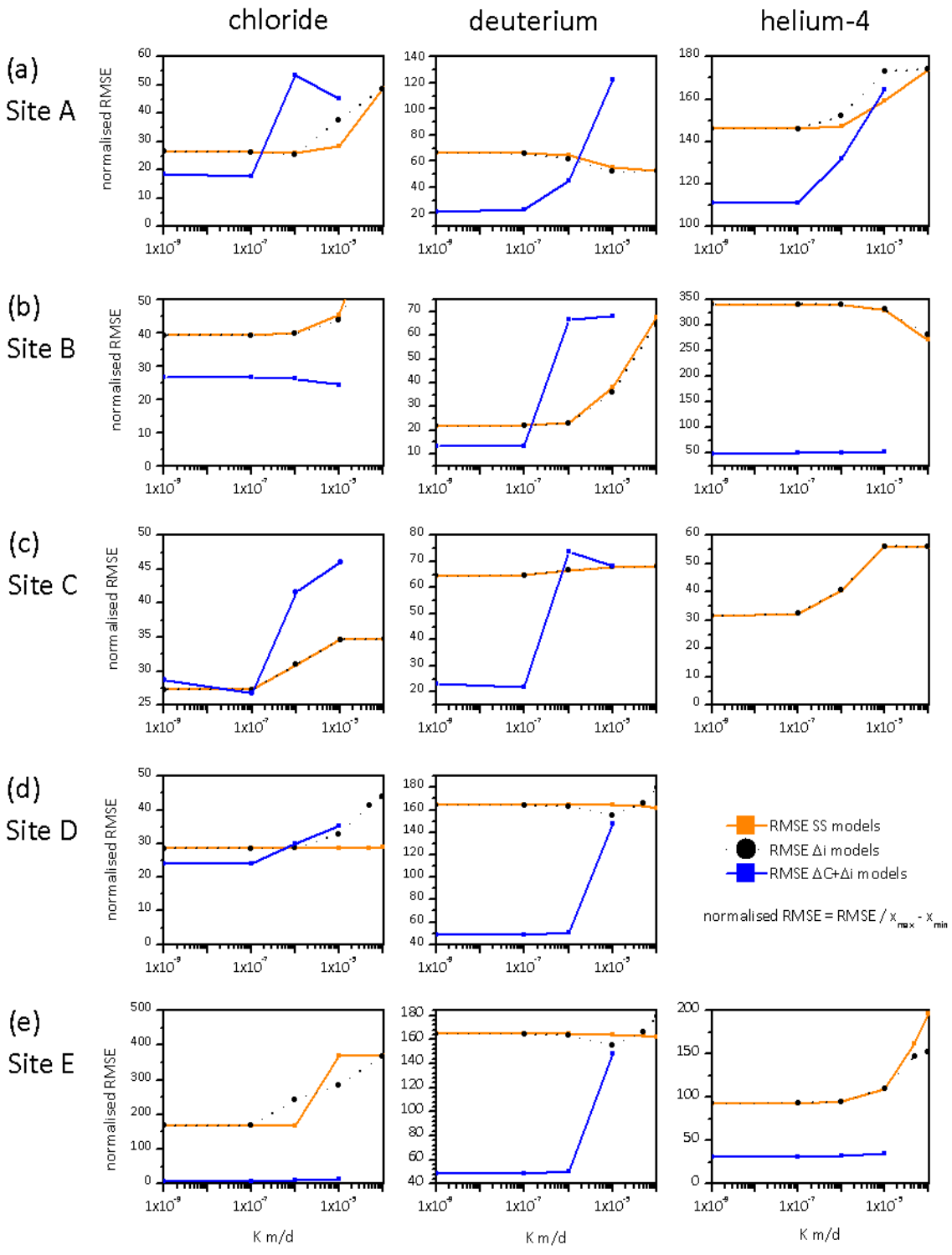

Figure 4.8: Normalised RMSE, where nRMSE (%) = RMSE / ymax – ymin x 100 for all core profiles. SS in black, Δi is shown in orange, and Δi +ΔC in blue. An acceptable model result is considered to be nRMSE below 30%.

4.5.2 Changing hydraulic gradients (Δi)

For these simulations boundary conditions were applied at each site that replicate the vertical hydraulic gradients taken from the best calibrated 3D groundwater flow model, which was run with a transient sea level model boundary condition (Chapter 3). These are shown in Figure 4.9.

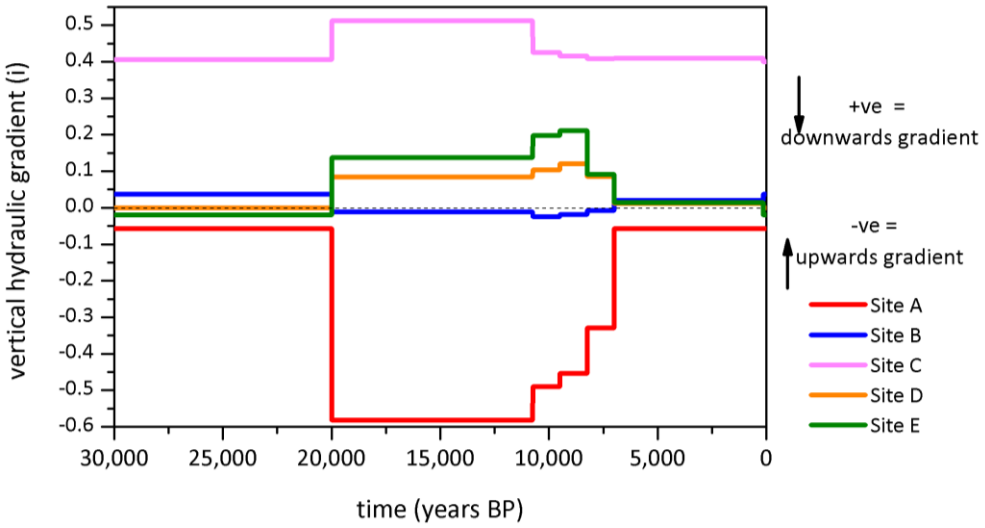

Figure 4.9: Vertical hydraulic gradient boundary conditions (Δi), modified from numerical 3-D model results (Chapter 3).

Figure 3.12 demonstrates how heads change over time in both aquifers in the sea level change model (ΔSL). The head change difference in the Port Willunga Formation between 20,000 and 150 years BP is small, and the propagation distance of the head change through the aquifer is only 3000 m inland. In the Maslin Sands aquifer the model predicts a head decline of up to 20 m close to the coast during the last glacial maxima, and this propagates through the full length of the aquifer.

The resulting vertical hydraulic gradients across the aquitard during the sea level low stand of -130 mAHD are an increasing downward gradient across the aquitard closer to the coast, and an increasing upwards gradient in the upper portion of the system relative to the current hydraulic gradients.

Aquitard profiles that are modelled using the current aquifer concentrations with these changing vertical gradients are shown by a black dashed line in Figure 4.6. Despite a significant change in gradients, the results are not an improvement from the steady state models. In Figure 4.7 and Figure 4.8, the concentration RMSE are the same when K is below $1x10^{-7}$ m/d and diffusive transport dominates. Increasing K to $1x10^{-6}$ m/d and greater introduces some advective solute transport but this does not improve any model results to an nRMSE below 30%.

4.5.3 Changing aquifer solute concentrations (ΔC+Δi)

A prominent feature observed within the solute profiles is that at most sites the concentrations of chloride and deuterium in the aquitard exceed the range of measured concentrations in the bounding aquifers. This means that regardless of any hydraulic gradient changes, it is necessary to change the chloride and deuterium concentrations within the aquifers to successfully model the solute profiles. Helium-4 concentrations in the aquitard above those in the aquifer are expected because helium-4 is produced within the aquitard.

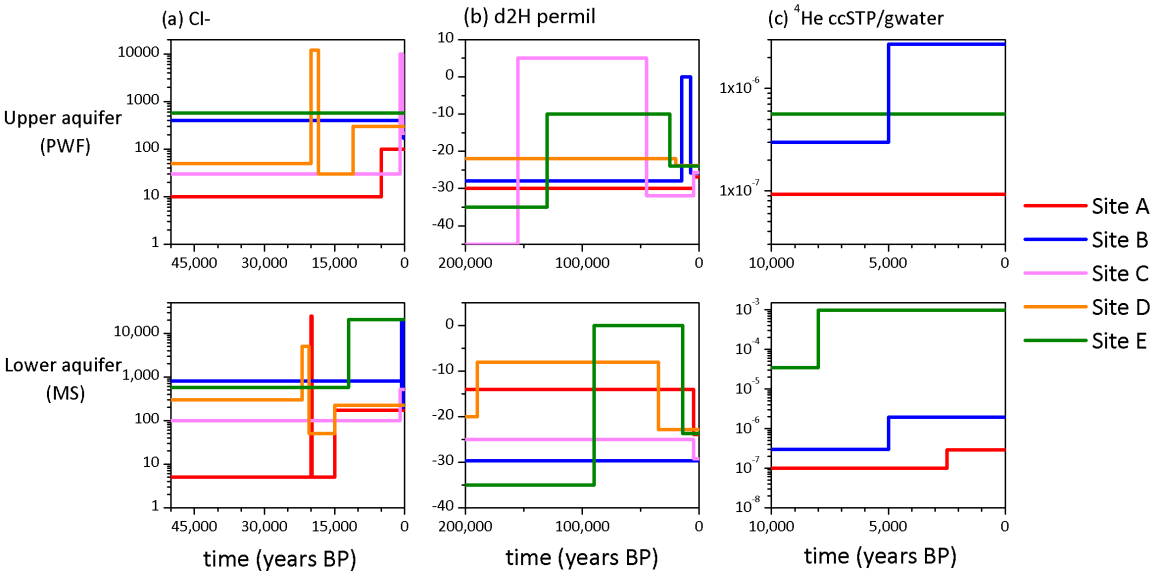

Figure 4.10: Solute concentration boundary conditions that were applied to core models for (a) chloride (b) deuterium (c) helium 4. All models were run for 300,000 years, the shorter time lengths are shown where boundary conditions were varied.

Figure 4.10 describes the aquifer concentration boundary conditions applied to the transient models. The profiles were modelled at hydraulic conductivities of 1 x 10^{-5} m/d, 1 x 10^{-6}, 1 x 10^{-7} and 1 x 10^{-9} m/d however only K = 1 x 10^{-7} m/d are shown on Figure 4.6.

The rationale for the aquifer concentration boundary conditions used in these simulations are the presence of solute concentrations within the aquitard that exceed those in the aquifers. The profiles generated are dependent on the boundary condition concentration and time applied as demonstrated in Figure 4.11. A concentration boundary condition change that is half the magnitude and applied for twice as long can produce a similar profile. The adopted boundary conditions shown in Figure 4.10 therefore only provides an indication of timing and scale of concentration changes in the aquifers that need to have occurred to generate the observed aquitard concentrations. Generally the more pronounced the concentration fluctuation observed in the aquitard core porewaters, the more rapid the concentration change is required in the bounding aquifer.

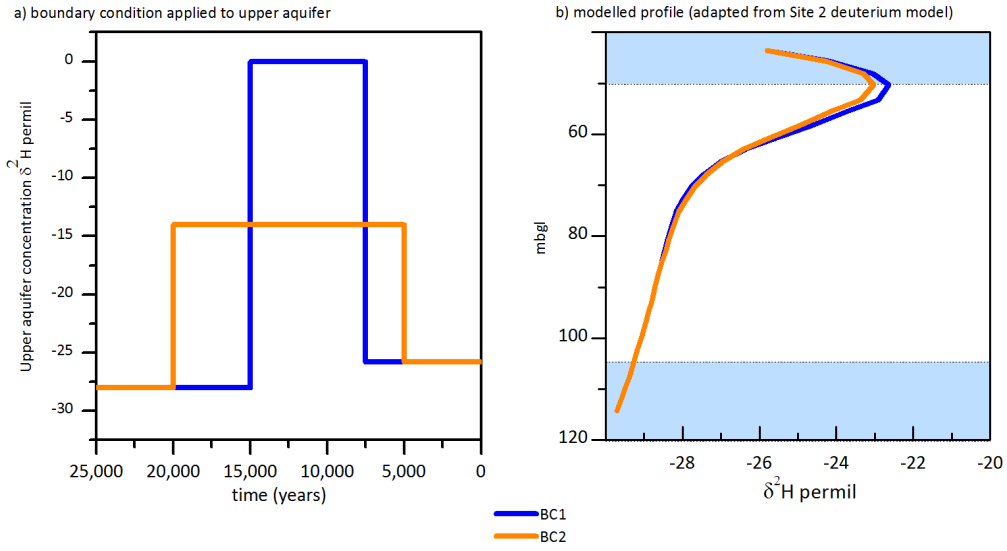

Figure 4.11: Two different boundary conditions are applied in the upper aquifer of the same model to demonstrate influence of concentration and timing. a) concentration vs time of boundary conditions, BC2 is half the concentration of BC1, and applied for twice as long b) depth vs modelled concentration profiles for BC1 and BC2, when applied to the upper aquifer. The lower aquifer boundary condition is constant for all time (-29.7 δ^2H permil).

4.5.3.1 Chloride

Chloride concentrations in the aquitard porewater at sites A, B, C and D vary beyond the current aquifer concentrations (Figure 4.6). Chloride profiles at Site C and D show two peaks in concentration in the upper and lower half of the aquitard, with a lower concentration in between.

To improve model fits to below 30% nRMSE, the following boundary conditions were used. At 20 kyrs BP a peak in chloride concentrations up to 25,000 mg/L is modelled in the upper aquifer at Site D, and in the lower aquifer at Sites A, D and E. At 9 kyrs BP a peak in chloride concentration to 10,000 mg/L was modelled in the upper aquifer at Site C. At Site B, a further peak in concentration of 10,000 mg/L is modelled at 700 yrs BP. The high chloride concentration in the aquitard at Site E is modelled to have increased in the lower aquifer 8000 years before present (Figure 4.10).

4.5.3.2 Deuterium

Deuterium values in the aquitard porewater profiles are more enriched than the aquifers at Sites A, C, D and E. Only the concentrations at Site B are within the range of the current aquifer boundary conditions.

The deuterium profiles show a single enriched peak for Sites A to D, and two enrichment peaks at site E. At sites A and D the enriched deuterium compositions are within the lower part of the aquitard profile, the change in concentration was modelled within the lower aquifer. At sites B and C the enriched deuterium compositions are within the upper half of the aquitard, so the change in concentration was modelled from the upper aquifer (Figure 4.10).

Model simulations indicate that enriched δ^2H waters occurred in the upper and lower aquifers both prior and post the last glacial maxima. Enriched deuterium of up to 5 δ^2H permil are modelled prior to 25 kyr BP at Sites E and D in the lower aquifer, and Sites E and C in the upper aquifer. More recent enriched aquifer conditions were modelled in the upper aquifer at Site B at 7 kyr BP, and in the lower aquifer at Site A prior to 5 kyrs BP. The models indicate that the current aquifer range

between -22 to -30 δ^2H permil has been in place for the last 5000 years, coinciding with the late Holocene (7000 years) and the current sea level of 0 mAHD.

4.5.3.3 Helium

Helium-4 concentrations in the aquifer and aquitard porewaters increase from Site A to Site E down the flow path, which is expected from production of helium-4 within the aquifers and aquitard. In three sites the helium concentrations are higher in the aquitard than in the adjacent aquifers. Higher helium in the aquitard occur at Site B, at Sites A and E closest the deeper aquifer, and at Site C near the shallower aquifer.

Sites A and C potentially represent diffusion profiles between upper and lower end member concentrations and the base case models would be suitable. At Sites A the lower aquifer helium-4 concentration is higher than would be anticipated based on the aquitard porewater concentrations, and was modelled by increasing the concentration in the lower aquifer at Site A at 5000 years BP

At Site C, the deeper aquifer helium-4 concentration is less than the shallower aquifer. This is counter intuitive, as the deeper aquifer has a longer flow path than the upper aquifer, and the upper aquifer is assumed to be recharged through the Quaternary sediments along the full length of the flow path (Chapter 2). The steady state model is able to adequately represent the profile, but the profile shows that older water exists over younger waters at this location, which is unlikely. Carbon-14 data from this location indicate that waters in the upper aquifer are younger than the lower aquifer (Chapter 2).

Helium-4 at Site E was modelled by changing the aquifer concentrations, by increasing the helium-4 concentration of the lower aquifer at 8000 years.

Site B is the most perplexing profile. Site B was modelled by having lower concentrations in the upper and lower aquifer, and then increasing to the current concentrations 5000 years before present, which improved the nRMSE to below 30%. The helium-4 concentrations in both the upper

and lower aquifers exceed the helium-4 concentrations in the aquitard porewaters. It is possible that helium could have been removed from the core during degassing of the sampling canisters (Photo 7). However all the samples in this profile (Site B), except the samples closest the upper and lower aquifer, had concentrations of neon-20 in excess of the assumed atmospheric equilibrium concentration. This indicates that the samples contained excess air in accordance with the bulk of groundwater samples measured within the Willunga Basin, so gas loss appears unlikely. It could be possible in the short time that the cores were exposed to the atmosphere between drilling and sampling that diffusion of helium-4 to the atmosphere occurred. The process of fractionation would mean that helium-4 would be lost more rapidly than neon-20. During drilling it was noted that the cores were sometimes friable in texture so this is considered a possibility, but at this site the cores were relatively solid.

4.5.4 Fluxes

The model results indicate that the hydraulic conductivity of the aquitard is $1x10^{-7}$ m/d or lower; at higher values of K the model fits become poorer.

Based on a K value of $1x10^{-7}$ m/d or less and the measured vertical hydraulic gradients across the aquitard the maximum flux through the aquitard would be 0.014 mm/yr at Site C. This site is located in the centre of the basin, with a hydraulic gradient of 0.4 in the downwards direction.

The smallest maximum flux occurs closest the coast, Site D, at $2.6x10^{-5}$ mm/yr in the upwards direction where the head gradient is -0.0007, and Site E adjacent the coast of with a maximum flux of $6.9x10^{-4}$ mm/yr in the upwards direction. The two furthest inland sites have a maximum flux of 0.002 mm/yr upwards at Site A, and 0.001 mm/yr downwards at Site B.

Table 4.3 provides an estimate of the regional flux based on approximated surface areas of the aquitard, the measured vertical hydraulic gradients and an estimated maximum hydraulic conductivity of 1×10^{-7} m/d (3.65×10^{-5} m/yr). The sum of the total regional flux between the

aquitard and aquifers is 283 m^3/ year in the downwards direction, or 284 kL/yr. Most of the flux is calculated at the centre of the basin, where the vertical hydraulic gradient is two orders of magnitude greater than all other measured vertical gradients, at 0.4. The overall estimated sustainable yield of the aquifers is 6000 ML/yr, so the proportion of water moving from the aquitard to the aquifers is a very small compared to recharge. It should be emphasised that these leakage rates are maximum values, based on the maximum values for K_v from the aquitard modelling.

Table 4.3: Estimated regional vertical flux across aquitard where Kv is 1 x 10^{-7}m/d

Site	Q (m^3/yr)	K_v (m/yr)	i	Area (m^2)
A	-41	3.65E-05	-0.0572	19,700,000
B	34	3.65E-05	0.037	25,400,000
C	310	3.65E-05	0.4	21,200,000
D	1	3.65E-05	0.0007	23,700,000
E	-20	3.65E-05	-0.019	28,600,000

4.6 Discussion

The models show the K_v of the aquitards is a maximum of 1 x 10^{-7} m/d, but possibly lower. This vertical hydraulic conductivity is the point where diffusion becomes the dominant solute transport mechanism and not advection. The optimised 3D regional model from Chapter 3 resulted in a K_v value for the aquitard of 2.36 x 10^{-12} m/d, 5 orders of magnitude lower. Permeability tests on cores in the literature measured the K_v as being between 5.9 x 10^{-13} to 1.5 x 10^{-15} m/d.

The results indicate that the current hydraulic gradients and groundwater solute concentrations in the aquifers can not explain the development of the aquitard solute profiles, and that solute concentration changes in the aquifers are required to model these profiles (ΔC+Δi results). Modelling of solute profiles by altering concentrations in the aquifer boundary conditions has been used in the past to infer how aquifers have changed over time. These studies have not included the changing vertical hydraulic gradients.

Mazurek, Alt-Epping et al. (2011) modelled solute tracers profiles for 9 sites across Europe, all solute profiles with the exception of one site (Boom Clay at Essen) reflected transient conditions, generally with higher concentrations in the aquitards than the aquifers. For example, modelling of a chloride profile Couch Silteus at Marcoule France required initial concentrations up to 25,875 mg/L,where current aquifer conditions were less than 1000 mg/L. The shapes of the profiles enabled a different modelling approach than applied here to generate aquitard concentrations by modifying the aquifer boundary conditions. Mazurek, Alt-Epping et al. (2011) modelled the solute profiles by allowing the initial aquitard concentrations in all nodes to be set at the highest concentration of the solute profile, and then applied aquifer boundary conditions at current concentrations to commence at different times (in the millions of years) to determine the time that the current aquifer concentrations occured. The aquitards in the European study were all between 200 and 1000 m thick so profiles were modelled over millions of years, whilst our study of the Willunga Basin has aquitard thicknesses between 30 and 90m, so the time taken to develop the profiles is much shorter.

Love, Herczeg et al. (1996) found that in the Otway Basin, South Australia, the range of deuterium and chloride was also higher in the aquitard than in the aquifers, although the chloride are only up to ~ 8000 mg/L and dueterium up to -15 δ^2H permil. These cores were only up to 50 m thick, so the times taken for diffusion are similar to those in this study of the Willunga Basin.

Solute transport in aquitards resulting from changes in concentration in bounding aquifers are a result of both advection and diffusion processes, dependent on the hydraulic conductivity of the aquitard. In this study diffusive solute transport was shown to be dominant when the hydraulic conductivity of the aquitard is $1x10^{-7}$ m/d or lower. At K values greater than $1x10^{-6}$ m/d advective solute transport becomes evident. The best model fits were acheived at K ≤ $1x10^{-7}$ m/d and lower.

Different aquifer boundary conditions can produce similar results for the modelled aquitard profiles. In the case ofa short period of increase aquifer concentrations, the concentration boundary condition in an aquifer can be doubled and applied for only half the time to produce the same model profile. Despite this, the timing of an aquifer concentration change is approximately constrained by the depth of the change in solute concentration in the aquitard. With the timing constrained, it is therefore possible to establish the scale of the concentration change in the aquifer.

Some estimates can therefore be made of how aquifer concentrations have changed in the past. The models show two time periods where aquifer chloride concentrations have increased, at around the time of the last glacial maxima and a more recent increase within the Holocene. In the models the maximum boundary condition concentration was 25,000 mg/L. Site E, closest to the coast has a current chloride concentration measured in the lower aquifer of 20,664 mg/L, and the modelling approach leads us to conclude that the chloride concentration of the groundwater would have increased around 22 kyrs BP. This timing coincides with the sea level low stand of the last glacial maxima, but the mechanism of how such an increase in chloride occurs in unclear. Common methods of increasing chloride concentrations would be evaporation processes or sea water

intrusion, but this sample is deep beneath the surface and the timing is at sea level decline away from the coast.

Increased chloride concentrations in groundwater used in the model scenarios are not unrealistic for groundwater in this region. Several groundwater sites sampled in the Willunga Basin and wider St Vincent Basin have observed hypersaline waters, with measured chloride concentrations up to 80,000 mg/L (Post and Banks in press).

The enrichment of deuterium in the groundwater at each site was modelled as occurring around the last glacial maxima. In the last 5,000 years all deuterium were modelled as being within the current aquifer range of -20 to -30 permil; however a chloride increase was modelled to have occurred within the last 1000 years.

Studies have shown that in this region, the period of warming since the last glacial maxima occurred in two rapid stages, interrupted by a cooling phase, with further cooling during the late Holocene (6 kyr BP to now) (Calvo, Pelejero et al. 2007, Petherick, Bostock et al. 2013, Reeves, Barrows et al. 2013). The last glacial maxima had a colder drier climate with increasing $\delta^{18}O$ values, deglacial warming periods associated with warmer sea surface temperatures and periods of increased precipitation, yet were broken by the Antarctic cold reversal a rapid period of cooling. Climate trends from 10 kyr BP to the present show decreasing ocean $\delta^{18}O$ values, and a progressive decrease in sea surface temperature from 6.5 kyr to modern times (Calvo, Pelejero et al. 2007), with a period of increased precipitation between 6 and 8 kyr (Petherick, Bostock et al. 2013). This rapidly changing climate appears to have caused changing aquifer conditions beyond the influence of sea level change that makes the use of solute tracers to measure flux difficult. Deuterium values are assumed in this study to behave in a similar way to $\delta^{18}O$ values from the climate studies cited herein.

Sources of enriched deuterium compositions in groundwater could have originated from evaporated seawaters, or from these changing climatic conditions. The range of deuterium

measurements in the aquitard and aquifers are within the range of the precipitation record for Adelaide, −76.9 ~ 18.8 δ^2H permil recorded from 1962 (Liu, Fu et al. 2010). The range of deuterium measured in the aquifers of the Willunga basin is between -15.5 and -27.9 δ^2H permil (Table 3.6).

The inability of the current helium-4 concentrations in the aquifers to constrain the concentrations in the aquitard porewaters complicates the analysis of this data. Within the normal expectations of error in the core sampling or analysis, the helium-4 concentrations within the aquitard are still significant showing water of long residence times that increase down the flow path as expected. The fitted models for Site A, B and E have assumed changing aquifer conditions, including increasing the helium-4 concentrations at two sites. The mechanisms of how this could occur in an aquifer are difficult to explain and justify. Possibilities include a reversal of horizontal hydraulic gradients, moving older water 'up' the aquifer, or an increased flux of helium-4 from deeper aquifers, potentially induced by pumping. In terms of human induced system changes, land clearing in the Willunga Basin occurred 150 years ago, and groundwater extraction around 30 years ago. The modelling indicates that if aquifer conditions have changed, then the high diffusion rate of helium constrains this change to occurring within the last 8000 years, coinciding with the Holocene.

4.7 Conclusion

This study shows that the use of environmental tracers to measure flux in this coastal groundwater system is not complicated by transient hydraulic conditions, but by changing solute concentrations within the groundwater.

Modelling demonstrates that current aquifer concentrations and vertical hydraulic gradients do not provide an adequate explanation of how these aquitard solute profiles were developed. Numerical modelling of the profiles was only possible through altering the concentration boundary conditions of the upper and lower aquifers over time, for all three tracers, chloride, deuterium and helium-4. Chloride and deuterium boundary conditions were required to be hypersaline and enriched at times. The modelling of helium profiles again required changing aquifer conditions to

provide an adequate fit to the aquitard profiles, within the last 8000 years. Using the solute profiles we are able to resolve the upper limit of the hydraulic conductivity of the aquitard to $1x10^{-7}$ m/d. The maximum downward flux is 0.014 mm/yr at Site C in the centre of the basin, and maximum upward flux is 0.002 mm/yr at Site A the high point in the basin. An estimate overall flux from the aquitard to the aquifers is made of 284 kL/yr downward, which is a very small proportion of the overall water balance for Willunga Basin. Most of this flux is calculated to occur at the centre of the basin where the vertical hydraulic gradient is highest at 0.4.

A rapidly changing climate as identified in previous studies appears to have caused changing aquifer conditions beyond the influence of sea level change, making the use of environmental tracers to measure aquitard flux difficult. Whilst dynamic groundwater solute conditions limit the usefulness of the technique to measure flux across an aquitard, they do provide longer term insights into groundwater evolution and what might be expected in system variability for future management.

Table 4.4: Aquifer solute concentrations and parameters for steady state models

			Chloride		Deuterium		Helium 4	
			D_e 0.0081 m^2/yr		D_e 0.00419 m^2/yr		D_e 0.0126 m^2/yr	
			n_e 0.4		n_e 0.5		n_e 0.5	
							γ 2.4x10^{-12} $cm^3STP/gwater$	
	Aquitard thickness (m)	Vertical hydraulic gradient	PWF (mg/L)	MS (mg/L)	PWF (permil)	MS (permil)	PWF (cm^3STP/gwater)	MS (cm^3STP/gwater)
A	30	↑ -0.0572	99	171	-26.9	-23.9	9.25x10^{-8}	2.93x10^{-7}
B	55	↓-0.037	170	670	-25.8	-29.7	1.96x10^{-6}	2.65x10^{-6}
C	68	↓ 0.4	214	523	-25.7	-29.3	1.42 x10^{-6}	4.21 x10^{-7}
D	82	↑-0.0007	304	224	-23.8	-22.8	-	-
E	72	↑-0.019	570	20,664	-24	-23.7	5.64x10^{-7}	9.92x10^{-5}

Chapter 5 Conclusions

5.1 Summary of findings

The studies presented in this thesis investigate how the use of environmental tracers in a coastal connected aquifer-aquitard system to determine recharge and aquitard flux are influenced by changes in climatic conditions during the last glacial maxima. Numerical modelling outputs of hydraulic changes from sea level variation from a 3D regional groundwater flow model were used in 1D models of five aquitard sites, to better understand how these processes influence solute transport and flux.

The key findings from the studies are as follows:

1. The process of sea level change in the aquifers was shown to change the heads in the aquifers by up to 20 m near the coast in the confined aquifer, but did not result in a significant difference in carbon-14 distributions when compared to a steady state coastal boundary condition model. The largest change in carbon-14 concentrations was nearest the the coast, up to 3 pmC.
2. The use of carbon-14 as an additional target in calibration was shown to improve the estimate of recharge by providing calibration results with a narrower range of best fits, while the model fit to heads was shown to be non-unique and not able to reliably predict recharge.
3. A chloride mass balance using local data predicts recharge of 15-16 mm/yr to the aquifers, and the model calibration predicts a post-land clearing (0-150 yrs BP) recharge between 15 and 60 mm/yr, with pre-land clearing recharge of 15 to 55 mm/yr.
4. Changing vertical hydraulic conditions were shown not to have an influence on solute transport within the aquitard. The maximum hydraulic conductivity is constrained to $1x10^{-7}$ m/d where the dominant solute transport process across the aquitard is diffusion.

5. Dynamic groundwater solute conditions limit the usefulness of solute profiles to measure flux across an aquitard. These profiles do provide insights into the longer term chemistry of groundwater and past climate.
6. This rapidly changing climate appears to have caused changing aquifer conditions beyond the influence of sea level change that makes the use of solute tracers to measure flux difficult.

Further work could clarify further how recharge has varied temporally over several climatic changes in the region. The mechanism by which aquifer chemistry has also changed is uncertain. The aquitard modelling constrain the increase in chloride concentrations of the aquifer up to ~20,000 mg/L to occurring around 18,000 years ago, but the mechanisms for this increase in the deep aquifer is unclear.

References

Aeschbach Hertig, W., F. Peeters, U. Beyerle and R. Kipfer (2000). "Palaeotemperature reconstruction from noble gases in ground water taking into account equilibration with entrapped air." Nature **405**(6790): 1040-1044.

Aldam, R. (1990). Report Book 90/71 Willunga Basin Groundwater Investigation Summary Report, Groundwater and Engineering, Department of Mines and Energy, Government of South Australia.

Allison, G. B., P. G. Cook, S. R. Barnett, G. R. Walker, I. D. Jolly and M. W. Hughes (1990). "Land clearance and river salinisation in the western Murray Basin, Australia." Journal of Hydrology **119**(1–4): 1-20.

Allison, G. B. and M. W. Hughes (1978). "The use of environmental chloride and tritium to estimate total recharge to an unconfined aquifer " Australian journal of soil research, CSIRO Division Of Soils: pp.181-195

Appelo, C. A. J. and D. Postma (2005). Geochemistry, groundwater and pollution, 2nd edition Leiden : Balkema

Batlle-Aguilar, J. and P. G. Cook (2012). "Transient infiltration from ephemeral streams: A field experiment at the reach scale." Water Resources Research **48**(11): W11518.

Bensenouci, F., J. L. Michelot, J. M. Matray, S. Savoye, M. Massault and A. Vinsot (2014). "Coupled study of water-stable isotopes and anions in porewater for characterizing aqueous transport through the Mesozoic sedimentary series in the eastern Paris Basin." Marine and Petroleum Geology **53**(0): 88-101.

Bethke, C. M. and T. M. Johnson (2008). "Groundwater age and groundwater age dating." Annual Review of Earth and Planetary Sciences **36**: 121-152.

Bourman, R. P. and N. F. Alley (1999). "Permian glaciated bedrock surfaces and associated sediments on Kangaroo Island, South Australia: Implications for local Gondwanan ice-mass dynamics." Australian Journal of Earth Sciences **46**(4): 523-531.

Bredehoeft, J. D. and S. S. Papadopulos (1980). "A method for determining the hydraulic properties of tight formations." Water Resour. Res. **16**(1): 233-238.

Brown, K. G. (2004). Groundwater contributions to streamflow along Willunga Fault, McLaren Vale, South Australia.

Calvo, E., C. Pelejero, P. De Deckker and G. A. Logan (2007). "Antarctic deglacial pattern in a 30 kyr record of sea surface temperature offshore South Australia." Geophysical Research Letters **34**(13).

Cann, J. H., A. P. Belperio, V. A. Gostin and C. V. Murray-Wallace (1988). "Sea-level history, 45,000 to 30,000 yr B.P., inferred from Benthic foraminifera, Gulf St. Vincent, South Australia." Quaternary Research **29**(2): 153-175.

Canyon, P. L. (1998). Enchilada 1 Well Completion Report. Adelaide, Australia, Primary Industries and Resources, South Australian Government.

Castro, M. C. and P. Goblet (2005). "Calculation of ground water ages—A comparative analysis." Ground Water **43**(3): 368-380.

Clark, I. and P. Fritz (1999). Environmental Isotopes in Hydrogeology, CRC Press, Taylor and Francis Group.

Clark, I. D. and P. Fritz (1997). Environmental isotopes in hydrogeology. Boca Raton, FL, CRC Press/Lewis Publishers.

Cook, P. G. and A. L. Herczeg (2000). Environmental Tracers in Subsurface Hydrology, Kluwer Academic Publishers.

Cook, P. G. and D. K. Solomon (1997). "Recent advances in dating young groundwater: Chlorofluorocarbons, H-3/He-3 and Kr-85." Journal of Hydrology **191**(1-4): 245-265.

Cooper, B. J. and J. G. McKenzie (1979). Eocene to miocene stratigraphy of the Willunga embayment / by B.J. Cooper ; with an appendix Notes on ostracoda from Willunga embayment boreholes WLG38, WLG40 and WLG42 by K.G. McKenzie. G. S. o. S. A. Dept. of Mines and Energy, Adelaide : Govt. Pr., 1979.

Denham, T., C. Lentfer, E. Stuart, S. Bickford and C. Barr (2012). Multi-disciplinary investigation of 19th century European settlement of the Willunga Plains, South Australia. Terra Australis 34 Peopled landscapes : archaeological and biogeographic approaches to landscapes. S. G. Haberle and B. David. Australian National University, ANU E Press. **34**.

Doherty, J. (2010). PEST Model Independent Parameter Estimation.

Drexel, J. F. and W. V. Preiss, Eds. (1995). The Geology of South Australia. Vol 2, The Phanzerozic, South Australia Geological Survey.

Engdahl, N. B., T. R. Ginn and G. E. Fogg (2013). "Using groundwater age distributions to estimate the effective parameters of Fickian and non-Fickian models of solute transport." Advances in Water Resources **54**(0): 11-21.

Fetter, C. W. (2001). Applied hydrogeology. Upper Saddle River, N. J., Pearson Education.

Fontes, J. C. and J. M. Garnier (1979). "Determination of the Initial 14C activity of the Total Dissolved Carbon: A review of the existing model and a new approach." Water Resour Res **15**(2): 399-413.

Gardner, P. and D. Solomon (2009). "An advanced passive diffusion sampler for the determination of dissolved gas concentrations." Water Resources Research **45**(6).

Gardner, W. P., G. A. Harrington and B. D. Smerdon (2012). "Using excess 4He to quantify variability in aquitard leakage." Journal of Hydrology **468-469**: 63-75.

Ginn, T., H. Haeri, A. Massoudieh and L. Foglia (2009). "Notes on Groundwater Age in Forward and Inverse Modeling." Transport in Porous Media **79**(1): 117-134.

Harbaugh, A. W., E. R. Banta, M. C. Hill and M. G. McDonald (2000). MODFLOW-2000, the U.S. Geological Survey modular ground-water model -- User guide to modularization concepts and the Ground-Water Flow Process, U.S. Geological Survey Open-File Report 00-92, 121 p.

Harrington, G. A. (2002). Recharge mechanisms to Quarternary sand aquifers in the Willunga Basin, South Australia.

Harrington, G. A., W. P. Gardner, B. D. Smerdon and M. J. Hendry (2013). "Palaeohydrogeological insights from natural tracer profiles in aquitard porewater, Great Artesian Basin, Australia." Water Resources Research **49**(7): 4054-4070.

Harrington, G. A., G. R. Walker, A. J. Love and K. A. Narayan (1999). "A compartmental mixing-cell approach for the quantitative assessment of groundwater dynamics in the Otway Basin, South Australia." Journal of Hydrology **214**(1-4): 49-63.

Healy, R. W. and P. G. Cook (2002). "Using groundwater levels to estimate recharge." Hydrogeology Journal **10**(1): 91-109.

Heaton, T. H. E. and J. C. Vogel (1981). "Excess Air in Groundwater." Journal of Hydrology **50**(1-3): 201-216.

Hendry, M. and L. Wassenaar (2011). "Millennial-scale diffusive migration of solutes in thick clay-rich aquitards: evidence from multiple environmental tracers." Hydrogeology Journal **19**(1): 259-270.

Hendry, M. J., S. L. Barbour, K. Novakowski and L. I. Wassenaar (2013). "Paleohydrogeology of the Cretaceous sediments of the Williston Basin using stable isotopes of water." Water Resources Research **49**(8): 4580-4592.

Hendry, M. J. and L. I. Wassenaar (2009). "Inferring Heterogeneity in Aquitards Using High-Resolution δD and δ18O Profiles." Ground Water **47**(5): 639-645.

Herczeg, A. and F. Leaney (2002). Groundwater flow systems and recharge in Willunga Basin_report_10_CSIRO.

Herczeg, A. L. and W. M. Edmunds (2000). Inorganic Ions as Tracers. Environmental Tracers in Subsurface Hydrology. P. Cook and A. L. Herczeg. CSIRO Land and Water, Glen Osmond, Australia, Kluwer Academic Publishers. **1:** 31-77.

Hill, M. C. and C. R. Tiedeman (2007). Effective groundwater model calibration: with analysis of data, sensitivities, predictions, and uncertainty. Hoboken, New Jersey, John Wiley and Sons.

Jahne, B., G. Heinz and W. Dietrich (1987). "Measurement of the diffusion coefficients of sparingly soluble gases in water." Journal of Geophysical Resources **100**: 7083-7088.

Kalin, R. M. (2000). Radiocarbon dating of groundwater systems. Environmental Tracers in Subsurface Hydrology. P. Cook and A. L. Herczeg. CSIRO Land and Water, Glen Osmond, Australia, Kluwer Academic Publishers**:** 111-144.

Kipfer, R., W. Aeschbach-Hertig, F. Peeters and M. Stute (2002). "Noble Gases in Lakes and Ground Waters " Reviews in Mineralogy and Geochemistry: 615-700.

Kloppmann, W., L. Dever and W. M. Edmunds (1998). "Residence time of Chalk groundwaters in the Paris Basin and the North German Basin: a geochemical approach." Applied Geochemistry **13**(5): 593-606.

Liu, J., G. Fu, X. Song, S. P. Charles, Y. Zhang, D. Han and S. Wang (2010). "Stable isotopic compositions in Australian precipitation." J. Geophys. Res **115**.

Love, A. J., A. L. Herczeg, F. W. Leaney, M. F. Stadter, J. C. Dighton and D. Armstrong (1994). "Groundwater Residence Time and Paleohydrology in the Otway Basin, South Australia - H-2, O-18 and C-14 Data." Journal of Hydrology **153**(1-4): 157-187.

Love, A. J., A. L. Herczeg and G. Walker (1996). Transport of Water and Solutes Across a Regional Aquitard inferred from porewater dueterium and chloride profiles. Isotopes in Water Resources Management: Procedings of a Symposium on Isotopes in Water Resources Management, International Atomic Energy Agency.

Mahara, Y., M. A. Habermehl, T. Hasegawa, K. Nakata, T. R. Ransley, T. Hatano, Y. Mizuochi, H. Kobayashi, A. Ninomiya, B. R. Senior, H. Yasuda and T. Ohta (2009). "Groundwater dating by estimation of groundwater flow velocity and dissolved 4He accumulation rate calibrated by 36Cl in the Great Artesian Basin, Australia." Earth and Planetary Science Letters **287**(1–2): 43-56.

Maloszewski, P. and A. Zuber (1991). "Influence of Matrix Diffusion and Exchange Reactions on Radiocarbon Ages in Fissured Carbonate Aquifers." Water Resources Research **27**(8): 1937-1945.

Martin, R. R. (1998). Report Book 98/28 Willunga Basin - Status of Groundwater Resources 1998. P. I. a. R. SA. Adelaide, South Australia.

Martin, R. R. (2006). Hydrogeology and Numercial Groundwater Flow Model for the McLaren Vale Prescribed Wells Area Summary Report, REM, Adelaide and Mount Lofty Ranges Natural Resource Management Board.

Massoudieh, A. and T. R. Ginn (2011). "The theoretical relation between unstable solutes and groundwater age." Water Resources Research **47**.

Mazor, E. (2004). Chemical and isotopic groundwater hydrology. New York, Marcel Dekker.

Mazurek, M., P. Alt-Epping, A. Batch, T. Gimmi and H. Niklaus Waber (2009). Natural Tracer Profiles Across Argillaceous Formations: The CLAYTRAC Project, Nuclear Energy Agency, Organisation for Economic Co-operation and Development.

Mazurek, M., P. Alt-Epping, A. Bath, T. Gimmi, H. N. Waber, S. Buschaert, P. De Canniere, M. De Craen, A. Gautschi, S. Savoye, A. Vinsot, I. Wemaere and L. Wouters (2011). "Natural tracer profiles across argillaceous formations." Applied Geochemistry **26**(7): 1035-1064.

McCallum, J. L., P. G. Cook, C. T. Simmons and A. D. Werner (2013). "Bias of Apparent Tracer Ages in Heterogeneous Environments." Ground Water.

McCallum, J. L., N. B. Engdahl, T. R. Ginn and P. G. Cook (2014). "Nonparametric estimation of groundwater residence time distributions: What can environmental tracer data tell us about groundwater residence time?" Water Resources Research **50**(3): 2022-2038.

Niswonger, R. G., S. Panday and M. Ibaraki (2011). MODFLOW-NWT, A netwon forumation for MODFLOW 2005.

Osenbrück, K., J. Lippmann and C. Sonntag (1998). "Dating very old pore waters in impermeable rocks by noble gas isotopes." Geochimica Et Cosmochimica Acta **62**(18): 3041-3045.

Pearson, F. J. (1965). Use of C-13/C-12 ratios to correct radiocarbon ages of material initially diluted by limestone. Proceedings of the 6th International Conference on Radiocarbon and Tritium Dating, Pulman, Washington.

Pearson, F. J., D. Arcos, A. Bath, J.-Y. Boisson, A. M. Fernandez, H.-E. Gabler, E. Gaucher, A. Gautschi, L. Griffault, P. Hernan and H. N. Waber (2003). Mont Terri Project - Geochemistry of the Water in the Opalinus Clay Formation at the Mont Terri Rock Laboratory. Reports of the Federal Office for Water and Geology (FOWG), Geology Series No. 5.

Petherick, L., H. Bostock, T. J. Cohen, K. Fitzsimmons, J. Tibby, M.-S. Fletcher, P. Moss, J. Reeves, Mooney, B. S., K. T., J. J., N. J. and A. Dosseto (2013). "Climatic records over the past 30 ka from temperate Australia - a synthesis from the Oz-INTIMATE workgroup." Quaternary Science Reviews **74** 58-77.

Poole, J., G. McNeill, S. Langman and F. Dennis (1997). "Analysis of noble gases in water using a quadrupole mass spectrometer in static mode." Applied Geochemistry **12**(6): 707-714.

Post, V. E. A. and E. Banks (in press). Appendix G Seawater intrusion and sources of groundwater salinity. Adelaide Plains, Goyder Institute.

Rebeix, R., C. Le Gal La Salle, P. Jean-Baptiste, V. Lavastre, E. Fourré, F. Bensenouci, J. M. Matray, P. Landrein, O. Shouakar-Stash, S. K. Frape, J. L. Michelot and J. Lancelot (2014). "Chlorine transport processes through a 2000 m aquifer/aquitard system." Marine and Petroleum Geology **53**(0): 102-116.

Reeves, J. M., T. T. Barrows, T. J. Cohen, A. S. Kiem, H. C. Bostock, K. E. Fitzsimmons, J. D. Jansen, J. Kemp, C. Krause, L. Petherick, S. J. Phipps and O.-I. Members (2013). "Climate variability over the last 35,000 years recorded in marine and terrestrial archives in the Australian region: an OZ-INTIMATE compilation." Quaternary Science Reviews **74**: 21-34.

Reilly, T. E., L. N. Plummer, P. J. Phillips and E. Busenberg (1994). "The use of simulation and multiple environmental tracers to quantify groundwater flow in a shallow aquifer." Water Resources Research **30**(2): 421-433.

Sanford, W. (2011). "Calibration of models using groundwater age." Hydrogeology Journal **19**(1): 13-16.

Sanford, W. E., L. N. Plummer, D. P. McAda, L. M. Bexfield and S. K. Anderholm (2004). "Hydrochemical tracers in the middle Rio Grande Basin, USA: 2. Calibration of a groundwater-flow model." Hydrogeology Journal **12**(4): 389-407.

Seiler, K. P. and J. R. Gat (2007). Groundwater Recharge from Run-off, Infiltration and Percolation. Dordrecht, Springer.

Short, M. (2011). Submarine groundwater discharge from the Willunga Basin, South Australia, Flinders University.

Short, M. A., S. Lamontagne, P. G. Cook and R. Cranswick (2014). "Characterising the distribution of near-shore submarine groundwater discharge along a coastline using Rn-222 and electrical conductivity." Australian Journal of Earth Sciences **61**(2): 319-331.

Smith, S. D., D. K. Solomon and W. P. Gardner (2013). "Testing helium equilibrium between quartz and pore water as a method to determine pore water helium concentrations." Applied Geochemistry **35**: 187-195.

Solomon, D. K. (2000). 4He in Groundwater. Environmental Tracers in Subsurface Hydrology. P. G. Cook and A. L. Herczeg, Kluwer Academic Publishers**:** 425-439.

Solomon, D. K., A. Hunt and R. J. Poreda (1996). "Source of radiogenic helium 4 in shallow aquifers: Implications for dating young groundwater." Water Reources Research **32**(6): 1805-1813.

Solomon, K. (2000). ^{4}He in Groundwater. Environmental Tracers in Subsurface Hydrology. P. G. Cook and A. L. Herczeg. Boston ; London, Kluwer Academic Publishers**:** 425 - 439.

Tamers, M. A. (1975). "Validity of radiocarbon dates on ground water." Geophysical Surveys **2**(2): 217-239.

Timms, W., R. I. Acworth and J. Jankowski (2001). "Quantifying leakage and mixing in an alluvial aquifer system: a combined hydrochemical and hydrodynamic modelling approach constrained by isotopic evidence." New Approaches Characterizing Groundwater Flow, Vols 1 and 2: 419-423.

Timms, W., R. I. Acworth, J. Jankowski and S. Lawson (2000). "Groundwater quality trends related to aquitard salt storage at selected sites in the Lower Murrumbidgee alluvium, Australia." Groundwater: Past Achievements and Future Challenges: 655-660.

Timms, W., M. J. Hendry, J. Muise and R. Kerrich (2009). "Coupling Centrifuge Modeling and Laser Ablation Inductively Coupled Plasma Mass Spectrometry To Determine Contaminant Retardation in Clays." Environmental Science & Technology **43**(4): 1153-1159.

Turnadge, C. and B. D. Smerdon (2014). "A review of methods for modelling environmental tracers in groundwater: Advantages of tracer concentration simulation." Journal of Hydrology **519**(PD): 3674-3689.

Van Der Kamp, G. (2001). "Methods for determining the in situ hydraulic conductivity of shallow aquitards – an overview." Hydrogeology Journal **9**(1): 5-16.

Van Der Kamp, G., D. R. Van Stempvoort and L. I. Wassenaar (1996). "The radial diffusion method. 1. Using intact cores to determine isotopic composition, chemistry, and effective porosities for groundwater in aquitards." Water Resources Research **32**(6): 1815-1822.

Vogel, J. C. (1967). Investigation of groundwater flow with radiocarbon. Isotopes in Hydrology, IAEA, Vienna.

Zheng, C. and P. P. Wang (1999). MT3DMS, A modular three-dimensional multi-species transport model for simulation of advection, dispersion and chemical reactions of contaminants in groundwater systems; documentation and user¡¯s guide, U.S. Army Engineer Research and Development Center Contract Report SERDP-99-1, Vicksburg, MS, 202 p.

Zuber, A., K. Rozanski, J. Kania and R. Purtschert (2011). "On some methodological problems in the use of environmental tracers to estimate hydrogeologic parameters and to calibrate flow and transport models." Hydrogeology Journal **19**(1): 53-69.